The Dissertation Committee for Deanna Helene Gates Certifies that this is the approved version of the following dissertation:

The Role of Muscle Fatigue on Movement Timing and Stability during Repetitive Tasks

Committee:

Jonathan B. Dingwell, Supervisor

Ronald Barr

Lisa Griffin

J. Steven Moore

H. Grady Rylander

The Role of Muscle Fatigue on Movement Timing and Stability during Repetitive Tasks

by

Deanna Helene Gates, B.S.; M.S.

Dissertation

Presented to the Faculty of the Graduate School of

The University of Texas at Austin

in Partial Fulfillment

of the Requirements

for the Degree of

Doctor of Philosophy

The University of Texas at Austin

May 2009

Acknowledgements

The Role of Muscle Fatigue on Movement Timing and Stability during Repetitive Tasks

Publication No._____

Deanna Helene Gates, Ph.D.

The University of Texas at Austin, 2009

Supervisor: Jonathan B. Dingwell

Repetitive stress injuries are common in the workplace where workers perform repetitive tasks continuously throughout the day. Muscle fatigue may lead to injury either directly through muscle damage or indirectly through changes in coordination, development of muscle imbalances, kinematic and muscle activation variability, and/or movement instability. To better understand the role of muscle fatigue in changes in movement parameters, we studied how muscle fatigue and muscle imbalances affected the control of movement timing, variability, and stability during a repetitive upper extremity sawing task.

Since muscle fatigue leads to delayed muscle and cognitive response times, we might expect the ability to maintain movement timing would decline with muscle fatigue. We compared timing errors pre- and post-fatigue as subjects performed this repetitive sawing task synchronized with a metronome using standard techniques and a goal-equivalent manifold (GEM) approach. No differences in basic performance parameters were found. Significant decreases in the temporal correlations of the timing errors and

velocities indicated that subjects made more frequent corrections to their movements post-fatigue.

Muscle fatigue may lead to movement instability through a variety of mechanisms including delayed muscle response times and muscle imbalances. To measure movement stability, we must first define a state space that describes the movement. We compared a variety of different state space definitions and found that state spaces composed of angles and velocities with little redundant information provide the most consistent results. We then studied the affect of fatigue on the shoulder flexor muscles and general fatigue of the arm on movement stability. Subjects were able to maintain stability in spite of muscle fatigue, shoulder strength imbalance and decreased muscle cocontraction.

Little is known about the time course for adaptations in response to fatigue. We studied the effect of muscle fatigue on movement coordination, kinematic variability and movement stability while subjects performed the same sawing task at two work heights. Increasing the height of the task caused subjects to make more adjustments to their movement patterns in response to muscle fatigue. Subjects also exhibited some increases in kinematic variability at the shoulder but no changes in movement stability. These findings suggest that people alter their kinematic patterns in response to fatigue possibly to maintain stability at the expense of increased variability.

Table of Contents

List of Tables

List of Figures

Chapter 1: Introduction

1.1 SIGNIFICANCE OF MUSCULOSKELETAL INJURIES

Musculoskeletal injuries occur when the mechanical properties of soft or hard tissues are overwhelmed by applied loads. They may result from a single event or an accumulation of microfractures or microtears over time (Goerlick et al., 2003). The latter are termed repetitive stress injuries (RSIs) or cumulative trauma injuries (Latko et al., 1999; Côté et al., 2005). Work-related musculoskeletal injuries affected over 375,500 people in the U.S. in 2005 resulting in 30% of all work days lost due to work-related injuries (U.S. Bureau of Labor Statistics, 2005). Injuries caused by repetitive motions like grasping tools, scanning groceries, and typing resulted in the longest absences from work (U.S. Bureau of Labor Statistics, 2005). Upper extremity RSI cost workers and the U.S. economy at least $12 to $14 Billion a year (Gardner-Morse and Stokes, 1998; Boden and Galizzi, 1999; Levenstein, 1999; Keogh et al., 2000). The true costs are significantly higher, since only 1 in 10 workers who suffer RSI seek compensation (Gardner-Morse and Stokes, 1998; Pransky et al., 1999). While the exact causes of RSIs are unknown, there are several common characteristics associated with their development. These include high force (Barr, 2002), a high number of movement repetitions (Latko et al., 1999), improper postures, muscular imbalances, and muscle fatigue (Côté et al., 2005).

Muscle fatigue is defined as a decrease in the force generating capacity of a muscle or muscle group after activity (Bigland-Ritchie and Woods, 1984; DeLuca, 1984; Gandevia, 2001). Fatigue is a combination of both central and peripheral processes (Gandevia, 2001). At the peripheral level, there is a loss of force generating capacity of individual motor units (Selen et al., 2007). To maintain force, the central nervous system can increase its drive to the muscles. This causes already active motor units to fire more

1

frequently and causes larger motor units to be recruited. This leads to an increased sense of effort (Gandevia, 2001). As fatigue progresses, the number of active motor units decreases, muscle fiber conduction velocity decreases (Farina et al., 2002), motor units fire more slowly (Bigland-Ritchie and Woods, 1984), and the motor units become more synchronized (Arihara and Sakamoto, 1999). These changes lead to decreases in the mean or median frequencies of the electromyogram (EMG) signal (Bigland-Ritchie and Woods, 1984) and eventually to task failure (Hunter et al., 2004).

1.2 FATIGUE AND INJURY

Muscle fatigue has been suggested to cause injury both directly and indirectly (Fig. 1.1). Muscle fatigue decreases the amount of energy that a muscle can absorb at the same degree of stretch. This leaves the muscle more susceptible to muscle strain injuries (Mair et al., 1996). In addition, exhausting stretch-shortening cycles can lead to microscopic structural damage of the contractile elements of the muscle (Friden et al., 1988), and extensive eccentric contractions can lead to disorganization of the sacromeric band pattern (Lieber et al., 1991). The relationship between fiber strain and muscle injury is complex (Butterfield and Herzog, 2005) however, and even more so in the case of fatigue.
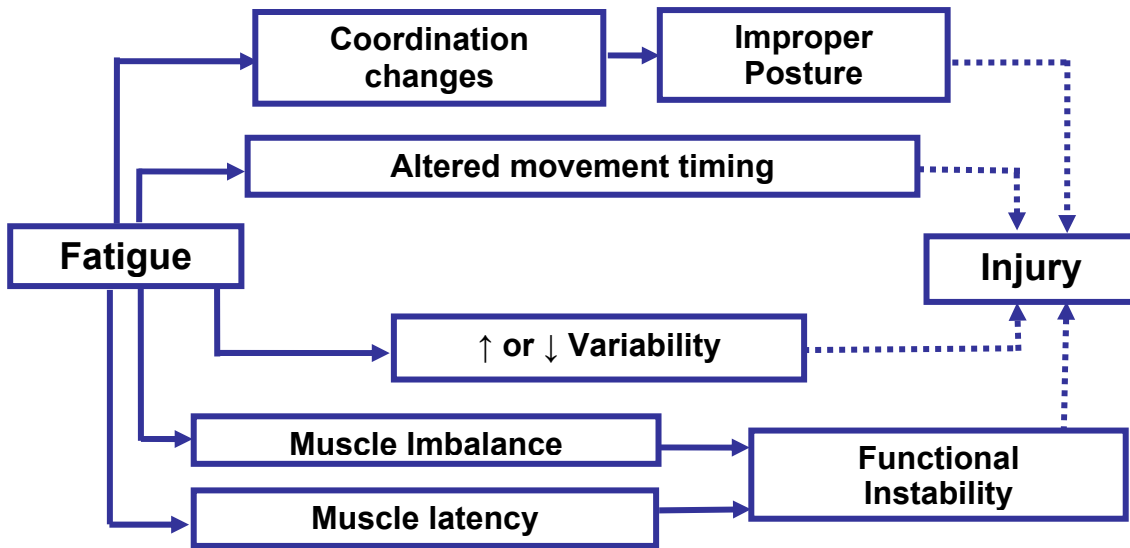
Figure 1.1: Proposed injury model
This schematic illustrates the possible relationships between muscle fatigue and injury based on the literature. Each link is described in a section of this introduction.

1.3 MUSCLE FATIGUE AND COORDINATION

Repeatedly performing manual tasks leads to muscle fatigue, which can induce changes in motor coordination (Viitasalo et al., 1993; Bonnard et al., 1994; Forestier and Nougier, 1998). Studies of single joint upper extremity movements have shown that fatigue leads to differential changes in the phasic firing rates of agonist and antagonist muscles and degradations in performance (Jaric et al., 1999; Corcos et al., 2002). Studies of sub-maximal jumping and hopping reported fatigue associated changes in both joint and muscle coordination (Viitasalo et al., 1993; Bonnard et al., 1994).

Certain changes in coordination may pre-dispose individuals to developing RSIs by inducing poor biomechanics (Rodgers et al., 1994; Sparto et al., 1997; Mizrahi et al., 2000). Studies of repetitive lifting (Marras, 1997; Sparto et al., 1997) showed that after fatigue subjects switched from a squat-lift to a stoop-lift strategy, which has been

3

associated with ligament and intervertebral disc damage (Burgess-Limerick, 2003). Fatigue has also been shown to alter the typical proximal-to-distal organization of joint coordination in throwing (Forestier and Nougier, 1998). In a whole body sawing task, subjects altered their inter-joint coordination patterns, such that while the individual segment movement characteristics changed with fatigue their endpoint trajectories did not (Côté et al., 2002). Such biomechanical changes resulting from fatigue may indicate an increased potential for injury (Sparto et al., 1997; Rodgers et al., 2003), or may alternatively reflect protective strategies used to decrease injury risk (Madigan and Pidcoe, 2003).

During many of these tasks, fatigue was localized to a specific muscle group. Localized muscle fatigue may also contribute to, or indicate risk of, chronic muscle pain (Nussbaum, 2001). It is unclear whether the same adaptations would also be present if the fatigue was not specific to any particular muscle. To our knowledge, only one study has investigated this distinction. In this study, subjects performed a repetitive lifting task after either a back extension fatigue protocol targeted at specific fatigue of the trunk extensor muscles or a rowing task to generate non-specific widespread fatigue. The specific fatigue protocol caused changes in muscle timing, while the non-specific fatigue protocol did not (Goerlick et al., 2003).

1.4 CONTROL OF MOVEMENT TIMING

Repetitive movements are common in daily life and numerous work environments. Typical repetitive motion activities include factory assembly work, typing, scanning groceries, walking, and running. Timing is often critical in these activities. For instance, in assembly line work, individuals lose productivity and increase

their potential for injury if they cannot maintain timing. Muscle fatigue adversely affects movement and muscle timing (Wilder et al., 1996; McQuade et al., 1998), as well as reaction time (Lorist et al., 2002). Increased activity in the prefrontal areas of the brain after muscle fatigue may contribute to increased processing time during congnitive reaction time tests (van Duinen et al., 2007). At the muscle level, fatigue increases the 'electromechanical delay', possibly due to decreased muscle fiber conduction velocity (Wilder et al., 1996). Muscle fatigue may also alter the ability to reproduce a movement. In a rapid elbow flexion/extension task, fatiguing the extensor muscles caused an undershoot of the final position during extension but had no affect on flexion movement (Jaric et al., 1999). In more complex multi-joint tasks, subjects may change their muscle activation strategies to maintain the same end-point trajectories (Lucidi and Lehman, 1992; Côté et al., 2002; Heuer et al., 2002; Selen et al., 2007).
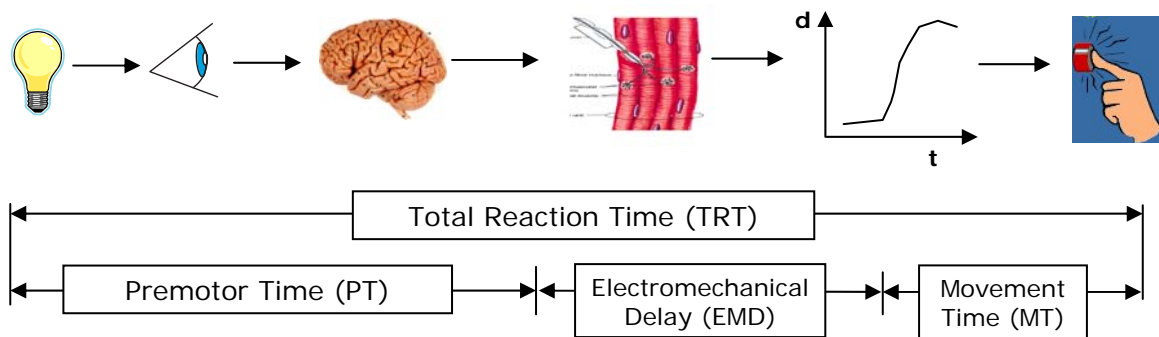
Figure 1.2: Schematic of a reaction time test
The time it takes for the brain to recognize a stimulus and decide to act is known as the 'Premotor Time'. The time for the brain to send a signal to the muscles to act is the 'Electomechanical delay' or 'muscle response time'. Finally the time it takes to complete the requisite movement is the 'movement time'. Each of these reaction times may be slowed by muscle fatigue.

Multi-joint tasks exhibit infinite movement solutions (equifinality), so determining an appropriate control strategy is difficult. One way to study control is to quantify how quickly subjects respond to deviations away from the task *goal*. For

5

redundant tasks, one can define a "goal equivalent manifold" (GEM) (Cusumano and Cesari, 2006), which yields an explicit mapping between variability of body state variables and variability of the goal variables defined by the task. All viable task solutions lie on the GEM. To determine how quickly deviations are corrected, we can quantify temporal correlations in a time series (Hausdorff et al., 1995; Peng et al., 1995; Gates, 2007; Gates et al., 2007). Deviations that go uncorrected lead to "persistent" correlations over consecutive movements. Thus, less "persistence" or greater "anti-persistence" in a time series indicates a highly controlled process where deviations are rapidly corrected (Gates and Dingwell, 2008); Ch.2). A previous study used similar techniques to look at movement of the center of pressure during quiet standing. They found that localized fatigue of the ankle plantarflexors caused increased anti-persistence of these movements indicating that more control was applied after fatigue, possibly to maintain stability (Corbeil et al., 2003).

1.5 MUSCLE FATIGUE AND VARIABILITY

Muscle fatigue can lead to increased muscle force unsteadiness proportional to the force level (Missenard et al., 2008a). This unsteadiness may in turn lead to increased kinematic and kinetic variability (Parnianpour et al., 1988; Selen et al., 2007). Muscle fatigue may also reduce cocontraction of opposing muscle groups (Missenard et al., 2008b), which can lead to decreased stiffness and increased variability (Gribble et al., 2003; Selen et al., 2005). In multi-joint dynamic tasks, people may alter their biomechanical coordination strategies (Sparto et al., 1997; Côté et al., 2002) or muscle activation patterns (Corcos et al., 2002; Goerlick et al., 2003). These adjustments may serve to minimize changes in overall kinematic variability.

6

It is debatable whether or not changes in variability of movements relate to increased risk of injury, however. Greater variability might lead to injury by increasing the likelihood of extreme movements (Potvin and O'Brien, 1998). Conversely, increased variability might be protective, because it prevents the joints from constantly being loaded in the same manner. Hamill et al. (1999) found that subjects with patellofemoral pain were less variable than asymptomatic individuals when running. They suggest that subjects with pain found a repeatable solution that minimized pain. This would further exacerbate the problem, however, since they continue to stress the joints in the same manner causing an accumulation of microscopic damage of the tissues and/or cartilage being stressed (Hamill et al., 1999; Madeleine et al., 2003). Madeleine et al. (2003) studied experienced butchers with no history of injury and healthy novice butchers. They found that the experienced butchers had more variable motions and suggested that this may be a protective strategy to prevent musculoskeletal injuries. It is unclear whether similar adaptations would be made in response to muscle fatigue, however.

1.6 MUSCLE IMBALANCES AND MUSCLE FATIGUE

Muscle imbalances were originally defined as an impaired relationship between muscles which are prone to develop tightness and shortness, and muscles which are prone to inhibition (Janda, 1993). This definition has been adapted to include any asymmetry of strength, power, endurance, or flexibility between opposing muscle groups (Beukeboom et al., 2000). Reduced activity of some muscles around a joint may lead to excessive motion in the direction in which the dominant muscle operates (Alizadehkhaiyat et al., 2007), or to improper joint loading (Goerlick et al., 2003). Imbalances may be inherent or they could result from prolonged static postures (Valachi

7

and Valachi, 2003), selective training of different muscles (Burnham et al., 1993), or alteration in endurance or 'fatiguability' between opposing muscle groups (Hagg and Milerad, 1997; Alizadehkhaiyat et al., 2007)

Localized muscle fatigue leads to altered muscle activation patterns in fatigued muscles (Goerlick et al., 2003), increased compensation of other joints (Madeleine et al., 1999; Côté et al., 2002), and can lead to muscle imbalance if only one muscle group crossing a joint is selectively fatigued (Alizadehkhaiyat et al., 2007). These studies support the "Differential Fatigue Theory" (Kumar, 2001), which proposed that during strenuous activity, the muscles surrounding a joint fatigue at different rates. Since muscle fatigue leads to a decrement in force production (Basmajian and DeLuca, 1985), this creates a force imbalance around the joint which could lead to abnormal stress distributions (Goerlick et al., 2003).

A few studies support the differential rate of fatigue of opposing muscle groups. Kumar and Narayan (1998) found different rates of fatigue in 14 lower back muscles during an isometric axial rotation contraction. Mizrahi et al. (2000) found greater fatigue in the ankle dorsiflexors than plantarflexors during prolonged running. Haag et al. (1997) found greater wrist extensor fatigue than flexor fatigue during gripping. And finally, Kilbom et al. (1993) observed greater fatigue on the flexor side during a one-handed carrying task. None of these studies concurrently measured force imbalances or stress distributions, however.

Muscle imbalances may play an important role in the development of musculoskeletal injuries, such as tennis elbow (Kamien, 1990). Possible causes of tennis elbow include decreased strength (Alizadehkhaiyat et al., 2007) and fatigability (Hagg and Milerad, 1997) of the wrist extensors compared to wrist flexors. Another study showed that runners suffering from overuse injuries had greater muscle imbalances about

their hip than non-injured runners (Niemuth et al., 2005). Muscle strength imbalance of the shoulder rotators has also been associated with increased prevalence of shoulder injuries (Wang and Cochrane, 2001). In addition, an imbalance between the flexor and extensor strength of the trunk can significantly influence the lordotic curve of the lumbar spine, potentially resulting in low back pain (Kim et al., 2006).

1.7 MOVEMENT STABILITY & COORDINATION

The body controls stability in many ways. The central nervous system integrates afferent information about joint position, kinesthesia and proprioception to generate muscular responses to maintain functional stability during movement (Bowman et al., 2006). If any of these feedback mechanisms are adversely affected, the muscular responses may also be altered. Fatigue has been linked to decreased proprioception (Myers et al., 1999), decreased kinesthesia (Pedersen et al., 1999), altered reflexes (Wojtys et al., 1996) and increased muscle response time (Wilder et al., 1996; Wojtys et al., 1996). Muscle fatigue may in turn lead to decreased stability. One difficulty is that the definition of 'stability' varies greatly. Stability is often equated to joint stiffness. To compensate for fatigue, people may co-contract their muscles leading to increased joint stiffness (Psek and Cafarelli, 1993), which may protect the joint from injury. However, muscle fatigue also results in decreased muscle response times (Wilder et al., 1996), so any shocks due to sudden perturbations must be absorbed by the passive tissues (Sparto et al., 1997). Thus, stiffness alone may not predict the likelihood of injury in the presence of sudden loading or perturbations.

As an alternative, we can measure stability as the capacity of a system to respond to perturbations (Full et al., 2002). In particular, "local dynamic stability" measures

directly quantify the resilience of the motor system to small perturbations that occur naturally during movement (Dingwell and Cusumano, 2000; Dingwell and Marin, 2006; Dingwell et al., 2007). To examine the response to perturbations, we must first define a state space that describes the movement. The state space can be composed of any variables that adequately describe the motion (refer to Ch. 3 for additional details). For example we can look at a simple pendulum. The equation of motion for the pendulum is

$$\ddot{\theta} = -\frac{g}{L}\sin\theta \qquad (1.1)$$

The state of the pendulum is characterized by defining its angular displacement from the vertical position, θ, and its corresponding angular velocity, $\dot{\theta}$ (Fig. 1.3). A plot of θ versus $\dot{\theta}$ is known as the 'state space' (Fig. 1.3B) since it uniquely describes the state of the system for all time points (Kantz and Schreiber, 2004). If this system had noise you would see small deviations away from the mean trajectory. These represent what might happen if a small perturbation were applied to the system. We can track these 'perturbations' over time in state space by measuring the distance between two nearest neighbors at any time point (Fig. 1.3C). We look at all the distances between nearest neighbors and then add them up to find the average logarithm of the divergence (Fig. 1.3D). This tells us whether trajectories converge together over time or diverge apart. The slope of the mean log divergence curve is the local divergence exponent. Positive exponents indicate that the trajectories diverge apart and thus the system is unstable. Higher values indicate a more rapid divergence and thus greater instability.
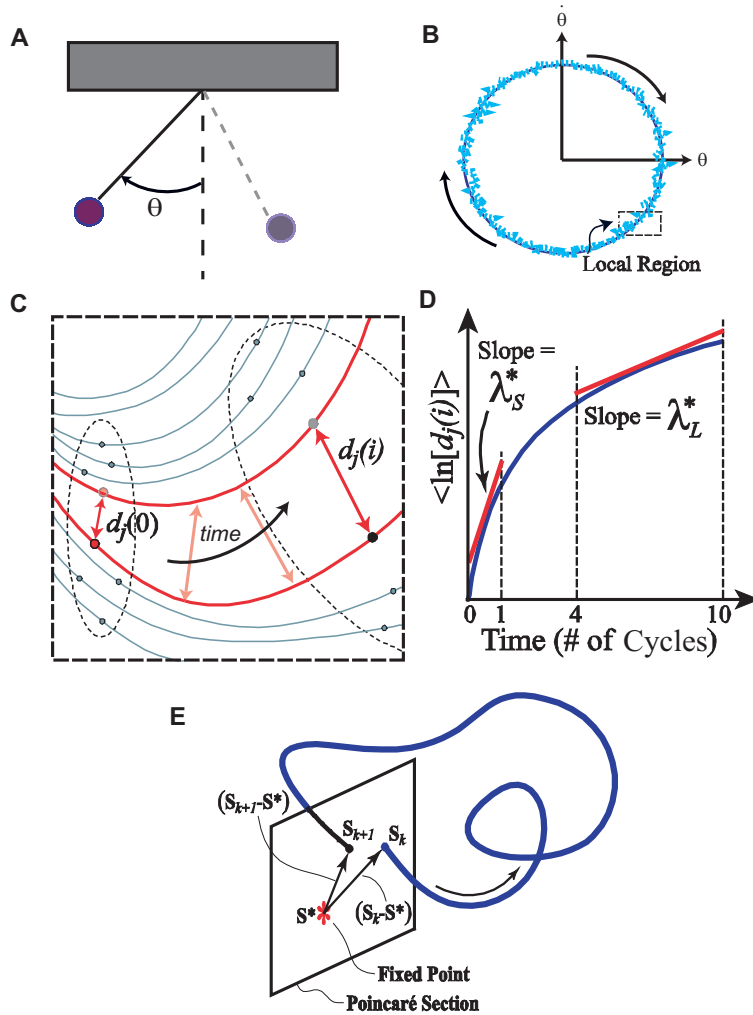
Figure 1.3: Schematic representations of local and orbital stability analyses.
A) Illustration of a simple pendulum. **B)** The state space of the pendulum is defined by the angular position and velocity of the mass. The solid line represents an ideal pendulum while the dashed line represents what would happen if the system had noise. **C)** The distance between nearest neighbors in state space is measured as time evolves. **D)** The mean logarithm of the divergence, $\langle \ln(d_j(i)) \rangle$, is calculated for each time increment. The slope of the mean log divergence curve over 0 to 1 cycles is known as the short-term local divergence exponent, λ_S^*, while the slope over 4 to 10 cycles is the long-term local divergence exponent, λ_L^*. **E)** Representation of a Poincaré section transecting the state space perpendicular to the system trajectory. The system state, $\mathbf{S}_k$, at cycle k evolves to $\mathbf{S}_{k+1}$ one cycle later. The Floquet multipliers quantify whether the distances between these states and the system fixed point, $\mathbf{S}^*$, grow or decay on average across many cycles. (Figure adapted from (Kang and Dingwell, 2008)

11

Two studies have examined the effect of muscle fatigue on local dynamic stability. Yoshino et al. (2004) measured local dynamic stability during prolonged walking. Subjects who showed greater leg muscle fatigue after prolonged walking compensated by slowing down, which increased their trunk stability. Subjects who showed moderate fatigue did not slow down and became more unstable. Granata and Gottipatti (2008) studied the effect of specific fatigue of the back extensors on repeated back flexion/extension. They found that the movement was more unstable post-fatigue. This is might suggest that people are more likely sustain an injury if they are perturbed (Sparto et al., 1997).

A second approach can be used to quantify local stability of periodic systems. This method requires that the movement has a limit cycle, which is a closed trajectory in state space that at least one other trajectory spirals into either as time approaches infinity or as time approaches minus-infinity. Orbital stability can be quantified using Floquet multipliers (Nayfeh and Balachandran, 1995), which quantify how the system's states respond to local perturbations discretely from one cycle to the next at a single point during the cycle. They quantify how a perturbation at cycle k will change after one full cycle. This analysis is done on specific pieces of the limit cycle, known as Poincaré sections. The trajectories of cycle k and cycle $k+1$ both intersect the Poincaré section (Fig. 1.3E). The relationship of cycle k to $k+1$, each relative to the limit cycle, or the mapping of cycle k to $k+1$ at a particular part of the cycle, is called the Jacobian matrix, whose eigenvalues are the Floquet multipliers. The largest Floquet multiplier defines the stability of the system. A Floquet multiplier greater than 1 indicates that a perturbation will increase by that factor at the next cycle, and the perturbation will become greater and greater, indicating instability. A Floquet multiplier less than 1 indicates that a perturbation will decrease by that amount by the subsequent cycle, indicating stability.

Presently, no one has studied the effect of muscle fatigue on the orbital stability of repetitive movements.

1.8 SPECIFIC AIMS

To date, the strategies people use to delay muscle fatigue are not known. Most work tasks require movements that fatigue more than just a single muscle group. It is also unclear whether both isolated and multi-muscle fatigue have the same affect on coordination changes. It is necessary, therefore, to look at the effect of both widespread muscle fatigue and localized muscle fatigue (which can create muscle imbalances) on low-load repetitive tasks, similar to those encountered in many work places. The goal of this dissertation was to determine how muscle fatigue and muscle imbalances alter the control of movement timing and movement stability. I proposed the following four specific aims.

Specific Aim #1: Determine how muscle fatigue affects the control of movement timing during a repetitive task.

To address this first aim, we looked at how muscle fatigue affected the subject's ability to synchronize repetitive movements with a metronome in the face of progressing muscle fatigue. The increased force variability and delayed reaction times associated with muscle fatigue (Bigland-Ritchie and Woods, 1984; Farina et al., 2002; Lorist et al., 2002; van Duinen et al., 2007) suggest that task performance should deteriorate with fatigue: i.e., that timing errors would increase in magnitude. Alternatively, subjects could alter their movement patterns to maintain task performance: i.e., they would continue to

achieve the task goal (Côté et al., 2002; Selen et al., 2007). Therefore, we proposed two alternative hypotheses:

Hypothesis 1a: Task performance will deteriorate with fatigue: i.e. timing errors would increase in magnitude.

Hypothesis 1b: Subjects will alter their movement patterns to maintain task performance: i.e. subjects would continue to achieve the task goal.

Hypothesis 2: Subjects will adopt a control strategy that aligns their movements with the GEM for this task: i.e. deviations perpendicular to the GEM would be much smaller in magnitude and would be corrected more rapidly than deviations along the GEM.

Specific Aim #2: Determine an appropriate state space for local stability analyses.

In order to study the local stability of kinematics, one must first define an appropriate state space for the movement. One difficulty is that the state space definition is not unique and it is not clear whether the measure of local stability, the local divergence exponent, is affected by this choice. We studied the effect of state space definition on the local stability measure for both experimental data and data for which the true local divergence exponent was known. We used various state space definitions that primarily had been used previously in the literature.

Specific Aim #3: Determine how widespread vs. localized muscle fatigue affect the control of movement stability.

Fatigue likely leaves subjects less able to respond to perturbations that can cause injury. However, how muscle fatigue and/or muscle imbalances affect the control of movement stability is not well understood. Subjects performed a five minute repetitive

14

sawing task before and after completing one of two fatiguing tasks. The first task primarily fatigued the shoulder flexor muscles while the second caused general fatigue of the arm. We quantified local dynamic stability for each five minute trial to test the following hypotheses:

Hypothesis 4: Subjects will exhibit greater dynamic instability following both of the fatigue protocols.

Hypothesis 5: The increases in dynamic instability will be larger following specific fatigue of the shoulder flexors than widespread muscle fatigue.

Hypothesis 6: The muscles will become more unbalanced after the specific fatigue of the shoulder flexors than after the general fatigue of the arm (ie. the ratio of flexor to extensor strength will decrease).

Specific Aim #4: Determine how muscle fatigue affects stability and variability of movements performed at two heights.

In this aim we determined how coordination, kinematic variability and dynamic stability of the arm were affected by muscle fatigue while subjects performed a repetitive task at a constant rate until volitional exhaustion. Upper limb disorders are commonly associated with repetitive work performed with the arm elevated and abducted (Ohlsson et al., 1995), so this task was performed at both sternum and shoulder levels. We measured peak angles, kinematic variability and local dynamic stability over time to test the following hypotheses:

15

Hypothesis 1: Subjects would change their movement patterns more dramatically when the task was performed at a higher height since this was assumed to be more difficult to maintain.

Hypothesis 2: Kinematic variability would increase with fatigue in response to increase neuromuscular noise.

Hypothesis 3: Movement stability would decrease with fatigue.

Hypothesis 4: Movement variability and instability would be greater for movements performed at shoulder level where the incidence of injury is greater.

This dissertation determined how muscle fatigue and muscle imbalances affect the control of movement timing, variability, and movement stability. These components of control are critical for maintaining performance during repetitive goal-directed movement tasks. While this dissertation is not related to how these parameters relate to injury themselves, we hope that eventually these results will lay the groundwork for linking specific movement parameters with increased injury risk.

Chapter 2: The Effects of Neuromuscular Fatigue on Task Performance during Repetitive Goal-Directed Movements [1]

2.1 ABSTRACT

Proper movement timing is essential to the successful execution of many motor tasks and may be adversely affected by muscle fatigue. This study quantified how muscle fatigue affected task performance during a repetitive upper extremity task. A total of 14 healthy young adults pushed a low load back and forth along a low-friction horizontal track in time with a metronome until volitional exhaustion. Kinematic, force, and electromyography (EMG) data were measured continuously throughout the task. The first and last 3.5 min were analyzed to represent ''early'' and ''late'' fatigue. Means and standard deviations of movement distance, speed, and timing errors were computed. We also decomposed variations in movement distance and speed into deviations that directly affected achieving the task goal and those that did not, by identifying the goal equivalent manifold (GEM) of all valid solutions to this task. Detrended fluctuation analysis was used to quantify the temporal persistence in each time series. Principle components analysis provided a direct measure of alignment with the GEM. Median power frequencies of the EMG significantly decreased in six of the nine muscles tested indicating that subjects did fatigue. However, there were no differences in the means or variability of movement distance, speed, or timing errors. Thus, subjects maintained overall performance despite fatigue. Subjects applied slightly higher peak handle forces when they were fatigued ($p = 0.032$). Muscle fatigue caused significant reductions in the temporal persistence of movement speed ($p = 0.037$) and timing errors ($p = 0.046$),

---

indicating that subjects corrected errors more quickly when fatigued. Mean deviations and variability perpendicular to the GEM were much smaller than variability along the GEM (p < 0.001). Deviations perpendicular to the GEM were also corrected much more rapidly than those along the GEM (p < 0.001). Subjects aligned themselves very closely ($\pm7^{o}$), but not exactly (p < 0.001), with the GEM. These measures were not significantly affected by muscle fatigue. Overall, these results indicated that subjects altered their biomechanical movement patterns in response to muscle fatigue, but did so in a way that specifically preserved the goal relevant features of task performance.

2.2 INTRODUCTION

Rhythmic movements performed during daily activities are often triggered and sustained by external signals (e.g., auditory, visual, etc.) (Bove et al., 2007). Timing is often critical to these repetitive movement tasks. During coordinated movements, specific muscles must be activated and/or inactivated in both the correct sequence and at appropriate times (O'Boyle et al., 1996). Muscle fatigue can alter muscle timing (Wilder et al., 1996; Strange and Berg, 2007) and muscle coordination (Corcos et al., 2002; Goerlick et al., 2003; Billaut et al., 2005), thus impeding task performance. However, exactly how muscle fatigue affects the control of timing during repetitive tasks has not been established.

Muscle fatigue is defined as a decrease in the force generating capacity of a muscle or muscle group after activity (Bigland-Ritchie and Woods, 1984; DeLuca, 1984; Gandevia, 2001). Fatigue is a combination of both central and peripheral processes (Gandevia, 2001). At the peripheral level, there is a loss of force generating capacity of individual motor units (Selen et al., 2007). To maintain force, the central nervous system

can increase its drive to the muscles. This causes already active motor units to fire more frequently and causes larger motor units to be recruited. This leads to an increased sense of effort (Gandevia, 2001). As fatigue progresses, the number of active motor units decreases, muscle fiber conduction velocity decreases (Farina et al., 2002), motor units fire more slowly (Bigland-Ritchie and Woods, 1984), and the motor units become more synchronized (Arihara and Sakamoto, 1999). This leads to decreased mean or median frequencies of the electromyogram (EMG) signal (Bigland-Ritchie and Woods, 1984) and eventually to task failure (Hunter et al., 2004).

Muscle fatigue may impair a person's ability to properly execute a task. Reaction time during a choice reaction time task increased with muscle fatigue (Lorist et al., 2002). fMRI studies showed increased activity in the prefrontal areas of the brain after muscle fatigue, which may explain this increase in processing time (van Duinen et al., 2007). At the muscle level, fatigue causes an increase in muscle response time or 'electromechanical delay' (Wilder et al., 1996), possibly due to the decrease in muscle fiber conduction velocity. Muscle fatigue may also affect the body's ability to successfully reproduce a movement. In a study of rapid elbow flexion/extension, fatigue of the extensor muscles caused an undershoot of the final position during extension but had no affect on flexion (Jaric et al., 1999). However, other studies showed no affect of fatigue on the end-point trajectories in multi-joint tasks (Lucidi and Lehman, 1992; Côté et al., 2002; Heuer et al., 2002; Selen et al., 2007). In each of these studies, it was presumed that subjects changed their neural control (muscle activation) or coordination strategies to achieve the same overall task goal.

Little is known about how muscle fatigue affects movement control. To determine this, it is important to define what parameters humans actively try to control. Since movement variability may increase with muscle fatigue (Selen et al., 2007), there

may be active higher level processes occurring to combat this variability in order to retain accuracy. Many multi-joint tasks exhibit an infinite number of possible movement solutions (i.e., equifinality), so determining an optimal control strategy is difficult. One way to quantify the system's degree of control is to study how quickly subjects respond to deviations away from the task goal. Cusumano and Cesari (2006) introduced the idea of a 'goal equivalent manifold' (GEM) which provided a rigorous approach to quantifying motor redundancy in goal-directed movements. This method defines an explicit mapping between the variability of the body state variables (e.g., position, speed) and variability of the goal variables defined by the task. All possible solutions to the task lie along the GEM. Using this approach one can determine whether muscle fatigue affects the outcome (i.e., the 'goal'), the body, or both.

One way to determine how quickly deviations are corrected is to quantify the temporal correlation structure of the variations in a time series (Hausdorff et al., 1995; Peng et al., 1995). When deviations in one direction are more likely to be followed by deviations in the opposite direction, the time series exhibits "anti-persistent" correlations. This indicates a highly controlled process. When deviations in one direction are more likely to be followed by deviations in the same direction (i.e., the deviations get bigger in magnitude) the time series exhibits "persistent" correlations. To date, only one group has examined the affect of fatigue on such temporal correlations. Localized muscle fatigue of the ankle plantarflexors caused the center of pressure trajectories during quiet standing to become more anti-persistent (Corbeil et al., 2003). These results suggested that the actions taken by the postural control system to maintain balance were more frequent post-fatigue (Corbeil et al., 2003).

The goal of this project was to determine how muscle fatigue affected the control of repetitive goal-directed upper extremity movements. Subjects performed a repetitive

20

sawing-like task in time with a metronome until volitional exhaustion. The increased force variability and delayed reaction times associated with muscle fatigue (Bigland-Ritchie and Woods, 1984; Farina et al., 2002; Lorist et al., 2002; van Duinen et al., 2007) suggest that task performance should deteriorate with fatigue: i.e., that timing errors would increase in magnitude. Alternatively, subjects could alter their movement patterns to maintain task performance: i.e., they would continue to achieve the task goal (Côté et al., 2002; Selen et al., 2007). We hypothesized that subjects would adopt a control strategy that aligned their movements with the GEM for this task: i.e., that deviations perpendicular to the GEM would be much smaller in magnitude and would be corrected more rapidly than deviations along the GEM. We further hypothesized that while subjects would alter their movement patterns to combat the effects of muscle fatigue, those features of motor performance that were specifically "goal relevant" would not change.

2.3 METHODS

Subjects

14 healthy right-handed subjects (9 male, 5 female) participated. Their mean ± standard deviation age, body mass, and height were 27 ± 2.7 yr, 72.5 ± 16.9 kg and 1.72 ± 0.10 m, respectively. All participants signed institutionally approved informed consent forms and were screened to ensure that no subject had a history of medications, surgeries, injuries, or illnesses that might have affected their upper extremity joint movements. To determine handedness, subjects completed a modified version of the Edinburgh Inventory (Oldfield, 1971) (Appendix B). This inventory indicates the level of dominance of one hand over another. A score of 0/10 indicates a complete left-handed preference, while a

score of 10/10 indicates a complete right-handed preference. All subjects scored at least 9/10 on the Edinburgh Inventory, indicating a strong right-handed dominance.

Experimental Protocol

To monitor timing parameters during fatigue, we built a device to simulate a repetitive work task similar to sawing (Fig. 2.1). Subjects made bi-directional horizontal movements in the anterior-posterior direction with their right arm while holding a handle mounted to a carriage riding on a low friction track attached to a support frame. Inertial resistance was supplied by an adjustable set of weights mounted on the carriage. Therefore, the resisting load was always opposed to the direction of motion so the arm extensors were the primary agonists during the pushing stroke, while the flexors were the primary agonists on the pulling stroke.
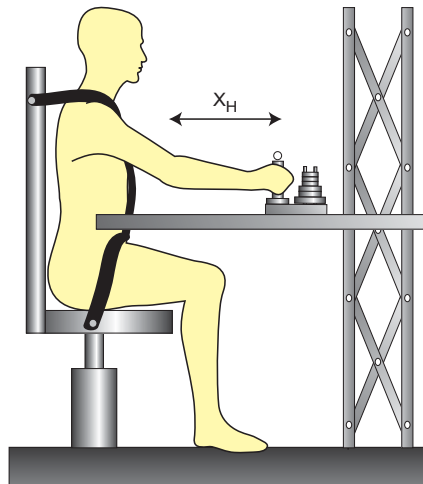
Figure 2.1: Illustration of the experimental setup.
Subjects were seated in a high-back chair and restrained by belts across the waist and shoulders. Subjects pushed a handle with an adjustable weight across a low friction horizontal track. This track was adjusted to the level of the subject's sternum. A single marker on top of the handle quantified the anterior-posterior motions of the handle (X_H).

The device was adjusted so the subject's legs were at a 90˚ angle with the ground. The height of the bar was adjusted so the midpoint between the third and fourth finger was in line with the xiphoid process. The front/back position of the chair was adjusted to be comfortable for the subject and allow for a full range of motion. This was defined as a maximum point almost to full extension (no hyperextension) and a minimum point at the level of the sternum.

To ensure the task resistance was comparable across subjects, we first measured each subject's maximum pushing/pulling force using a second custom handle attached to a Baseline® dynamometer that was rigidly mounted on a table. Subjects alternately pushed and then pulled on this rigidly fixed handle as hard as they could for 5 seconds each, 3 times, with 60 seconds of rest in between each attempt. The average of these six peak forces applied during each maximal effort defined that subject's maximum isometric pushing/pulling strength.

Subjects were instructed to move in time with a metronome. To ensure the task was dynamically equivalent across subjects, the frequency of the metronome was set to twice the average of the predicted resonant frequencies of the upper arm and forearm segments of each subject (2 beats per cycle). The natural frequency, f_n, of a rigid body pendulum is

$$f_n = \frac{1}{2\pi}\sqrt{\frac{mgr}{I_o}} \tag{2.1}$$

where m is the mass of the limb segment, I_o is the moment of inertia of the limb segment about the axis of rotation, and r is the distance from the axis of rotation to the center of mass of the limb segment. Given each subject's height and weight, values for m, I_o, and r were estimated from standard anthropometric tables (Winter, 2005). The average natural frequency was 1.07 ± 0.03 Hz.

Subjects performed the sawing task with the weight mounted on the carriage (Fig. 2.1) set to 15% of this maximum pushing/pulling force. The actual forces experienced by each subject were a function of this external load, their hand acceleration (through $F = m \cdot a$), and to some extent friction. Because movement distance and frequency were also both scaled to each subject, so were these external forces. Therefore, the forces applied to the handle by each subject were monitored throughout the trial by a 6 axis load cell (JR3 Inc., Woodland, CA) mounted at the base of the handle.

Our goal was to quantify the effects of muscle *fatigue* on movement timing and coordination. However, our findings could have been potentially seriously confounded if subjects simultaneously exhibited changes due to *learning* of the task. Humans can adjust grip force to accommodate simple inertial loads imposed by typical rigid objects within as little as 135 ms during a single movement (Bock, 1993). When subjects lift objects of unusually high densities, they adapt their responses within fewer than five movements (Gordon et al., 1993). Even for more complex modifications of the arm's inertial properties, adaptation is typically completed within 40 to 50 movements (Sainburg et al., 1999). Thus, we expected subjects would "learn" to manipulate the simple inertial load used in the present experiment vary quickly. Pilot testing confirmed that subjects did indeed learn this task (i.e., their mean errors approached zero) within just a few (< 10) movements. Thus, to ensure that our results were not influenced by learning effects, subjects were asked to perform a warm up trial, moving in time with the metronome, for a minimum of 30 seconds (~30 cycles) or until they felt completely comfortable with the task. Subjects then rested for one minute to minimize any fatigue effects that may have occurred during this practice period.

Subjects then performed the fatigue task by sawing until they reached voluntary exhaustion. Once the fatigue trials began, data collection did not begin until subjects

visually reached steady-state (an additional ~20 cycles). Subjects were given strong verbal encouragement to continue and were told to "focus on the metronome and keep time with the beat" when they exhibited any difficulty maintaining timing. They were similarly instructed to maintain full range of motion if they began making smaller movements than specified.

A single reflective marker was placed on the top of the handle (Fig. 2.1) to define the beginning and end of each cycle. The 3D position of this marker was recorded continuously during each fatigue trial at 60 Hz using an 8-camera Vicon-612 motion analysis system (Oxford Metrics, Oxford, UK). Nine preamplified EMG surface electrodes (Delsys Inc., Boston, MA) were attached to the dominant arm and torso to record activity in the middle trapezius, pectoralis major, deltoids (anterior, lateral and posterior), triceps (lateral head), biceps, flexor carpi radialis, and extensor carpi radialis longus. Electrodes were positioned over each muscle according to accepted recommendations (Konrad, 2005). EMG and metronome data were recorded continuously at 1080 Hz during all trials. Additionally, ratings of perceived exertion (RPE) were recorded once every 3 minutes during each trial using the modified Borg scale (Borg, 1974; Borg, 1982), on which subjects subjectively rated their level of fatigue on a scale from 0 ("none at all") to 10 ("maximal exertion").

Data Analyses

Raw EMG data were band-pass filtered from 20 to 400 Hz. Time points defining the beginning, middle, and end of each cycle, as determined from the marker data were used to split each EMG signal into the push stroke and pull stroke. Median power frequencies (MdPF) of the EMG signals were used to indicate muscle fatigue (DeLuca, 1984). The MdPF for each stroke (either push or pull) was computed from the power

spectrum of the signal using Welch's method (MATLAB, Mathworks, Natick, MA). The MdPF for each complete movement cycle (push plus pull) was calculated as the average of the MdPFs for the push and pull strokes (MacIsaac et al., 2001). For each muscle, the average MdPF for the first 224 cycles and the last 224 cycles (approximately 3.5 minutes) were compared using paired t-tests. This range was chosen because the other analyses used (see below) required relatively long time series. The need for longer time series was balanced against the need to capture only the earliest stages of fatigue. Data from two subjects for the middle deltoid and one subject for the wrist flexor were omitted due to technical problems during data collection.

The kinematic data from the handle marker (Fig. 2.1) were filtered using a 5th order low-pass Butterworth filter with a cutoff frequency of 6 Hz. These marker data were then resampled to 1080 Hz using a piecewise cubic interpolant in Matlab (Mathworks, Natick, MA) to match the sampling frequency of the metronome. The beginning and end of each movement *stroke* (i.e., either push or pull) were defined as the minimum and maximum excursions of the marker in the anterior-posterior direction. These minima/maxima were found by first differentiating the marker trajectory data and then locating the zero crossings of the velocity. For each movement *cycle* (i.e., push followed by pull), i, movement distance, $d(i)$, was defined as the maximum minus the minimum anterior-posterior marker excursions for the push phase. Movement speeds, $s(i)$, were defined as the movement distance, $d(i)$, divided by the elapsed time for each movement cycle. Timing errors, $e(j)$ were calculated separately for each *stroke*, j, by subtracting the time the handle marker reached a maximum or minimum from the time of the nearest metronome signal (Fig. 2.2; (Chen et al., 1997; Ding et al., 2002). Thus, negative timing errors indicated that the subject lagged behind the metronome, while positive value indicated that they were ahead of it.

26
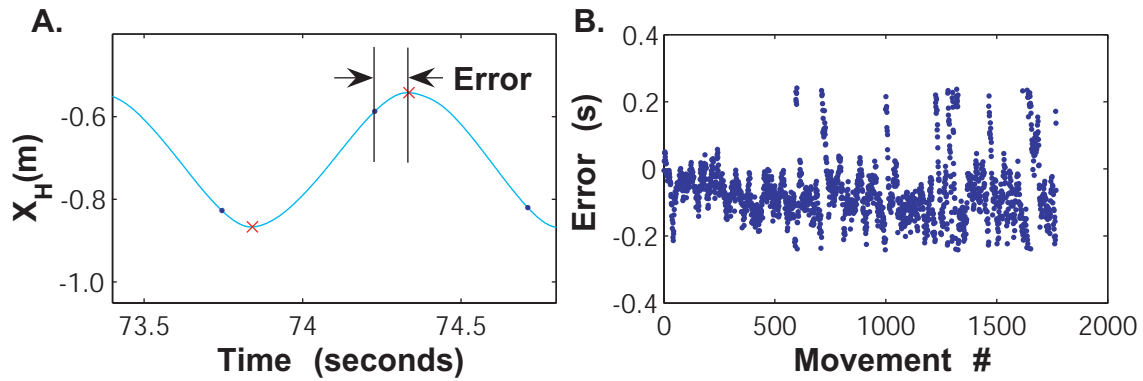
Figure 2.2: Example of calculating timing errors.

A) An example segment of the handle marker trajectory (X_H) is shown with points of minimum and maximum extension highlighted ('×'). Errors were defined as the elapsed time between these points and the metronome signal ('•'). **B)** Example time series of timing errors for the same representative subject: S12. This subject consistently lagged behind the metronome. Points where the errors switch sign indicate where the subject was so far behind that they became more aligned with the subsequent metronome signal.

To appropriately non-dimensionalize these variables (Hof, 1996), movement speed was rescaled by a factor $1/(H \cdot f_m)$, where H was the subject's height and f_m was the frequency of the metronome. Movement distance was rescaled by $1/H$. The non-dimensional distance, $D(i)$, was equal to the non-dimensional speed, $S(i)$, at every location where the goal, f_m, was reached. Because the same characteristic length (H) was used to non-dimensionalize both movement distance and speed, this choice did not affect the GEM analyses. Time series of non-dimensionalized $E(j)$, $D(i)$, and $S(i)$ values were analyzed to quantify task performance and the overall movement patterns subjects used to achieve that performance.

In addition to these measures, we also used a performance analysis based on the idea of body-goal variability mapping (Cusumano and Cesari, 2006). The primary *goal* of this task was to maintain movement *time*, T, with the metronome on each movement. However, there are an infinite number of combinations of movement distance, D, and speed, S, that will achieve this goal, so long as $D/S = T$. These [D, S] combinations

27

define the *goal equivalent manifold* (GEM) for this task (Fig. 2.3). It should be noted that this GEM is defined explicitly by the goal of the task itself. It exists independent of our choice of analyses and independent of whether and how (or even if) subjects choose to control their movements in relation to the GEM. Given the existence of this GEM, we can then decompose the variability in the body movement parameters, $D(i)$ and $S(i)$, into components that directly affect task performance (i.e., achieving the task goal) and those that have no effect on achieving the task goal (Fig. 2.3; Cusumano and Cesari 2006). Variability in $D(i)$ and $S(i)$ were thus decomposed into variability tangent to and perpendicular to the GEM:

$$\vec{\delta}(i) = \delta_T(i)\hat{e}_T + \delta_P(i)\hat{e}_P \qquad (2.2)$$

where $\vec{\delta}(i)$ was the vector-valued error in movement time for movement i, $\delta_T(i)$ was the corresponding magnitude of the deviation tangent to the GEM, $\delta_P(i)$ was the corresponding magnitude of the deviation perpendicular to the GEM, and $\hat{e}_T$ and $\hat{e}_P$ were unit vectors defining directions tangent to and perpendicular to the GEM (Fig. 2.3). Any scalar deviations $\delta_T(i) = \vec{\delta}(i) \cdot \hat{e}_T$ do *not* contribute to errors in movement time, while the deviations $\delta_P(i) = \vec{\delta}(i) \cdot \hat{e}_P$ *do*. Thus, changes in the magnitude, variability, and/or cycle-to-cycle dynamics of these $\delta_P(i)$ deviations would indicate changes in motor performance that were specifically "goal relevant."

Because the GEM is defined strictly by the task itself, this does not mean that subjects will take advantage of the GEM in regulating their movements. Computing the relative magnitudes of the variability of deviations in the δ_P and δ_T directions provides some insight as to how people regulate their movements. However, the ratio of these variances alone does not directly test the issue of *alignment* itself. To directly quantify how well each subject aligned their movements with the GEM, we also performed a principle components analysis (Wing et al., 2004) on the data obtained from each subject

28

during each trial. We computed the eigenvector associated with the largest eigenvalue of the covariance matrix. This vector is known as the first principle component (PC1) because it defines the direction in which the greatest variance occurs. We then computed the angle (θ) between this PC1 vector and the GEM using the dot product. Values of θ very close to zero would indicate that subjects were indeed aligning their movements with the GEM.
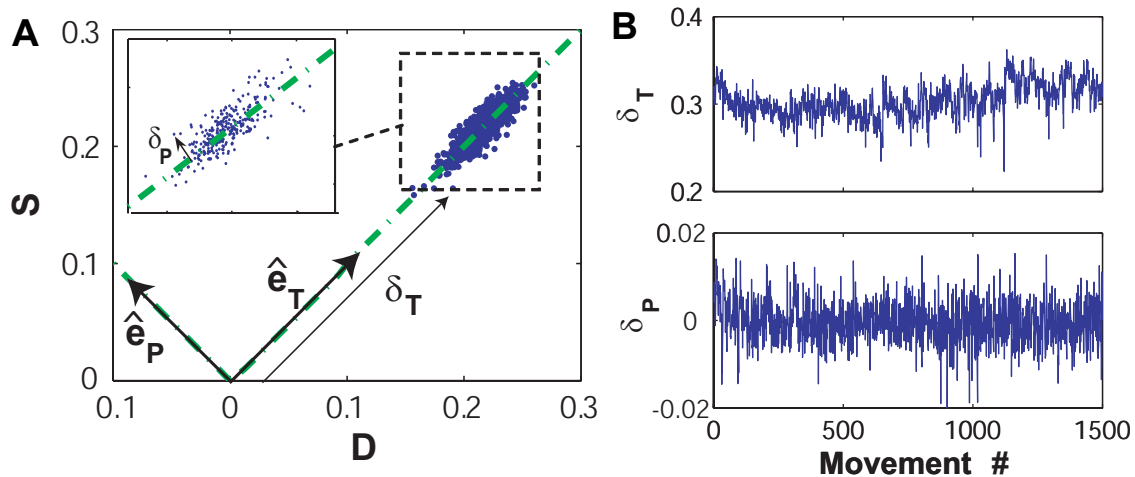
Figure 2.3: Example of the goal equivalent manifold (GEM) analysis.
A) The non-dimensional movement speed (*S*) is plotted versus non-dimensional movement distance (D). All combinations where *S* is equal to *D* achieve the 'goal' of matching the metronome frequency, and thus define the GEM (diagonal line). Deviations perpendicular to and tangent to the GEM are denoted δ_P and δ_T, respectively. **B)** Example time series of δ_P and δ_T fluctuations for a representative subject: S03. Fluctuations along the manifold were larger than those perpendicular to the manifold.

Detrended Fluctuation Analysis (DFA) was used to determine the degree to which each time series exhibited persistent or anti-persistent temporal correlations across successive movements. This method has been used extensively in the analysis of experimental time series because it reduces noise effects and removes local trends making it less likely to be affected by nonstationarities (Hausdorff et al., 1995). Complete details of the methodology are published elsewhere (Peng and Buldyrev, 1993;

29

Peng et al., 1994; Hausdorff et al., 1995; Peng et al., 1995). In brief, the data sequence of length N was first integrated and then divided into equal, non-overlapping segments of length n. In each segment, the series was detrended by subtracting a least squares linear fit to that segment. The squares of the integrated, detrended data points (i.e, residuals) were then averaged over the entire data set and the square root of the mean residual, $F(n)$, was calculated. This process was repeated for different values of segment lengths, n, ranging from 4 to $N/4$.

Typically, $F(n)$ increases with n and a graph of $\log[F(n)]$ versus $\log(n)$ will often exhibit an approximately power-law relationship indicating the presence of scaling, such that $F(n) \approx n^\alpha$ (Hausdorff et al., 1995; Peng et al., 1995). These $\log[F(n)]$ versus $\log(n)$ plots were fitted with a linear function using least squares regression. The slope of this line defined the scaling exponent α (Fig. 2.4). A value of $\alpha = 0.5$ indicates the time series is completely uncorrelated (i.e., random white noise). When, $\alpha < 0.5$, the time series contains anti-persistent temporal correlations. This indicates a highly controlled process where deviations in one direction are more likely to be followed by deviations (i.e., corrections) in the opposite direction. Persistent temporal correlations are present when $0.5 < \alpha \leq 1.0$ (Hausdorff et al., 1995). In this case, deviations in one direction are likely to be followed by deviations in the same direction (i.e., the deviations are *not* immediately corrected).

DFA was performed on the series of timing errors, $E(j)$, movement distances, $D(i)$ and movement speeds, $S(i)$, as well as the deviations perpendicular to, $\delta_P(i)$, and along, $\delta_T(i)$, the GEM. The first and last $i \in [1,...,224]$ movement cycles (i.e., $j \in [1,...,488]$ timing errors) from each experiment were analyzed (approximately 3.5 minutes) to obtain 'early' and 'late' fatigue measures. Early / Late comparisons for means, standard deviations, and α of each of these time series were made using paired t-tests (Minitab 14,

Minitab Inc, State College, PA). Comparisons between directions (tangent vs. perpendicular to the GEM) were also made using paired t-tests.
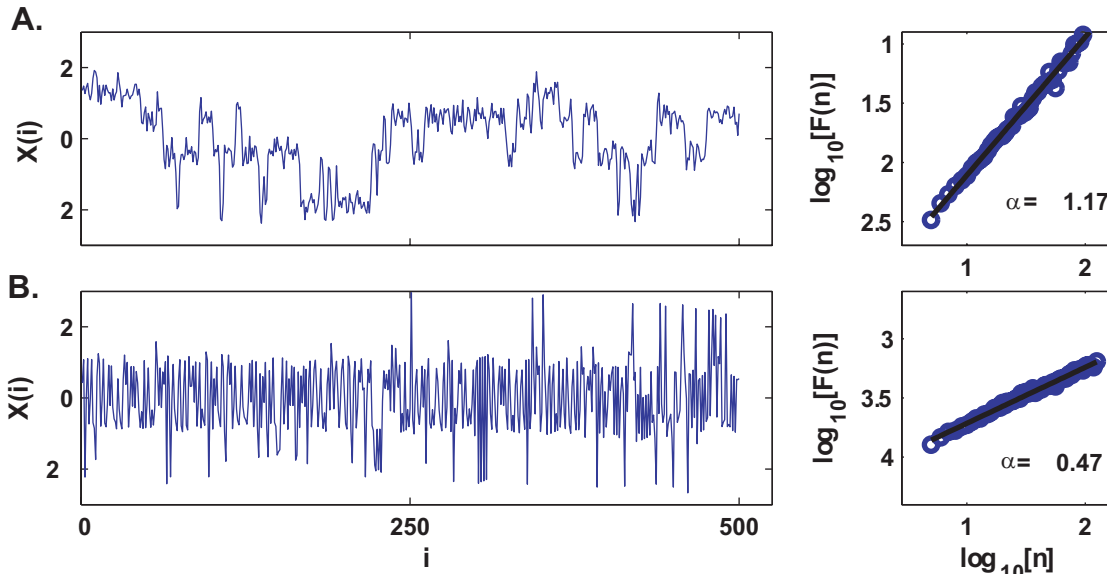
Figure 2.4: Example time series with equal variance and different correlation structures **A)** Two stochastic time series in arbitrary units are shown. Both have been normalized to unit variance. The top graph clearly shows temporal persistence, whereas the bottom graph fluctuates much more rapidly. **B)** DFA analyses of the two corresponding time series shown in A. The different temporal correlation patterns are clearly reflected in the different scaling exponent values obtained. Thus, the α exponent obtained from DFA quantifies temporal correlations (persistence vs. anti-persistence) in a time series, independent of the magnitude of the variance.

2.4 RESULTS

Subjects performed the task for 23.93 ± 10.44 minutes (range: 8.64 to 41.20 minutes). At the end of the first three minutes, subjects' rates of perceived exertion (RPE) ranged from 2 to 6 (mean = 3.8), while at the beginning of the last segment all subjects had an RPE of 9 or higher. All subjects exhibited localized muscle fatigue as measured by decreased MdPF of the EMG signals (Fig. 2.5). These decreases were statistically significant for six of the nine muscles tested ($p < 0.039$) and nearly significant ($p = 0.052$ and $p = 0.088$) for two others.
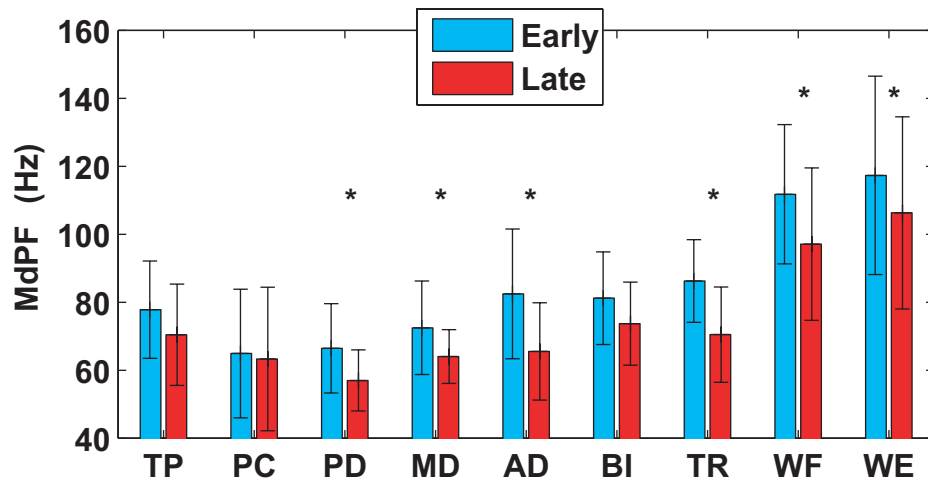
Figure 2.5: Median power frequencies of the EMG signals for the 9 muscles tested. All muscles showed a decrease in MdPF from early to late fatigue. These decreases were statistically significant for the posterior deltoid (PD, p = 0.006), middle deltoid (MD, p = 0.039), anterior deltoid (AD, p = 0.002), triceps (TR, p < 0.001), wrist flexors (WF, p = 0.006), and wrist extensors (WE, p<0.001). Decreases in MdPF were nearly statistically significant for the trapezius (TP, p =0.052) and biceps (BI, p = 0.088), but were not significant for the pectoralis (PC, p = 0.760). Error bars indicate ±1 between-subject standard deviations about the mean.

To verify that subjects had sufficiently "learned" the sawing task prior to data collection, the data from the first 240 cycles were divided into 24 non-overlapping bins of 10 movements each. Mean timing errors (E) and perpendicular distances from the GEM (δ_P) were computed within each bin to quantify performance accuracy. These data were compared statistically using a single-factor ANOVA to test for differences across the 24 bins. Neither timing errors nor δ_P deviations changed over this period (p = 0.336 and p = 0.770, respectively; Fig. 2.6). Indeed, the δ_P deviations tended to actually *increase* slightly, indicating that subjects were slightly *less* able to maintain proper timing. Thus, there was no evidence that any subject exhibited any further learning during the early fatigue phases of these experiments.
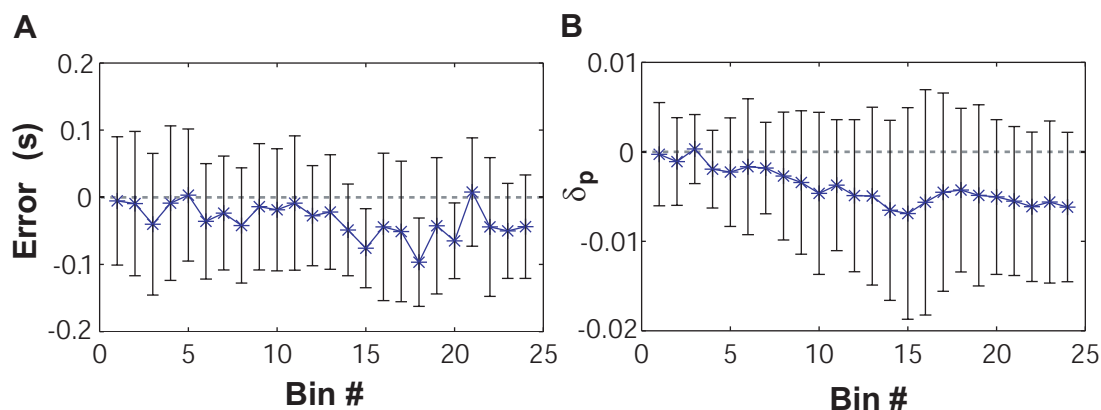
Figure 2.6: Mean timing errors and deviations across the first 240 movements.

A) Mean timing errors and B) Perpendicular deviations (δ_P) from the GEM across the first 240 cycles of each fatigue trial. For each subject, average values for each measure were computed within 24 non-overlapping bins of 10 movements each. Symbols (*) represent the mean values across all subjects. Error bars represent between-subject standard deviations. Both measures were very close to zero from the very beginning of the fatigue trials. Timing errors did not change over the first 240 cycles. Mean δ_P deviations grew slightly larger over time. These data demonstrate that subjects had fully learned the task prior to data collection.

Mean values of the non-dimensional movement distance (D), speed (S), and timing errors (E) were not affected by muscle fatigue (p = 0.958, 0.245, and 0.404, respectively; Fig. 2.7A). Timing errors were typically slightly negative, indicating that subjects were responding to the metronome signal rather than anticipating it. The magnitudes of the variability (Fig. 2.7B) for the task parameters D and S were unaffected by muscle fatigue (p = 0.695 and p = 0.538, respectively). The variability of timing errors exhibited a slight decrease with muscle fatigue that did not reach statistical significance (p = 0.192). However, α did decrease significantly with muscle fatigue (Fig. 2.7C) for both movement speed (p = 0.046) and timing errors (p = 0.037), but not for movement distance (p = 0.472). On average, all of these variables exhibited persistent temporal correlations ($0.5 < \alpha < 1.0$), suggesting that they were not tightly controlled.
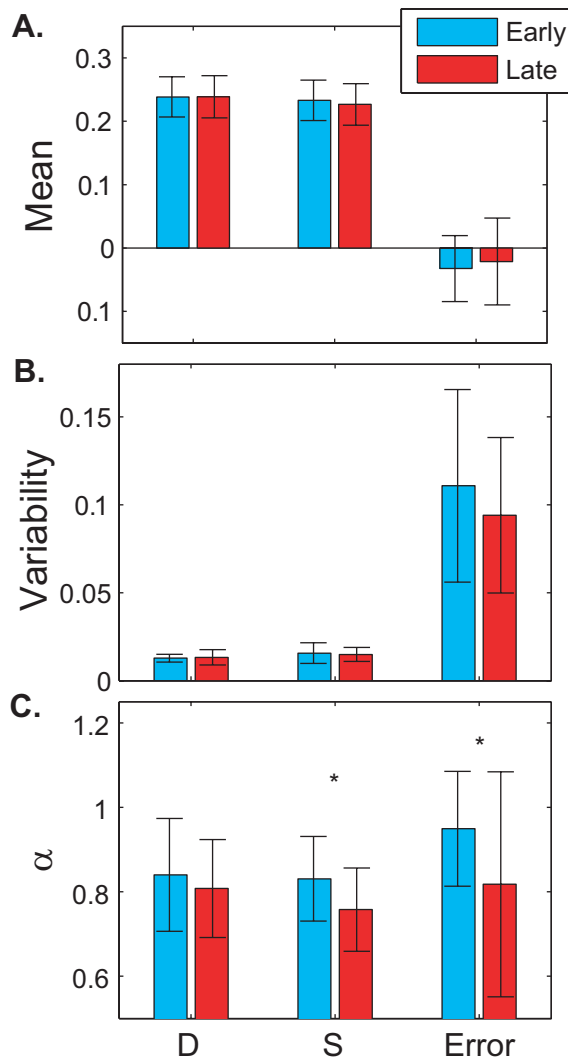
A) The mean values of the movement distance (*D*), speed (*S*), and timing errors (*E*) were not affected by muscle fatigue (p = 0.958, 0.245, and 0.407, respectively). **B)** Magnitudes of the variability (standard deviation) for these metrics were also not significantly affected by muscle fatigue (p = 0.695, 0.538, 0.192, respectively). **C)** There was a significant decrease in α with muscle fatigue for movement speed (*S*; p = 0.037) and timing errors (*E*; 0.046), but not distance (*D*; p = 0.472). On average, all variables exhibited persistent cycle-to-cycle correlations (0.5 < α < 1.0). Error bars indicate ±1 between-subject standard deviations about the mean.

Figure 2.7: Mean, standard deviation, and α of the basic timing parameters

Subjects' overall force profiles appeared quite similar during Early and Late fatigue (Fig. 2.8A). The mean magnitudes of the *peak* forces subjects applied to the handle increased significantly with muscle fatigue from 28.5 ± 6.0 % to 30.7 ± 7.5% of each subjects maximum pushing/pulling force (p = 0.032). This difference, while small, was consistent across subjects (Fig 2.8B).
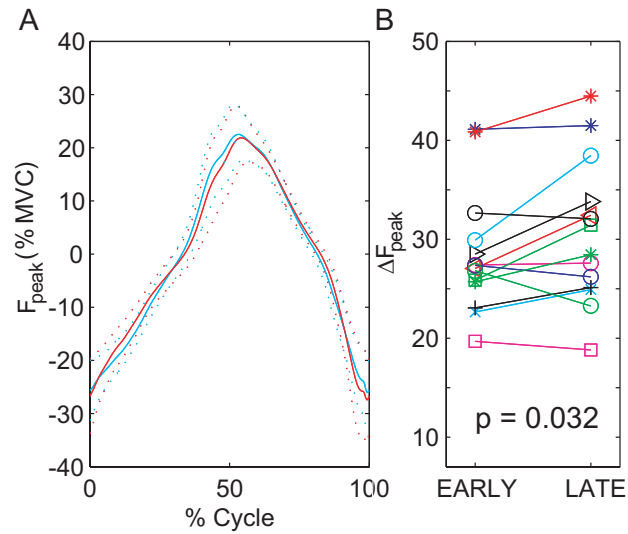
Figure 2.8: Average handle forces early and late fatigue.
A) Average handle force profiles for early and late fatigue movements, normalized to percent MVC and percent cycle time. Dotted lines represent ± between-subject standard deviation bands for each block of movements (Early and Late). **B)** Average peak handle forces (F_{peak}) for each subject for both Early and Late fatigue. Each symbol and line type represents the average value for one subject. While these changes were relatively small, they were consistent enough across subjects to be statistically significant (p = 0.032).

The initial GEM decomposition revealed a strong tendency for subjects to align themselves with the GEM. Deviations perpendicular to the GEM were much smaller than those tangent to the GEM (Figs. 2.9 & 2.10). There were differences between subjects in their responses to fatigue, however (Fig 2.9). Some subjects increased both movement amplitude and speed post-fatigue (Fig. 2.9A), while others showed a decrease (Fig. 2.9D). A few subjects became less variable after fatigue (Fig. 2.9B), while others were consistently unable to keep time with the metronome post-fatigue (Fig. 2.9C).
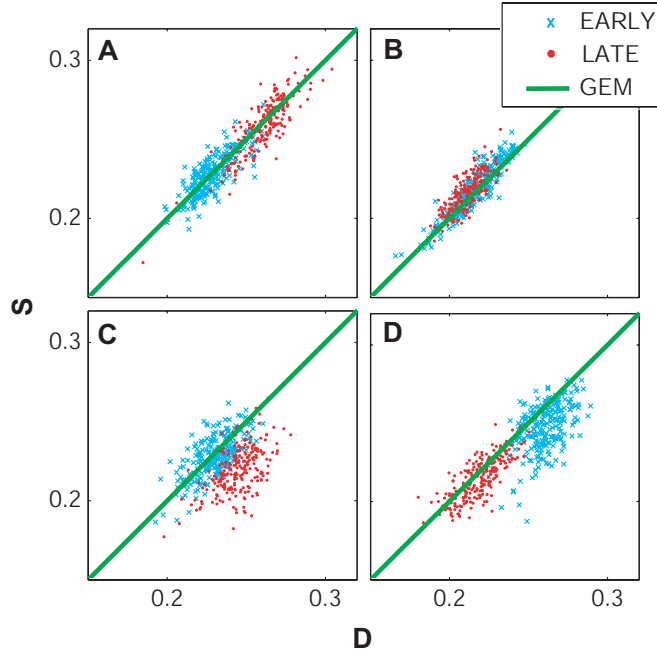
Figure 2.9: GEM decomposition for 4 representative subjects.

Points represent the combination of non-dimensional distance (*D*) and speed (*S*) for each movement. Symbols '×' and '•' represent the first and last 300 movements, respectively. The solid diagonal line is the goal equivalent manifold (GEM). Subjects tended to align with the GEM, such that there were greater deviations along the GEM than perpendicular to it. Two subjects showed an increase in movement amplitude and speed post-fatigue (e.g., **A**), while four others showed a decrease (e.g., **D**). Five subjects showed a decrease in variability post-fatigue (e.g., **B**). Three subjects showed an inability to keep time with the metronome post-fatigue (e.g., **C**).

The mean magnitudes of the deviations perpendicular to (δ_P) and tangent to (δ_T) the GEM were significantly different ($p < 0.001$; Fig. 2.10A). Fatigue did not affect the mean deviations tangent to the GEM ($p = 0.573$). Deviations perpendicular to the GEM tended to increase slightly post-fatigue ($p = 0.087$). The magnitude of the variability (Fig. 2.10B) was unaffected by muscle fatigue (δ_P: $p = 0.593$, δ_T: $p = 0.837$). The magnitude of variability perpendicular to the GEM was significantly less than that tangent to the GEM ($p < 0.001$). Deviations perpendicular to the GEM were also significantly less persistent (Fig. 2.10C) than deviations along the GEM ($\alpha_P < \alpha_T$; $p <$

0.001). This indicated that the δ_P deviations were corrected more quickly than δ_T deviations. There was also a slight tendency for α to decrease in late fatigue for δ_T deviations (p = 0.122), whereas temporal correlations in δ_P deviations were unaffected by fatigue (p = 0.497).
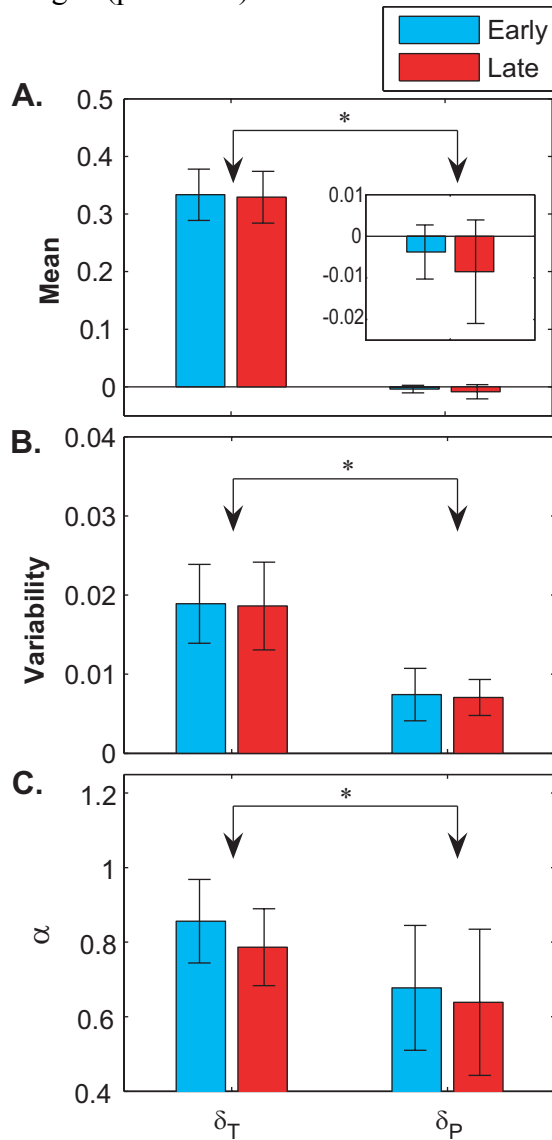
A) The mean magnitudes of the deviations perpendicular to (δ_P) to the GEM were significantly smaller than the deviations tangent to (δ_T) the GEM (p < 0.001). Perpendicular deviations tended to get slightly larger (i.e., more negative) with muscle fatigue (δ_P: p = 0.087). Deviations along the GEM were not affected by muscle fatigue (δ_T: p = 0.573). *B*) The variability of deviations perpendicular to the GEM was significantly smaller than that of deviations tangent to the GEM (p < 0.001). Variability was not affected by muscle fatigue (δ_P: p = 0.593, δ_T: p = 0.837). *C*) Deviations perpendicular to the GEM exhibited significantly less cycle-to-cycle temporal persistence (i.e., smaller α) than deviations tangent to the GEM (p < 0.001). There was a slight tendency for α to decrease with fatigue for deviations tangent to the GEM (δ_T: p = 0.122). Fatigue did not affect the persistence of deviations perpendicular to the GEM (δ_P: p = 0.497). Error bars indicate ±1 between-subject standard deviations about the mean.

Figure 2.10: The mean, standard deviation and α of deviations δ_P and δ_T

The principle components analyses (Fig. 2.11) revealed a slightly different view of how well subjects aligned their movements with the GEM. In most cases, the differences in alignment (θ) between the GEM and the first principle component (PC1) of the subjects' data were less than $\pm10°$ (Early: $5.9 \pm 7.8°$, Late: $6.1 \pm 6.8°$). Across subjects, however, θ was significantly positive (p < 0.001), as determined from a single sample t-test with the null hypothesis that $\mu = 0$. There were no significant changes in alignment of the data with the GEM between early and late fatigue (p = 0.93). Thus, even though subjects did exhibit positive ratios of δ_T to δ_P variability (Figs. 2.9 and 2.10B), their movements were not aligned *exactly* along the GEM itself (Fig. 2.11B).
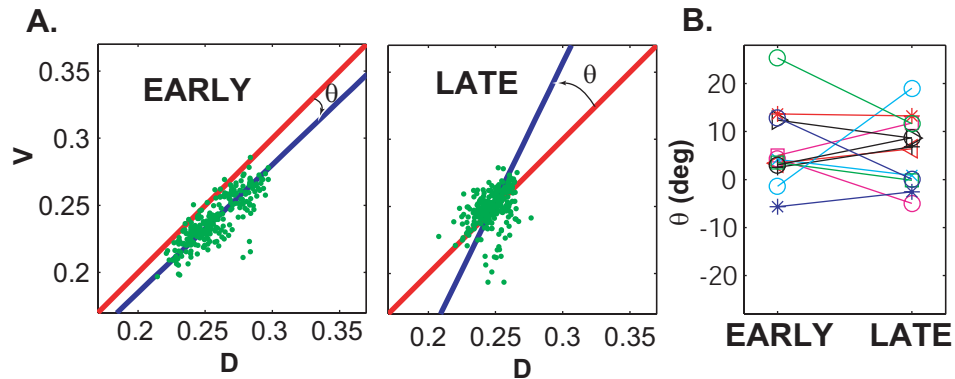
Figure 2.11: Determining degree of alignment with the goal equivalent manifold.
A) Plots of movement distance (*D*) vs. speed (*S*) for one example subject showing the orientation of the GEM as defined by the sawing task and the orientation of the first principle component (PC1) as determined from the subject's data. The angle θ defines the orientation of PC1 relative to the GEM. For this subject, $\theta = -1.4°$ during early fatigue and $\theta = +19.0°$ during late fatigue. **B)** Values of the angle θ for all subjects during both early and late fatigue. On average, these angles were slightly positive (p < 0.001) for most subjects, indicating that subjects did not align their movements exactly with the GEM. Across subjects, these angles did not change significantly from early to late fatigue (p = 0.93).

2.5 DISCUSSION

Muscle fatigue can alter movement timing (Lorist et al., 2002; van Duinen et al., 2007). However, little is known about how muscle fatigue affects performance and

control in repetitive tasks. This study was conducted to determine how muscle fatigue affected task performance during a repetitive sawing-like task. We analyzed the magnitudes, variations and temporal correlations of movement-to-movement timing errors, $E(j)$, and cycle-to-cycle distances, $D(i)$, and speeds, $S(i)$. We also analyzed performance by decomposing variations in the task variables (D and S) into those that directly affected achieving the task *goal* (δ_P) and those that did not (δ_T), by identifying the goal equivalent manifold (GEM) of all valid solutions to this task. Using these analyses, we could determine if muscle fatigue affected overall task performance at the 'goal' level, the biomechanical movement patterns subjects used to achieve this performance at the 'body' level, or both.

The increased rates of perceived exertion (RPE) and decreased EMG median frequencies (Fig. 2.5) demonstrate that the sawing task did induce significant muscle fatigue in these subjects. The primary task goal was to perform the reaching task in time with the metronome. The lack of significant changes in average movement distance, speed, and timing errors (Fig. 2.7A) demonstrate that overall task performance did not change with fatigue. Similar results were reported for other upper extremity repetitive tasks (Lucidi and Lehman, 1992; Côté et al., 2002; Heuer et al., 2002; Selen et al., 2007). The trend for mean deviations perpendicular to the GEM (δ_P) to increase slightly (but not quite significantly) with fatigue (Fig. 2.10A) suggests that there was *some* (albeit slight) deterioration in task performance. However, the lack of any significant changes (p > 0.49) in either the variability (Fig. 2.10B) or the temporal correlation structure (Fig. 2.10C) of δ_P deviations or in the alignment of subjects' movements with the GEM (Fig. 2.11) shows that subjects also maintained the same *goal relevant* performance with respect to the GEM.

Conversely, the cycle-to-cycle temporal persistence (α) of movement speed (S) and timing errors (E) both significantly decreased with fatigue (Fig. 2.7C). This indicates that subjects corrected timing errors more quickly when their muscles were fatigued. These decreases in α are supported by similar decreases found with fatigue during standing (Corbeil et al., 2003). Subjects also exhibited small but consistent increases in the peak forces they applied to the handle (p = 0.032; Fig. 2.8B). Likewise, 6 of the 14 subjects shifted their operating point along the GEM by making either longer faster movements (Fig. 2.9A) or shorter slower movements (Fig. 2.9D) with fatigue. The remaining subjects exhibited other qualitative changes in their movement patterns relative to the GEM (Fig. 2.9B & 2.9C). Together, these findings indicate that subjects significantly altered their biomechanical movement patterns in response to fatigue. However, these changes were made in such a way that those features of motor performance that were specifically "goal relevant" (Figs. 2.10 & 2.11) did not change.

The goal equivalent manifold (GEM) approach adopted here is similar in some respects to the uncontrolled manifold (UCM) approach described in recent literature (Scholz and Schöner, 1999; Latash et al., 2002; Schöner and Scholz, 2007). Both approaches identify a sub-set of body-level variables, assumed to have the structure of a manifold, that define a full set of motor solutions that equally achieve a given task goal (Cusumano and Cesari, 2006). The UCM approach then attempts to tie the resulting geometrical structure of this manifold directly to control by assuming control will be exerted only orthogonal to this manifold and not along it. Based on this assumption, putative control variables are identified by quantifying the ratio of the variance components parallel and perpendicular to the manifold (Latash et al., 2002). Conversely, the GEM approach makes no *a priori* assumptions about which variables are being "controlled." This is because the GEM exists even for purely passive systems where no

control is applied at all. Also, there is no particular reason to necessarily associate "control" with only *one* of the variance components (Cusumano and Cesari, 2006). *If* (but only if) the body variables being analyzed do turn out to be the variables that *are* controlled, then the GEM would also be a UCM. However, this is not necessary and the ratio of the parallel and perpendicular variance components alone does not guarantee this. The GEM approach is thus both more general and more precise than the UCM approach.

Additionally, there were several technical differences between the analyses presented here and those associated with the UCM approach. First, the UCM approach assumes that stability can be equated with variability (Latash et al., 2002; Schöner and Scholz, 2007). However, standard deviations only quantify the average magnitudes of the variations that occur across many cycles and do not directly quantify how a system responds to perturbations from one cycle to the next (Dingwell and Cusumano, 2000; Dingwell and Kang, 2007). The DFA analyses presented here (Figs. 2.4, 2.7C, and 2.10C) provide an additional measure of cycle-to-cycle *dynamics* that is *independent* of variability (Peng et al., 1994; Hausdorff et al., 1995). Furthermore, variance ratios alone (Latash et al., 2002) do not directly quantify how closely each subject's movements are aligned with the GEM. To assess this, we also conducted principle components analyses (PCA; Fig. 2.11) on our data. While previous authors have commented on the relationship between UCM and PCA (Schöner and Scholz, 2007), the present analyses are the first we know of to simultaneously apply both approaches to directly assess alignment with the GEM. Even though subjects exhibited greater variability along the GEM than perpendicular to it (Fig. 2.10B), their performance was not aligned *exactly* with the GEM (Fig. 2.11). This suggests, contrary to the UCM interpretation, that there was indeed at least some coupling between performance (and likely also control), both perpendicular to *and* along the GEM.

The results presented here provide some new insights into the general nature of movement timing control and how this control is affected by muscle fatigue. For example, it is clear that subjects altered their biomechanical movement patterns in response to fatigue only in such a way that they specifically preserved the goal *relevant* features of their motor performance. However, these findings do not reveal which specific variables were being "controlled" or whether the changes that were observed were caused by physical changes in the plant (i.e., the musculoskeletal system being controlled), by changes in the underlying control policy (i.e., the specific instructions that define how to produce the desired output) each subject adopted, or possibly both. This issue is particularly complicated in the context of fatigue since the physical properties of the end effectors (i.e., the muscles) change due to fatigue. Therefore, it is possible that even the same governing control policy could induce different behaviors of these effectors. Therefore, contrary to the typical UCM interpretation (Schöner and Scholz, 2007), we make no claims that subjects actively controlled their movements perpendicular to the GEM but not along it (Cusumano and Cesari, 2006), nor that this control was preserved in the face of fatigue. What we can say is that the lack of fatigue-related changes in the goal relevant (i.e., δ_P) performance measures (Figs. 2.10 & 2.11) suggests that any peripheral changes that might have directly affected these variables were compensated for by concurrent changes in the control policies subjects adopted.

As subjects tried to maintain time with the metronome, they oscillated between leading it and lagging behind it (e.g., Fig. 2.2B). The mean errors were negative (Fig. 2.7A), indicating that most subjects reacted to the stimulus rather than anticipating it. This result differs from previous findings on finger tapping (Aschersleben, 2002). One reason for this is likely the larger inertial load involved in this task. This was substantiated by the DFA results (Figs. 2.7C & 2.10C), which showed that all five time

42

series measures quantified in this study exhibited statistical persistence (i.e., $\alpha > 0.5$). To exhibit anti-persistence (i.e., $\alpha < 0.5$), subjects would have to be able to make *immediate* adjustments to each movement based on the error from the previous movement (e.g., Fig. 2.4; Bottom row). The significant inertial load involved in this task likely did not allow for such rapid corrections to be possible. Nevertheless, the finding that the δ_P deviations perpendicular to the GEM were significantly less persistent than the δ_T deviations along the GEM (i.e., $\alpha_P < \alpha_T$; Fig. 2.10C) strongly suggests that subjects adopted a general control strategy that corrected deviations in δ_P more rapidly than deviations in δ_T.

As mentioned, all five time series measures quantified in this study exhibited statistical persistence (i.e., $\alpha > 0.5$). It has previously been proposed that findings of $\alpha > 0.5$ from the DFA algorithm used here indicate the presence of "long-range correlations" such that the underlying time series can be characterized as having an infinite decorrelation time (Peng and Buldyrev, 1993; Peng et al., 1994; Hausdorff et al., 1995; Peng et al., 1995). However, this algorithm was recently shown to yield "false positives" for many processes with *finite* correlation times (so-called "short-range correlations"). For example, many linear auto-regressive models can also result in findings of $\alpha > 0.5$ (Maraun et al., 2004; Gates et al., 2007). Thus, here we make no claims that these α values represent true "long-range correlations" (Maraun et al., 2004). For our purposes, however, α still remains a valid measure of how rapidly the time series is fluctuating and thus provides a valid indication of how rapidly subjects were correcting deviations from each movement to the next.

We expected that the variability of the performance measures might increase with muscle fatigue (Selen et al., 2007). Instead, the variability of the timing errors actually decreased while the distance, speed, and deviations perpendicular and tangent to the GEM remained relatively constant (Figs. 2.7 & 2.9). Although kinematic variability and

43

force variability have been shown to increase in static tasks such as target tracking (Selen et al., 2007), these changes have not been documented in goal-directed movement tasks that require varying forces to achieve the goal.

Despite making the task as dynamically equivalent as possible, differences between subjects remained, particularly for time to exhaustion. One reason for this is that since this task was inherently redundant, there were numerous alternative modalities subjects could use to compensate for those that were altered by fatigue. Thus, it is easily possible different subjects compensated for fatigue in different ways. For example, each subject showed a unique pattern as to which muscles were most affected by fatigue during the task. By using different muscles, they were still able to perform the task accurately with no increase in movement variability. So while overall muscle force variability may increase (Selen et al., 2007), this effect could be counteracted by changing coordination strategies to use less fatigued muscles. The between-subject variability observed in this study was similar to that observed in previous studies of fatigue in complex multi-joint tasks (Nussbaum, 2001; von Tscharner, 2002; Madigan and Pidcoe, 2003; Voge and Dingwell, 2003).

Another possible explanation is that the subjects fatigued to different degrees. Subjects could stop the experiment as soon as they felt they could no longer continue the task. This 'threshold' could be different for the different subjects, depending on their motivation level and previous experience pushing themselves past the early stages of fatigue. To test this possibility, we correlated the difference between 'early' and 'late' fatigue for each dependent measure to each subject's time to exhaustion. Early-late differences in variability of movement distances (D) were positively correlated with time to exhaustion ($r^2 = 37.8\%$; $p = 0.019$). Subjects who performed longer showed greater decreases in movement distance variability, while subjects who stopped sooner showed

greater increases. Early-late differences in α of timing errors (E) were negatively correlated with time to exhaustion ($r^2 = 29.8\%$; $p = 0.044$). Subjects who performed longer showed smaller decreases to slight increases in α of timing errors. None of the other 13 comparisons were statistically significant ($0.4\% < r^2 < 23.2\%$; $0.82 > p > 0.08$). Thus, while time to exhaustion had some impact on some of our results, the overall effects were not particularly strong.

It is possible that subjects experienced mental fatigue as well as muscle fatigue, since trials lasted up to 41 minutes and were fairly tedious. Cognitive factors can affect these processes during finger tapping where increasing the mental challenge of the task can lead to more persistent (i.e., larger α) temporal correlations (Ding et al., 2002). Previous work using fMRI has shown that after motor fatigue, activity in the prefrontal areas of the brain increases during reaction time task performance (van Duinen et al., 2007). This results in increased reaction times during auditory choice reaction time tasks (Lorist et al., 2002). Therefore, if the task became more mentally challenging, it is possible that this could offset the effect of muscle fatigue in some subjects. This may explain why the affect in α is smaller in subjects who performed the task for a longer duration.

In summary, subjects significantly altered their biomechanical movement patterns in response to muscle fatigue. Muscle fatigue caused the deviations in movement speed and timing errors to become more anti-persistent. This suggests that subjects made more frequent corrections when their muscles were fatigued. Subjects also increased the peak forces they applied to the handle and exhibited qualitative changes in their behavior relative to the GEM when they were fatigued. However, the lack of significant changes in either the variability or temporal dynamics of the δ_P deviations perpendicular to the GEM

45

demonstrate that these changes were made only in such a way that they specifically preserved the goal *relevant* features of task performance.

Chapter 3: A Comparison of Different State Space Definitions for Local Dynamic Stability Analyses [2]

3.1 ABSTRACT

Measures of local dynamic stability, such as the local divergence exponent $\left(\lambda_s^*\right)$ quantify how quickly small perturbations deviate from an attractor that defines the motion. When the governing equations of motion are unknown, an attractor can be reconstructed by defining an appropriate state space. However, state space definitions are not unique and accepted methods for defining state spaces have not been established for biomechanical studies. This study first determined how different state space definitions affected λ_s^* for the Lorenz attractor, since exact theoretical values were known *a priori*. Values of λ_s^* exhibited errors < 10% for seven of the nine state spaces tested. State spaces containing redundant information performed the poorest. To examine these effects in a biomechanical context, 20 healthy subjects performed a repetitive sawing-like task for five minutes before and after fatigue. Local stability of pre- and post-fatigue shoulder movements was compared for six different state space definitions. Here, λ_s^* decreased post-fatigue for all six state spaces. Differences were statistically significant for three of these state spaces. For state spaces defined using delay embedding, increasing the embedding dimension decreased λ_s^* in both the Lorenz and experimental data. Overall, our findings suggest that direct numerical comparisons between studies that use different state space definitions should be made with caution. However, trends across experimental comparisons appear to persist. Biomechanical state spaces

---

constructed using positions and velocities, or delay reconstruction of individual states, are likely to provide consistent results.

3.2 INTRODUCTION

Nonlinear dynamics methods for determining the local stability of kinematics have gained increased interest in recent literature. For experimental data, the governing equations are typically unknown. During most repetitive movements, the dynamics of such movements can be represented geometrically within an n-dimensional 'state space' where n is the number of state variables (Dingwell and Cusumano, 2000; Kantz and Schreiber, 2004). Typically, these experimental data exhibit the structure of an attractor, i.e., a sub-space of the n-dimensional state space to which neighboring trajectories converge (Strogatz, 1994; Dingwell and Kang, 2007).

Measurable biomechanical state variables typically include linear and/or angular displacements, velocities, and/or accelerations. State spaces may also be defined using delay embedding, which allows reconstruction from a single scalar recording, once an appropriate time lag and embedding dimension are determined (Kantz and Schreiber, 2004). This can greatly simplify data collection and may be advantageous for situations where data for some measurable dimensions are prone to error. However, since divergence in one dimension may be compensated by contraction in another (Granata and Gottipati, 2008), analyzing one single trajectory may not adequately represent the movement. One proposed way to compensate for this is to perform delay embedding on the Euclidean norm of the three Euler angles at a joint (Granata and Gottipati, 2008)[3]. Another option is to analyze a state space composed of all angles and angular velocities

---

[3] The Euclidean norm of 3 Euler angles is *not* an appropriate measure of the "distance" between two angular orientations, as it would be for linear displacements. This measure should be interpreted here merely as a weighted average of the 3 joint angles.

at that joint. However, this will typically include redundant information which could negatively impact the results. One way to define state variables with minimum redundancy is to perform a principal components analysis (PCA) on the data (Wing et al., 2004). Many state spaces have been applied in biomechanical stability analyses (Table 3.1). To date, however, researchers have not explored how different definitions of these state spaces affect local stability measures.

Table 3.1: State Space Definitions used in the literature.

State Space Definition	References
All angular and linear motion and velocities of a segment	Kang and Dingwell, 2006a,b Kang and Dingwell, 2008
All angles and angular velocities at a joint	Lee and Granata, 2008 Slota et al., 2008
Delay embedding of sagittal plane angles	England and Granata, 2007 Manor et al., 2008 Segal et al., 2008 Stergiou et al., 2004
Delay embedding of linear motion of a single marker	Buzzi et al., 2003 Dingwell and Marin, 2006 Dingwell et al. , 2008 Jordan et al., 2009
Delay embedding of linear acceleration	Dingwell et al., 2000 Yoshino et al., 2004
Delay embedding of the Euclidean norm of three Euler angles at a joint	Granta and England, 2006 Granata and Gottipati, 2008

This study determined how including different state variables and/or different numbers of variables in the state space altered short-term local divergence exponents, λ_s^*, a measure of local dynamic instability (Dingwell and Cusumano, 2000). Data for which the true λ_s^* was known *a priori* were analyzed to determine how different state space definitions affect the resulting values of λ_s^*. Experimental data were then analyzed to determine how different state space definitions might affect the answers to research

questions attempting to quantify differences in stability between conditions. The state space definitions examined here were chosen primarily from previously published studies (Table 3.1).

3.3 METHODS

The Lorenz attractor (Strogatz, 1994) was used to test the effect of different state space definitions on λ_s^*. The Lorenz system is defined by three coupled nonlinear differential equations:

$$\dot{x} = \sigma(y - x)$$
$$\dot{y} = x(\rho - z) - y$$
$$\dot{z} = xy - \beta z$$

$$(3.1)$$

where σ, ρ, and β are fixed parameters that were set to $\sigma = 16$, $\rho = 45.92$ and $\beta = 4$ (Rosenstein et al., 1993). These equations were integrated in Matlab using a fourth order Runge-Kutta method (ode45) to generate ten trials of 155 seconds at 100 Hz. The first five seconds were removed to eliminate transients. The first derivative of each trajectory was estimated using a three point difference formula. Uniformly distributed random noise was added to attain a minimum signal-to-noise ratio of 100:1, which is considered 'moderate' (Rosenstein et al., 1993). Because the Lorenz attractor for these parameter values is chaotic, λ_s^* in this case defines the maximum finite-time Lyapunov exponent, which should be 1.50 (Rosenstein et al., 1993).

We defined nine different state spaces for this Lorenz attractor. The "Full" state space was defined by the three $x(t)$, $y(t)$, and $z(t)$ trajectories (Eq. 3.1). A "Redundant" state space was defined from these three trajectories and their derivatives:

$$\text{Redundant SS}(t) = \left[x(t), y(t), z(t), \dot{x}(t), \dot{y}(t), \dot{z}(t)\right]$$

$$(3.2)$$

We performed principal components analysis (Daffertshofer et al., 2004) on both the Full and Redundant state spaces. Principal components analysis is a method that

50

transforms a number of possibly correlated variables into a smaller number of uncorrelated variables called principal components. The first principal component accounts for the greatest amount of variability in the data. Each succeeding component accounts for as much of the remaining variability as possible. PCA can be used for reduce the dimensionality of the data while retaining those characteristics of the data set that contribute most to its variance, by keeping lower-order principal components and ignoring higher-order ones.

First we defined a matrix of all the state variables, $x_i(t)$

$$q(t) = [x_1(t), x_2(t), x_3(t)...x_n(t)]$$ (3.3)

In cases where the state variables did not have the same units, we normalized each to unit variance. This prevented the first principal component from being dominated by higher value terms (such as velocity relative to position). This choice of non-dimensionalization is not unique and others might be used. Then we took the covariance matrix of the data set defined by $q(t)$. The eigenvalues, e_i, of this covariance matrix represent the percent of the variance that is explained by each variable. The principle components are determined by multiplying the eigenvectors, v_i, associated with those eigenvalues by the original state space matrix,

$$PC1(t) = v_1 \cdot q(t)$$ (3.4)

We then redefined the state space using these principle components.

$$SS(t) = [PC_1(t), PC_2(t), PC_3(t)...PC_n(t)]$$ (3.5)

To explain ≥ 95% of the variance, two principal components were needed for the Full state space and 4 were needed for the Redundant state space (Fig. 3.1). However, since this system is three-dimensional (Eq. 3.1), we tested state spaces composed of both three and four principal components.
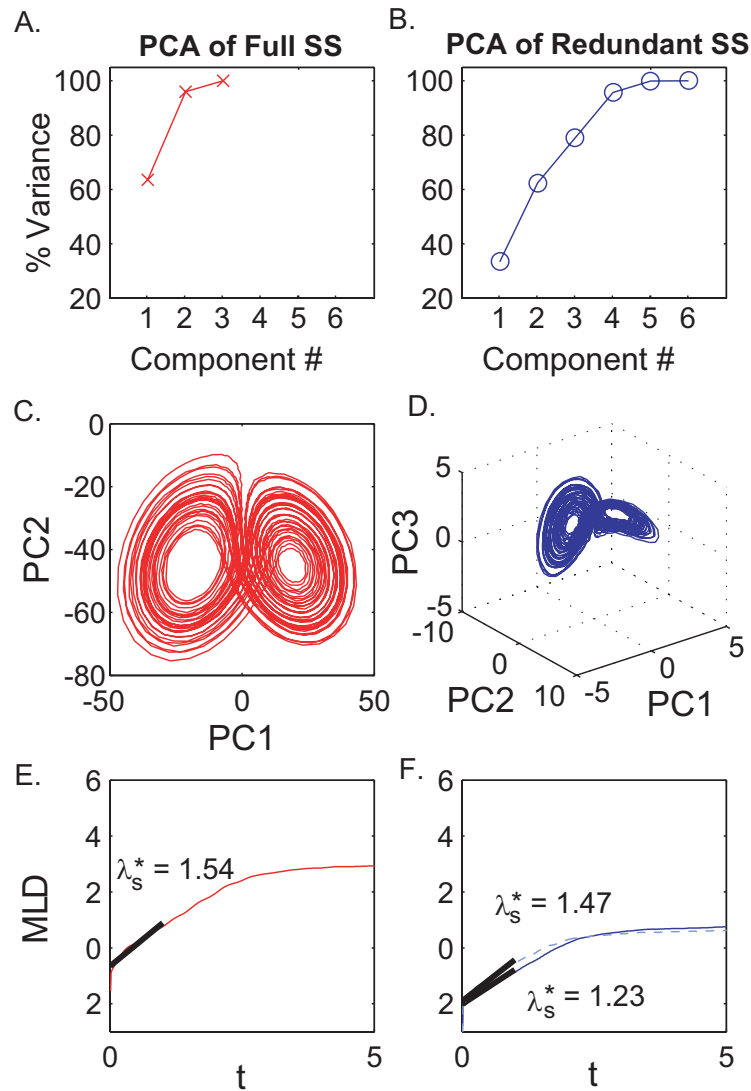
Figure 3.1: Principal components analysis (PCA) of the Lorenz attractor.

A-B) PCA revealed the percentage of the variance explained by each principal component. This percent is shown as a cumulative sum. Two principal components explained >95% of the variance for the Full state space while four were needed for the redundant state space. **C-D)** State spaces are shown for the principal components of the Full (C) and Redundant (D) state spaces. **E)** Mean log divergence (MLD) curves are shown for one trial of a state space of the first two principal components of the Full state space. **F)** MLD curves for a state space with the first three (dashed line) and first four (solid line) principal components of the Redundant state space. The amount and rate of divergence for the Redundant SS was less than for the Full SS.

Four additional state spaces were defined using delay embedding (Kantz and Schreiber, 2004) of $x(t)$, $y(t)$, $z(t)$ and $r(t) = \sqrt{x^2 + y^2 + z^2}$ (Granata and Gottipati, 2008). Multi-dimensional state spaces were reconstructed from each original time series and its time-delayed copies (Takens, 1981):

$$Q(t) = [q(t), q(t+T), q(t+2T), \ldots, q(t + (d_E - 1)T)] \tag{3.6}$$

where $Q(t) \in \{X(t), Y(t), Z(t), R(t)\}$ was the d_E-dimensional state vector, $q(t) \in \{x(t), y(t), z(t), r(t)\}$ was the original 1-dimensional data, T was the time delay, and d_E was the embedding dimension (Fig. 3.2). Time delays were calculated as the first minimum of the average mutual information function of each signal (Fraser and Swinney, 1986).

Maximum local divergence exponents $\left(\lambda_s^*\right)$ were calculated from the exponential rates of divergence of small perturbations in state space (Rosenstein et al., 1993; Dingwell and Cusumano, 2000). Positive exponents indicate local instability. Larger exponents indicate greater sensitivity to local perturbations. Short-term λ_s^* were estimated from:

$$\lambda_s^* = \frac{1}{\Delta t} \left\langle \ln[d_j(t)] \right\rangle \tag{3.7}$$

where $\left\langle \ln[d_j(t)] \right\rangle$ represents the mean log divergence for all pairs of nearest neighbors, j (Rosenstein et al., 1993), over $0 \leq t \leq 1$ seconds. To test the effects of embedding dimension, we calculated λ_s^* for $X(t), Y(t)$, and $Z(t)$ for $d_E \in \{2, 3, 4, 5, 6, 7, 15, 20\}$. Kennel et al. (1992) recommend using a d_E that is twice the true dimension (i.e., $d_E = 6$), while Rosenstein et al. (1993) suggest using a d_E equal to the true dimension (i.e., $d_E = 3$).
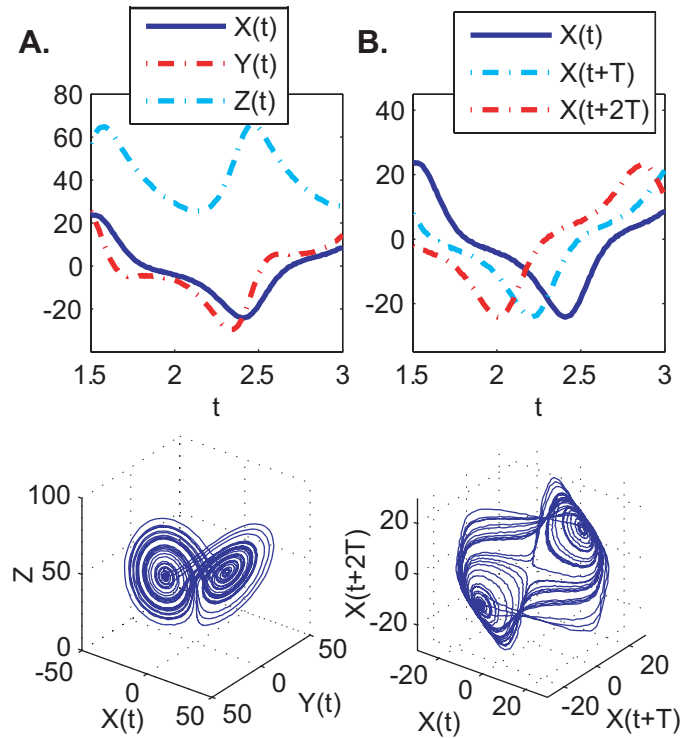
Figure 3.2: Illustration of delay embedding using the Lorenz Attractor

A) Data for the Lorenz attractor is shown with $\sigma = 16$, $\rho = 45.92$, and $\beta = 4$. A 3-D was created from the *x(t), y(t)* and *z(t)* data. **B)** Using the method of delays, a state space can be created by reconstruction of a single trajectory, *x(t)*. The time delay, *T*, is determined as the first minimum of the average mutual information function. A 3-D was created using the original time series, *x(t),* and its time delayed copies, *x(t+T)* and *x(t+2T)*. While the state spaces for the two methods appear different, their dynamics should be the same.

Experimental Data

Twenty healthy right-handed adults (nine female, eleven male) participated. Their mean ± SD age, body mass, and height were 25 ± 2.2 years, 71.2 ± 14.9 kg, and 1.71 ± 0.10 m respectively. Subjects were seated in a device built to simulate a repetitive work task similar to sawing. The device was adjusted so that subjects sat with a knee angle of 90˚. The height of the bar was adjusted so the midpoint between the third and

fourth finger was at the level of the xiphoid process. Subjects also wore a five-point harness across their waist and shoulders, to restrict trunk motion (Corbeau, Sandy, UT).

Subjects made bi-directional horizontal movements in the anterior-posterior direction with their right arm while holding a handle mounted to a metal platform sliding on a low friction track attached to a support frame. Inertial resistance was supplied by an adjustable set of weights mounted on the platform. To ensure the sawing task resistance was comparable across subjects, we first measured each subject's maximum pushing/pulling force using a Baseline® dynamometer that was rigidly mounted to the base of the handle. Subjects alternately pushed and then pulled on this rigidly fixed handle as hard as they could for five seconds each, three times, with 60 seconds of rest in between each attempt. The average of these six peak forces applied during each maximal effort defined that subject's maximum isometric pushing/pulling strength. The weight was set to 10% of the subject's maximum pushing/pulling force to minimize the effects of fatigue during the first portion of the experiment and minimize recovery during the second block of sawing.

Subjects performed this task continuously for five minutes while kinematic data was collected at 120 Hz from 19 reflective markers on the right arm and trunk using an 8 camera Vicon motion analysis system (Oxford Metrics, Oxford, UK). Movement time during the task was enforced by a metronome. For consistency across subjects, the frequency of the metronome was set to twice the average of the predicted resonant frequencies of the upper arm and forearm segments of each subject (two beats per cycle) (Gates and Dingwell, 2008).

The fatigue protocol was designed to specifically fatigue the shoulder flexors. During this task, the subjects lifted a weight (~10% of their maximum isometric shoulder flexion strength) in the sagittal plane with their elbows extended. They completed the

lifting task for three minutes or until they felt they could no longer continue. Eight of the 20 subjects were unable to complete the full three minutes, and all subjects were fatigued at the end of this protocol (RPE $\geq$ 8).

Marker data were filtered using a 5th order Butterworth filter with a cutoff frequency of 15 Hz. The joint centers were determined from a static calibration trial (Schmidt et al., 1999). Segment coordinate systems were calculated from the marker positions with a least-squares algorithm (Veldpaus, 1988). The joint centers at each instant in time were then calculated based on the position of the joint markers during the static trial (Schmidt et al., 1999). The coordinate systems for the trunk and humerus were defined using previous recommendations (Wu et al., 2005; Hingtgen et al., 2006). The three-dimensional movements of the humerus relative to the trunk were determined using Euler angles (Wu et al., 2005). These angles were calculated from the transformation matrix for a *Y-X-Y* rotation sequence (See Appendix C for details).
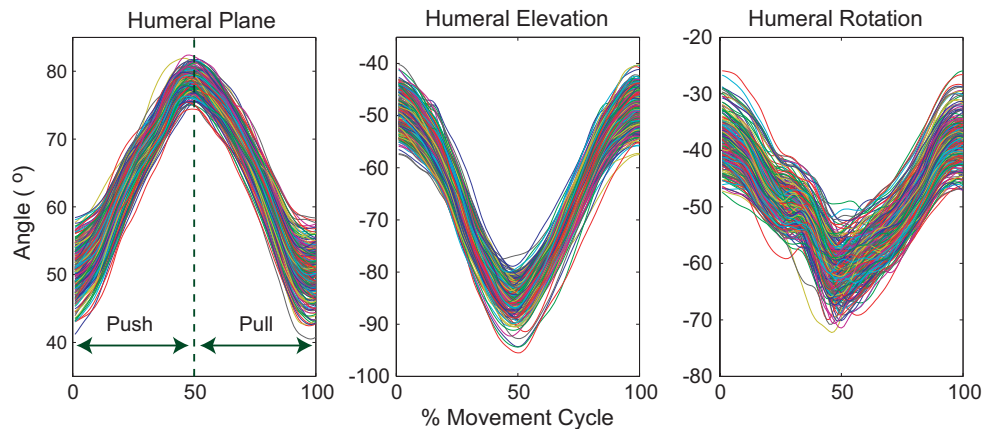
Figure 3.3: Example Euler angles for the shoulder during the sawing task
Angle data for one trial of a representative subject is shown. Each line represents one complete movement cycle. Data were normalized to 100 points per cycle for viewing.

We defined six state spaces for shoulder movement. The "Full" state space was composed of the three rotational angles and their angular velocities. Each state was then

56

normalized to unit variance and PCA was performed. Four principal components explained > 95% of the data variance. The second state space consisted of these four principle components. Four state spaces were defined using delay embedding. Global false neighbors analyses (Kennel et al., 1992) suggested $d_E = 5$ for all three rotational angles (Fig. 3.4). Therefore, we tested $d_E \in \{3, 4, 5, 6, 7\}$. Short-term local divergence exponents (λ_s^*, Eq. 3.4) were calculated over $0 \leq t \leq 1$ cycle (Dingwell and Marin, 2006).

Stability estimates are sensitive to time series length (Granata and England, 2006; Bruijn et al., 2009). Therefore, each time series was first normalized to exactly 36,000 points. This resulted in a < 1% change in the length of each time series. Pre- and post-fatigue λ_s^* from each trial were compared using paired t-tests for each state space.
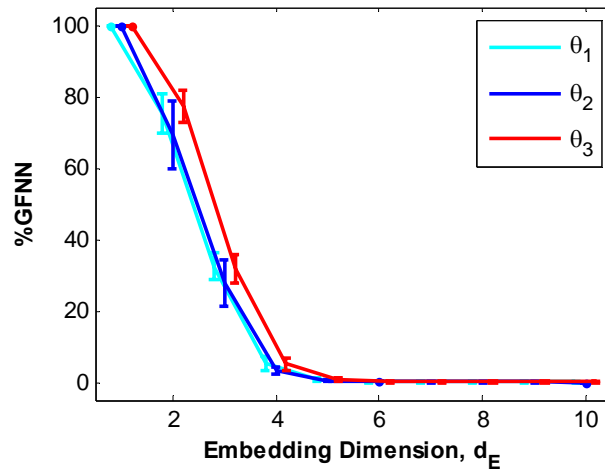
Figure 3.4: Results of the global false nearest neighbors analysis.
The percent of global false nearest neighbors (%GFNN) for each of the three angles dropped to zero after an embedding dimension of five. This signifies that there is some degree of redundancy in the system.

57
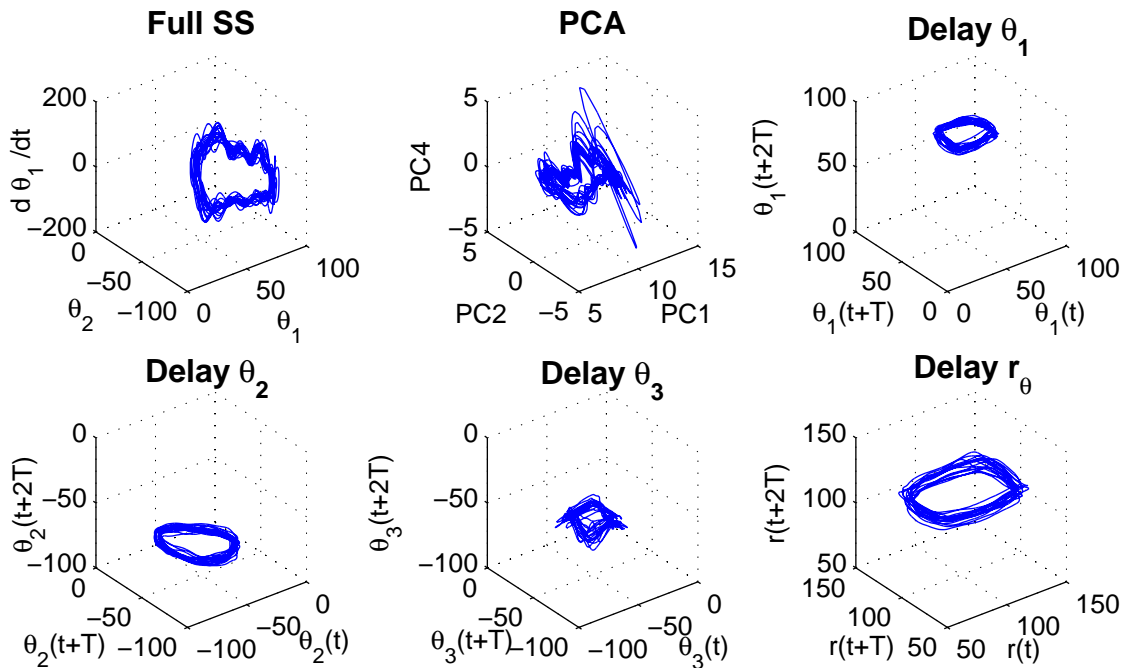
Figure 3.5. Example state spaces for one representative subject.
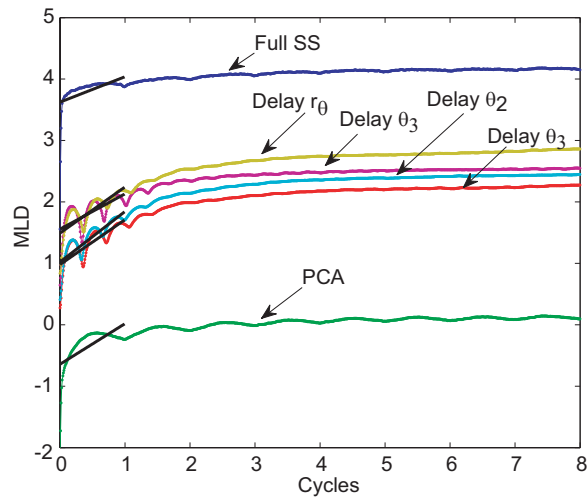
Figure 3.6: Example mean log divergence (MLD) curves for different state spaces

Data is shown for the same representative subject as Figure 3.5. The slope of the divergence curves changed depending on how the state space was defined. The trends between conditions did not change, however.

3.4 RESULTS

For the Lorenz attractor, λ_s^* differed depending on which state space was used (Fig. 3.7A; Table 3.2). Redundant state spaces containing derivatives performed the poorest (errors > 10%). Taking only three principal components of the redundant state space decreased this error from 20.4% to 7.53%. All methods correctly indicated that the Lorenz attractor is locally unstable ($\lambda_s^* > 0$).

As the embedding dimension was increased, λ_s^* decreased (Fig. 3.7B). We expected that a minimum of three (Rosenstein et al., 1993) to six (Kennel et al., 1992) states would reconstruct the state space with minimal error. Large errors were obtained when either too many or too few states were used.
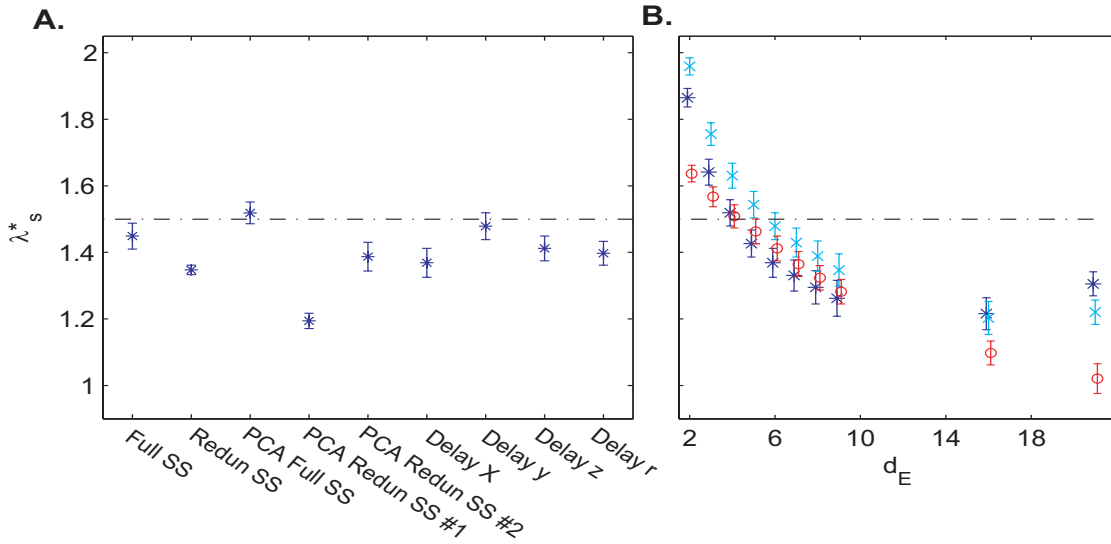
Figure 3.7: Local stability results for the Lorenz attractor.
A) The short-term local divergence exponent, λ_s^*, was calculated for 10 simulations with seven different state space definitions. Error bars represent the mean ± 95% confidence interval for each method defined in Table 2. The dotted line represents the expected value of 1.50. **B)** λ_s^* is shown as a function of the embedding dimension. '*' is λ_s^* for the delay embedding of *x(t)*, '×' is the delay embedding of *y(t)*, and '○' is the delay embedding of *z(t)*. Error bars represent ± 95% confidence interval for each method.

59

Table 3.2: Percent error in λ_s^* for different state spaces for the Lorenz attractor.

Method	State Space	% Error
Full SS	$S = [x(t), y(t), z(t)]$	3.40
Redundant SS	$S = [x(t), y(t), z(t), \dot{x}(t), \dot{y}(t), \dot{z}(t)]$	10.17
PCA of Full SS	$S = [PC1(t), PC2(t)]$	1.25
PCA of Redundant SS #1	$S = [PC1(t), PC2(t), PC3(t), PC4(t)]$	20.40
PCA of Redundant SS #2	$S = [PC1(t), PC2(t), PC3(t)]$	7.53
Delay X	$X(t) = [x(t), x(t+T), x(t+2T), \ldots, x(t+6T)]$	8.75
Delay Y	$Y(t) = [y(t), y(t+T), y(t+2T), \ldots, y(t+6T)]$	1.41
Delay Z	$Z(t) = z[x(t), z(t+T), z(t+2T), \ldots, z(t+6T)]$	5.87
Delay R	$R(t) = [r(t), r(t+T), r(t+2T), \ldots, r(t+6T)]$ Where $r(t) = \sqrt{x^2 + y^2 + z^2}$	6.85

For the experimental data, λ_s^* values also changed across different state spaces.

Shoulder motion was always locally unstable, both pre- and post-fatigue. For all state

spaces, λ_s^* tended to decrease post-fatigue (Fig. 3.8A). This decrease was statistically

significant for 3 of the 6 methods (Fig. 3.8A). As with the Lorenz attractor (Fig 3.7B),

increasing the embedding dimension caused λ_s^* to decrease (Fig. 3.8B). However, pre-

versus post-fatigue differences remained.
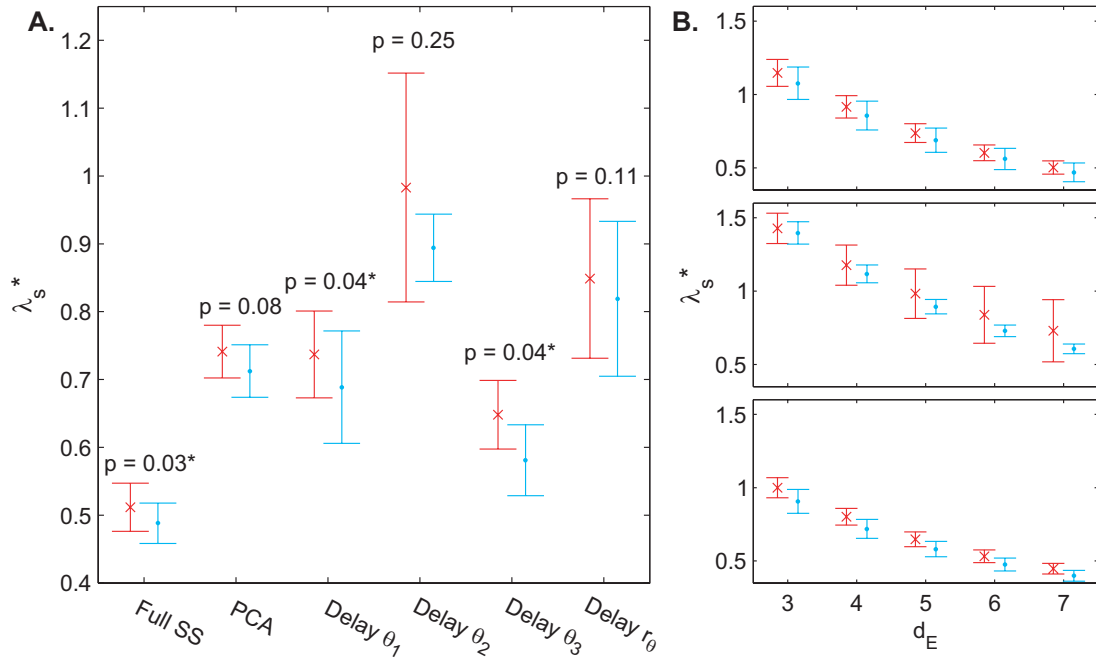
Figure 3.8: Local stability results for the experimental data.

A) The short-term local divergence exponent, λ_s^*, is shown pre- and post-fatigue for 6 state space definitions. From left to right, these are the full state space defined by $[\theta_1, \theta_2, \theta_3, \dot{\theta}_1, \dot{\theta}_2, \dot{\theta}_3]$, the principal components of the full state space, and delay embedding of θ_1, θ_2, θ_3, r_θ (where $r_\theta = \sqrt{\theta_1^2 + \theta_2^2 + \theta_3^2}$), and. Symbols '×' and '•' represent Pre- and Post-fatigue trials, respectively. While the numerical values differed depending on the state space definition, there was generally a decrease from pre to post fatigue. This decrease was statistically significant when using the delay embedding of θ_3 (p=0.04) and the full state space (p = 0.03). **B)** λ_s^* pre- and post-fatigue are plotted versus embedding dimension, d_E, for the delay embedding of θ_1 (Top), θ_2 (Middle), and θ_3 (Bottom). Error bars represent ± 95% confidence interval for each method. λ_s^* decreased as embedding dimension increased, similarly to the Lorenz data. This did not appear to affect the differences in λ_s^* pre and post fatigue.

3.5 DISCUSSION

The only formal requirement for a valid state space is that it uniquely defines the state of a system at all points in time (Kantz and Schreiber, 2004). Thus, any proposed

61

state space is not unique. Here, we explored how several different state spaces affect local dynamic stability (λ_s^*) calculations. The formulations presented here are by no means exhaustive. It is quite possible that other state space definitions might perform as well or better.

Reasonably accurate results were obtained when PCA was performed on the full Lorenz state space and when the correct number of principal components was chosen from the redundant state space. PCA may overestimate the true dimension of the system (Clewley et al., 2008) and poor results were in fact obtained when too many principal components were included (Table 3.2). PCA also requires prior normalization of states that have different units. These normalizations are not unique and can affect the value of λ_s^*. We therefore do not recommend using PCA to define the state space.

While there were quantitative differences in λ_s^* for the different experimental state spaces (Fig. 3.8), all methods demonstrated whether trajectories were locally more or less stable. Differences between experimental conditions persisted, although the statistical significance of these differences did vary. Similarly, previous work demonstrated qualitatively similar changes in walking stability with changes in speed (Dingwell and Marin, 2006; England and Granata, 2007; Kang and Dingwell, 2008), despite using different state space definitions. Thus, while it may be difficult to make direct numerical comparisons between studies that use different state space definitions, it seems that qualitative trends persist. Overall, our findings suggest that biomechanical state spaces constructed using positions and velocities, or delay reconstruction of individual states, are likely to provide more consistent results than those constructed using principal components. Efforts should also be made to avoid using redundant information wherever possible.

Chapter 4: Muscle Fatigue Affects Dynamic Stability of Repetitive Movements

4.1 ABSTRACT

Muscle fatigue alters neuromuscular responses. This may lead to increased sensitivity to perturbations and possibly to subsequent injury risk. We studied the affect of muscle fatigue on movement stability during a repetitive upper extremity task. Twenty healthy young subjects performed a repetitive work task, similar to sawing, synchronized with a metronome before and after performing one of two fatiguing tasks. The first fatigue task ("LIFT") primarily fatigued the shoulder flexor muscles, while the second fatigue task ("SAW") fatigued all of the muscles of the arm. Subjects performed each task in random order on two different days. Instantaneous mean frequencies (IMNF) decreased over both fatiguing tasks indicating that subjects did experience significant muscle fatigue. The slopes of the IMNF over time and the decreases in maximum force measurements demonstrated that the specific fatigue task successfully fatigued the shoulder flexors to a greater extent than any other muscle. On average, subjects exhibited more locally stable shoulder movements post-lifting ($p = 0.035$). They also exhibited more orbitally stable shoulder ($p = 0.039$) and elbow ($p = 0.008$) movements after the sawing task. Subjects also exhibited decreased cocontraction at the wrist post-fatigue for both tasks and at the elbow and shoulder post-lifting. Therefore, subjects movements did not become more dynamically stable as a result of increased muscle cocontraction.

4.2 INTRODUCTION

Muscle fatigue is common in activities that are performed repeatedly over extended periods of time, such as in the workplace. Stability during these movements is

crucial to both maintain performance and prevent injury. Here, we define stability as the ability to return to the same movement pattern after a small perturbation. Stability is regulated during movement through feedback control (Reeves et al., 2007). Feedback mechanisms include intrinsic properties of joints and muscles (i.e. stiffness and damping), and the central nervous system, which integrates information about joint position (i.e. proprioception) and movement (i.e. kinesthesia) to generate muscle (Bowman et al., 2006) and reflex responses (Fig. 4.1). If any of these feedback mechanisms are adversely affected, the resulting muscular responses may not adequately adjust for perturbations. Muscle fatigue causes decreased proprioception (Myers et al., 1999), decreased kinesthesia (Pedersen et al., 1999), altered reflexes (Wojtys et al., 1996), increased muscle response time (Wilder et al., 1996; Wojtys et al., 1996), and increased central processing time (van Duinen et al., 2007). Therefore, muscle fatigue likely leaves people less able to respond to perturbations.
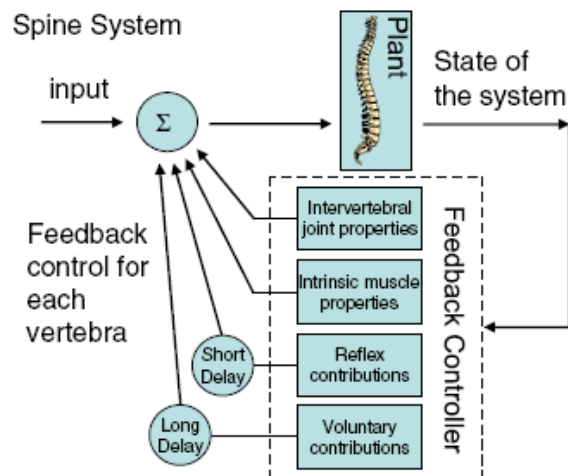
Figure 4.1 Diagram of the feedback control system of the spine for stability regulation
From (Reeves et al., 2007)

To compensate for decreased feedback and delayed responses, the body can increase muscle cocontraction to increase muscle stiffness. For instance, if perturbations

64

are introduced by imposing an external force field, the body can selectively stiffen the muscles in that direction to maintain stability of reaching movements (Franklin et al., 2004). Individuals may (Stokes et al., 2000), or may not (Granata et al., 2001; Grondin and Potvin, In Press) increase muscle cocontraction in anticipation of expected perturbations. People may also increase stiffness through cocontraction after muscle fatigue (Potvin and O'Brien, 1998; Granata et al., 2001; Grondin and Potvin, In Press), possibly to maintain stability. Increased stiffness does not always lead to more stable movements, however. Reeves et al. (2006) found that actively increasing trunk stiffness resulted in decreased postural control. They speculated that increased signal dependent noise from the increased trunk muscle recruitment was responsible. In addition, using cocontraction to maintain stability may be unfavorable in the case of fatigue since it can initiate a vicious cycle as higher muscle activity is energetically costly and may further accelerate fatigue.

Nonlinear dynamics estimates of movement stability can provide insight into the control of dynamic movement tasks (Dingwell and Cusumano, 2000). To our knowledge, only two studies have examined the effect of muscle fatigue on local dynamic stability. Trunk flexion movements were more locally unstable after fatigue of the trunk extensors (Granata and Gottipati, 2008). In contrast, fatigue of the ankle muscles during prolonged walking caused subjects to slow down and trunk movements became more locally stable (Yoshino et al., 2004). The differences in results between these two studies may have occurred due to the nature of the fatiguing contractions. In the first study, fatigue was localized to the trunk extensors. In the second study, fatigue was induced through prolonged walking and so it likely occurred in all muscles of the leg. Specific fatigue of a single muscle group may cause greater changes in muscle activation patterns (Goerlick et al., 2003), or muscle imbalances (Alizadehkhaiyat et al., 2007). However, how muscle

65

fatigue and/or muscle imbalances affect the control of movement stability is not well understood.

In this study, we quantified dynamic stability for a continuous sawing task before and after subjects performed one of two fatiguing tasks. The first task was designed to primarily fatigue the shoulder flexors. The second task caused general fatigue of the arm. We tested four hypotheses. First, subjects will exhibit greater dynamic instability following both fatiguing tasks. Second, these increases in dynamic instability will be larger following the specific fatigue of the shoulder flexors. Third, the muscles will become more unbalanced after specific fatigue of the shoulder flexors than general fatigue of the arm. Finally, subjects will exhibit increases in cocontraction post-fatigue in an attempt to maintain stability.

4.3 METHODS

Subjects

A total of 20 healthy right-handed adults (nine female, eleven male) participated. Their mean ± SD age, body mass, and height were 25 ± 2.2 years, 71.2 ± 14.9 kg, and 1.71 ± 0.10 m respectively. All participants signed institutionally approved informed consent forms and were screened to ensure no subject had a history of medications, surgeries, injuries, or illnesses that might have affected their upper extremity joint movements. To determine handedness, subjects completed a modified version of the Edinburgh Inventory (Oldfield, 1971)Appendix A). This inventory indicates the level of dominance of one hand over another. A score of 0/10 indicates a complete left-handed preference, while a score of 10/10 indicates a complete right-handed preference. All

subjects scored at least 9/10 on the Edinburgh Inventory, indicating a strong right-handed dominance.

General Procedure

Subjects came to the lab for two visits at least one week apart. Each experimental session followed the same general protocol (Fig. 4.2A). First, subjects were seated in a device built to simulate a repetitive work task similar to sawing (Fig. 4.2B). The device was adjusted so that subjects sat with a knee angle of 90˚. The height of the metal track was adjusted so the midpoint between the third and fourth finger was at the level of the xiphoid process. The front/back position of the chair was adjusted to be comfortable for the subject and allow for a full range of motion. This was defined as at a maximum point when almost to full extension (no hyperextension) and at a minimum point at the level of the sternum. Subjects wore a five-point harness across their waist and shoulders to restrict trunk motion (Corbeau, Sandy, UT).

Maximum Voluntary Contraction (MVC) Testing

To ensure the sawing task resistance was comparable across subjects, we first measured each subject's maximum pushing/pulling force using a Baseline[®] dynamometer rigidly mounted to the base of the handle. Subjects alternately pushed and then pulled on this rigidly fixed handle with maximal effort three times for five seconds each time, with 60 seconds of rest in between each attempt. The average of these six peak forces applied during each maximal effort defined that subject's maximum voluntary isometric contraction (MVC) for pushing/pulling. These measurements were taken only at the beginning of the first trial.
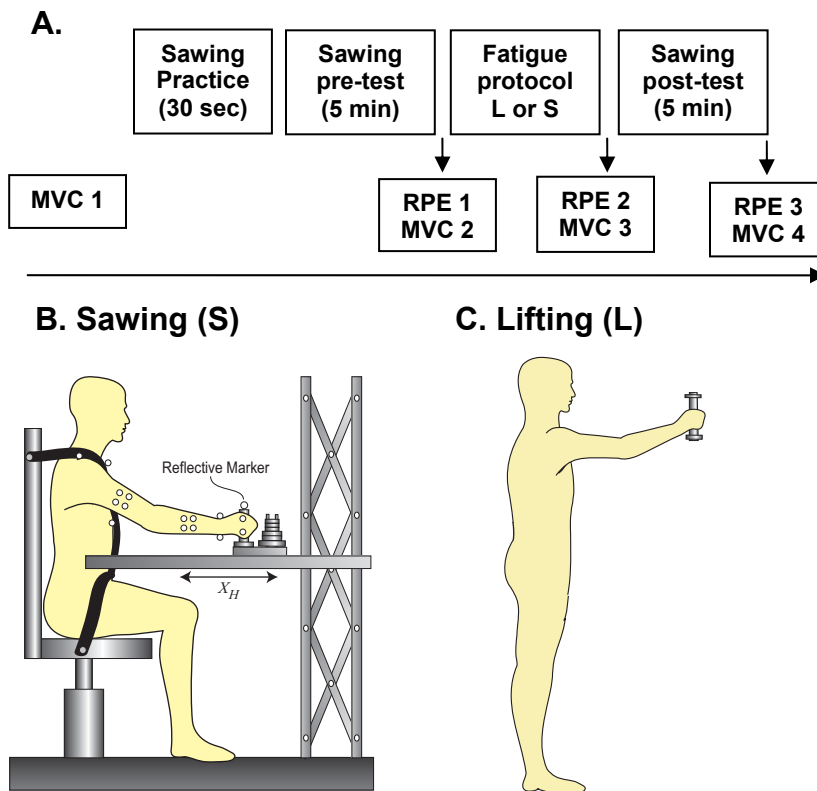
Figure 4.2: Illustration of the experimental protocol
A) General protocol for the experiment. On both visits, subjects completed all activities. Only the fatigue task differed. **B)** During the sawing task subjects were seated in a high-back chair and restrained by belts across the waist and shoulders. A handle with an adjustable weight stack was able to slide with low friction across a horizontal track. This track was adjusted to the level of the subject's sternum. **C)** In the sawing (S) fatigue task subjects pushed 25% of their pushing/pulling MVC for four minutes. In the lifting (L) fatigue task, subjects lifted 10% of their shoulder flexion MVC in the sagittal plane for three minutes. In both tasks, subjects could stop at any point they felt they could no longer continue.

To test for specific muscle imbalances, each subject's maximum strength was measured in six directions at various points throughout the experimental session. Subjects sat, strapped into the device, and adjusted their arms to specific positions (Table 4.1). They then pushed against a hand-held load cell (Lafayette Instruments, Lafayette, IN) with maximal effort two times for five seconds each time, with 30 seconds of rest in between. The peak of the two forces applied during each trial was taken as each subject's

68

MVC strength. Measurements were performed on the right arm only. To compare across subjects, MVCs were normalized to the maximum that they achieved at any of the four time points. Additionally, ratings of perceived exertion (RPE) were recorded using the modified Borg scale (Borg, 1974; Borg, 1982). Subjects subjectively rated their level of fatigue on a scale from 0 ("none at all") to 10 ("maximal exertion"). These measurements were taken periodically throughout the session (Fig. 4.2A).

Table 4.1: Positions of the arm during strength testing

Shoulder Flexion	Humerus extended and elbow flexed 90˚ in sagittal plane
Shoulder Extension	Humerus and elbow extended (~0˚ in sagittal plane)
Shoulder Internal / External Rotation	Humerus and elbow flexed to 90˚ and resting on a board
Elbow Flexion / Extension	Humerus and elbow flexed to 90˚ and resting on a board

Sawing Task

Subjects made bi-directional horizontal movements in the anterior-posterior direction with their right arm while holding a handle mounted to a metal platform sliding on a low friction track attached to a support frame (Fig 4.2B). Inertial resistance was supplied by an adjustable set of weights mounted on the handle platform. Therefore, the resisting load was always opposed to the direction of motion so the arm extensors were the primary agonists during the pushing stroke, while the flexors were the primary agonists on the pulling stroke. The weight was set to 10% of the subject's maximum pushing/pulling force to minimize fatigue during the sawing pre-test and minimize recovery during the sawing post-test. Subjects performed this task continuously for 5 minutes while kinematic and electromyography (EMG) data were collected.

Movement time during the task was imposed by a metronome. For consistency across subjects, the frequency of the metronome was set to twice the average of the predicted resonant frequencies of the upper arm and forearm segments of each subject (2 beats per cycle) (Gates and Dingwell, 2008). To ensure results were not influenced by learning effects, subjects performed a warm-up trial, moving in time with the metronome, for a minimum of 30 seconds (~30 cycles) or until they felt completely comfortable with the task. Subjects then rested for a few minutes to minimize fatigue that may have occurred during this practice period. Previous studies confirmed that subjects were able to learn this simple task within just a few (< 10) movements (Gates and Dingwell, 2008).

Nineteen reflective markers were placed on the right arm and trunk to define the movements of four body segments. Markers were placed on the trunk at the right and left acromion processes, the sternal notch, and the seventh cervical vertebra. Clusters of four markers each were placed on the upper and lower arms to define the arm segments. The hand was defined by four markers at the radial and ulnar epicondyles of the wrist and third and fifth metacarpal-phalangeal joints. Additional markers were placed on the medial and lateral humeral epicondyles during the static calibration trial. A final marker was placed on the top of the handle to define the beginning and end of each cycle. The 3D positions of these markers were recorded continuously during all trials at 120 Hz using an 8-camera Vicon-612 motion analysis system (Oxford Metrics, Oxford, UK).

Nine pairs of preamplified EMG surface electrodes (Delsys Inc., Boston, MA) were attached to the muscles of the trunk and right arm to record activity in the pectoralis major, upper trapezius, deltoid (anterior, middle and posterior), biceps, triceps, flexor carpi radialis, and extensor carpi radialis longus. Electrodes were positioned over each muscle according to accepted recommendations (Konrad, 2005). All analog data were collected at 1080 Hz using a 64-channel A/D board.

Each subject completed two fatigue tasks on separate days. The first task, SAW, involved general fatigue of all muscles of the right arm. Thus, subjects performed the same sawing task described above, except with a resistance that was increased to approximately 25% of their pushing/pulling MVC. Subjects performed this task for four minutes, or until they felt they could no longer continue. Two of the 20 subjects fatigued in less than four minutes. Six subjects who were not fatigued at the end of four minutes (RPE < 6) were asked to continue for an additional four minutes, or until they reached an RPE of eight or higher. The remaining 12 subjects were fatigued (RPE $\geq$ 8) at the end of four minutes.

The second fatigue task, LIFT, was designed to primarily fatigue the shoulder flexor muscles. During this task, the subjects lifted a weight (~10% of their maximum isometric shoulder flexion strength) in the sagittal plane with their elbows extended. They performed the lifting task for three minutes or until they felt they could no longer continue. Eight subjects were unable to complete the full three minutes. All other subjects were fatigued at the end of three minutes (RPE $\geq$ 8).

Data Analysis

Marker data were filtered using a 5th order Butterworth filter with a cutoff frequency of 15 Hz. Segment coordinate systems were calculated based on the marker positions with a least-squares algorithm (Veldpaus, 1988). The joint centers at each instant in time were then calculated based on the position of the joint markers during the static trial (Schmidt et al., 1999). Local coordinate systems were defined using the International Society of Biomechanics' (ISB) recommendations for the shoulder and elbow (Wu et al., 2005) and a modified coordinate system for the trunk (Hingtgen et al.,

71

2006) and wrist (Rao et al., 1996). Three dimensional movements of the right arm were determined using Euler angles in accordance with ISB recommendations (Wu et al., 2005). All joints were assumed to have three rotational degrees of freedom. The second rotational angle of the elbow, the carrying angle, was not analyzed since it changes only minimally due to biomechanical constraints.

EMG data were filtered to a bandwidth between 20 and 450 Hz (Fig. 4.3A). The *instantaneous* mean power frequency (IMPF) was calculated using a continuous wavelet transform algorithm (Matlab 7.0, Mathworks, Natick, MA) (Hostens, 2004). A 'debauchies' wavelet (db5) with a center frequency of 720 Hz at the lowest scale was used for all analyses. This wavelet was scaled in 1-scale intervals from 1–38, which corresponds to center frequencies ranging from approximately 19–720 Hz. The power density function, or 'Scalogram', of the continuous wavelet transform (*CWT*) was computed as

$$SCAL(\tau, s) = |CWT(s, \tau)|^2 \qquad (4.1)$$

where *s* represented the scale (frequency band) and τ was time (Fig. 4.3B). The instantaneous mean frequency (*IMNF*) was calculated by

$$IMNF = \frac{\int_1^{38} s \times SCAL(s)\,ds}{\int_1^{38} SCAL(s)\,ds} \qquad (4.2)$$

(Fig. 4.3C). The *IMNF* was then averaged over each cycle to give a single value per cycle. The slope of the *IMNF* vs. cycles curve was used to quantify trends across the trial (Fig. 4.3D). *IMNF* slopes during fatigue trials for each condition were compared using a single factor ANOVA to test for differences between muscles. These *IMNF* values quantified how the local fatigue state of each muscle changed across consecutive cycles

during the trial. Localized muscle fatigue would cause the EMG mean frequencies to decrease (DeLuca, 1997).
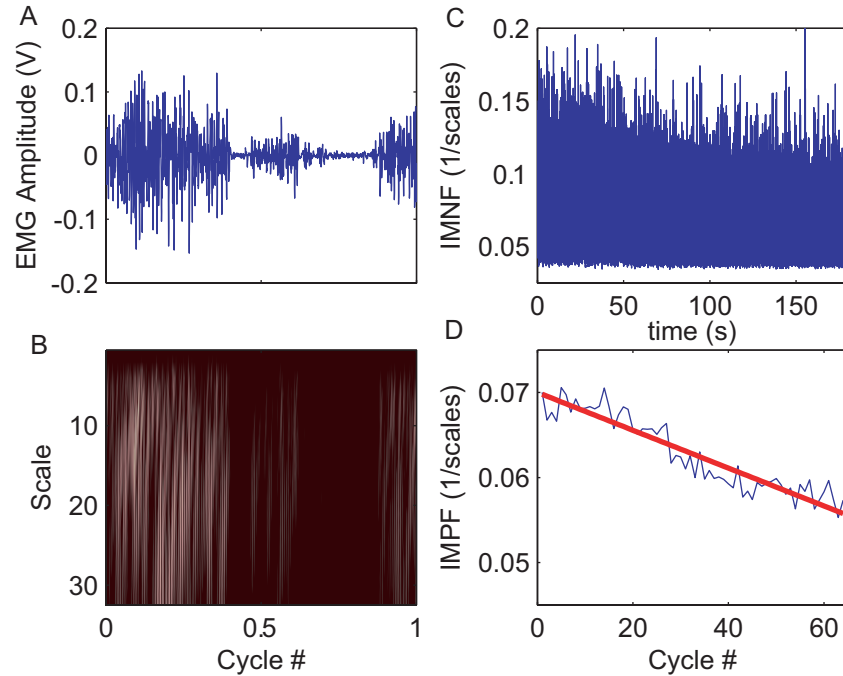
Figure 4.3: Illustration of wavelet analysis to measure instantaneous mean frequency
A) The raw EMG data for the anterior deltoid is shown for a representative subject during the lifting task. **B)** The scalogram of the EMG signal shown in A. **C)** The instantaneous mean frequency (IMNF) was measured at each instant in time. **D)** The average IMNF for each cycle was plotted versus cycle to quantify trends over time.

Separately, raw EMG data were also full wave rectified and filtered with a zero lag 2nd order Butterworth low-pass filter with a cut-off frequency of 6 Hz to obtain linear envelopes (Missenard et al., 2008b). EMG linear envelopes were normalized to the average peak muscle activation across the pre-sawing trial. Muscle cocontraction was estimated using an index of cocontraction (CCI) modified from (Kellis et al., 2003; Missenard et al., 2008b).

$$CCI = \frac{\int_0^{100} EMG_{min} dp}{\int_0^{100} \left(EMG_{ago} + EMG_{ant} \right) dp} \times 100 \qquad (4.3)$$

73

where p was the percent of the movement cycle, EMG_{min} was the EMG signal of the muscle which as the lower normalized activity at each sampling point, EMG_{ago} was the EMG of the agonist muscle, and EMG_{ant} was the EMG of the antagonist muscle (Fig. 4.4). CCIs were calculated for three muscle pairs, shoulder: anterior and posterior deltoid, elbow: biceps and triceps, and wrist: extensor and flexor carpi radialis. CCIs were calculated for each movement cycle and then averaged across cycles to obtain a single value for each subject pre- and post-fatigue under each condition.
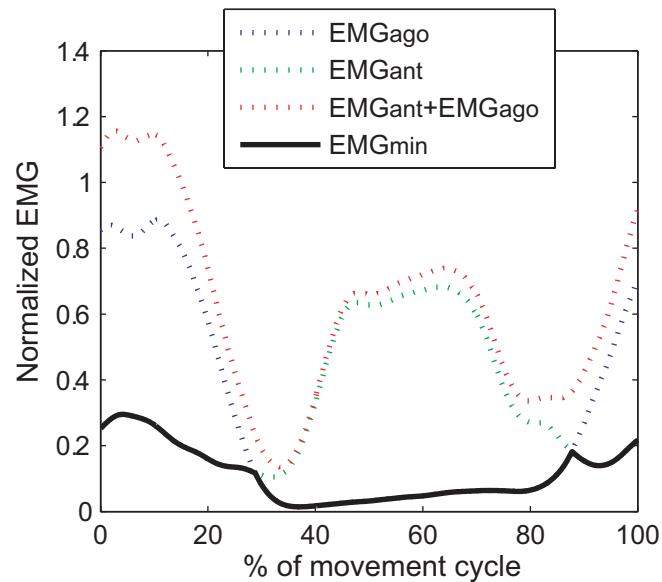
Figure 4.4: Illustration of calculating the cocontraction index (CCI).

EMG linear envelopes for one trial of a representative subject are shown. Here EMG_{ago} is the anterior deltoid, EMG_{ant} is the posterior deltoid and EMG_{min} is whichever had the lower value at that percent of the movement cycle. Subjects push the weight forward during the first 50 % of the movement cycle and then bring it back toward them during the last 50 %.

Responses to small inherent perturbations for the shoulder, elbow and wrist were quantified in two ways (Kang and Dingwell, 2008). First, local dynamic stability of the joint motions was quantified. This measures the quantitative response of the system's

state variables to small perturbations (Dingwell and Cusumano, 2000). We first defined a multi-dimensional state space for each joint (Gates and Dingwell, In Press). At the shoulder and wrist, these consisted of three rotational angles and three angular velocities. The elbow state spaces consisted of only two angles and two angular velocities (Fig. 4.5):

$$\mathbf{S}(t) = \left[\theta_1(t), \theta_2(t), \theta_3(t), \dot{\theta}_1(t), \dot{\theta}_2(t), \dot{\theta}_3(t)\right] \tag{4.4}$$

Euclidean distances between neighboring trajectories in state space were computed as a function of time and averaged over many original pairs of initially nearest neighbors using a previously published algorithm (Rosenstein et al., 1993). For any trajectory in state space, that trajectory's nearest neighbor represents what might happen if a small local perturbation were applied to the system. Local divergence exponents were estimated from the slopes of linear fits to curves using:

$$\lambda^* = \frac{1}{\Delta t}\left\langle \ln\left[d_j(t)\right]\right\rangle \tag{4.5}$$

where $\left\langle \ln\left[d_j(t)\right]\right\rangle$ was the mean logarithm of the divergence, for all pairs of nearest neighbors, j, throughout a time span (Rosenstein et al., 1993). Positive local divergence exponents indicate local instability (i.e., small perturbations grow larger with time). Larger exponents indicate greater sensitivity to local perturbations.

Because the intrinsic time scales were different for each subject (i.e. different average cycle times), the time axes of these curves were re-scaled by multiplying time by the average cycle frequency for each subject. Short-term exponents (λ_S^*) were calculated from the slopes of linear fits to the divergence curve between 0 and 1 cycle. Long-term exponents (λ_L^*) were calculated as the slope between 4 and 10 cycles (Dingwell et al., 2007). These calculations are sensitive to the number of sample points (Granata and England, 2006) and the number of cycles (Bruijn et al., 2009). Each Pre/Post trial was therefore normalized to exactly 36,000 data points. This resulted in less than one percent

75

change in the length of each time series. The frequency of the task was governed by a metronome so it was the same for all trials of each subject. Therefore the number of cycles was approximately the same for each trial of that subject (± 2 cycles).
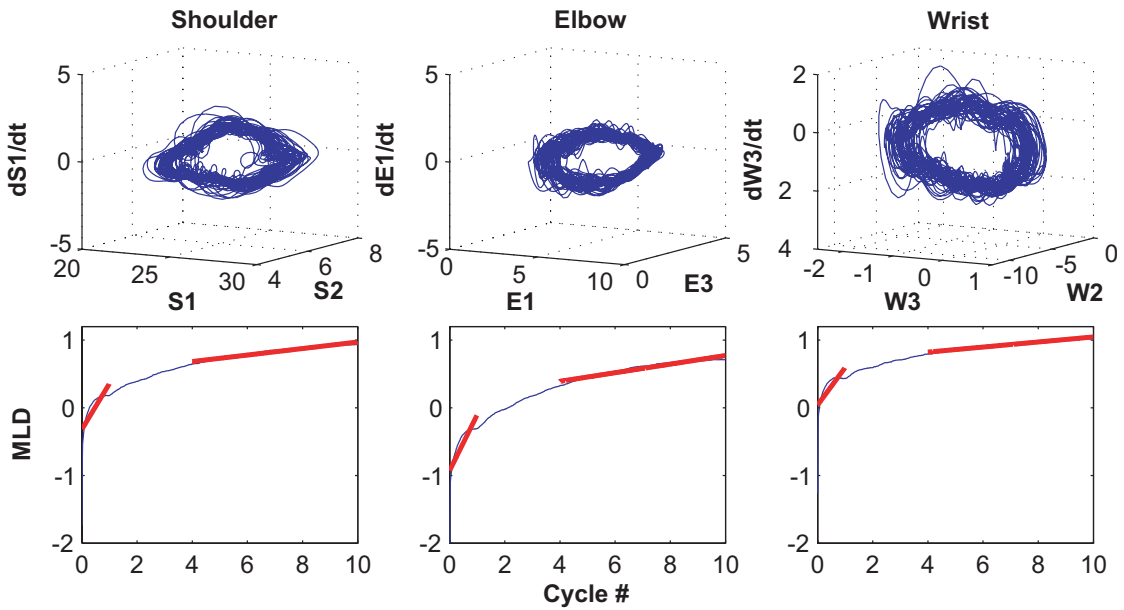
Figure 4.5: Example 3-D state spaces for the shoulder elbow, and wrist and their corresponding mean log divergence curves for a representative subject.

Second, orbital stability was quantified by calculating maximum Floquet Multipliers (FM) (Nayfeh and Balachandran, 1995) based on established techniques (Hurmuzlu et al., 1996; Kuo, 1999; Donelan et al., 2004). The state space data for each individual cycle were time-normalized to 101 samples (0% to 100%). We defined a Poincaré section for each percent of the movement cycle, which defined 101 Poincaré sections for the system. 0% and 100% were minimum positions of the handle marker while 50% was the maximum position (Fig. 4.5). The state space, S_k, for each cycle at that Poincaré section evolved to the state at the following cycle, S_{k+1} according to the Poincaré map:

76

$$\mathbf{S}_{k+1} = F(\mathbf{S}_k) \tag{4.6}$$

The average trajectory across all cycles within a trial was chosen to represent the 'limit cycle' for the movement. Limit cycles correspond to single fixed points in each Poincaré plane (i.e., at each % of the cycle). Orbital stability at each Poincaré section was estimated by computing how quickly small perturbations away from these fixed points grow or decay, using a linearized approximation of equation 5.6:

$$[\mathbf{S}_{k+1} - \mathbf{S}^*] \approx J(\mathbf{S}^*)[\mathbf{S}_k - \mathbf{S}^*] \tag{4.7}$$

where k enumerates individual cycles, $\mathbf{S}_k$ is the system state for cycle k at that Poincaré section, and $\mathbf{S}^*$ is the system state at the fixed point. $J(\mathbf{S}^*)$ is the system Jacobian matrix for each Poincaré section. The FM are the eigenvalues of $J(\mathbf{S}^*)$ (Hurmuzlu and Basdogan, 1994; Nayfeh and Balachandran, 1995). In this case, $J(\mathbf{S}^*)$ is a 6 x 6 matrix so there were six eigenvalues. Since each Poincaré section occupied a 5 x 5 sub-space of S, only the first five eigenvalues were non-zero. If these FM had a magnitude < 1, perturbations shrank, on average, by the next cycle, and the system remained stable. Like λ_s^* and λ_L^*, larger FM imply greater instability (Hurmuzlu and Basdogan, 1994; Hurmuzlu et al., 1996; Kuo, 1999; Donelan et al., 2004). The magnitudes of the maximum FM for each percentage of the movement cycle were calculated for all cycles and pre- and post-fatigue. The maximum MaxFM across the movement cycle was recorded as 'MaxFM'.

IMNF slopes during fatigue trials for each condition were compared using a single factor ANOVA to test for differences between muscles. Significant differences across muscles were then explored using a Tukey's honestly significant difference test. MVCs were compared using 2-factor repeated measures ANOVAs (Time point (1-4) x Saw/Lift). All cocontraction indicies (CCI) and stability measures (λ_s^*, λ_L^*, and peak MaxFM) were compared using a 2-factor repeated measures ANOVA (Pre/Post x

Saw/Lift). We explored differences between Pre/Post trials for the different conditions using estimated marginal means. Significance level was set at $p < 0.05$ for all comparisons.

4.4 RESULTS

All subjects exhibited localized muscle fatigue as measured by decreased IMNF of the EMG during both fatigue tasks (Fig. 4.6). This decrease was significant for all muscles tested (95% confidence intervals did not include zero). The amount of fatigue (slope of IMNF vs. cycle) was significantly greater in the anterior deltoid than all other muscles ($p < 0.019$), except the posterior ($p = 0.101$) and lateral deltoid ($p = 0.803$) for the LIFT fatigue task (Fig. 4.6). In contrast, the SAW task fatigued all muscles fairly equally. The posterior deltoid was significantly less fatigued than the anterior deltoid ($p = 0.006$) and wrist extensor ($p = 0.024$). Therefore, the imbalance in fatigue rates of the anterior and posterior deltoid was more pronounced in the non-specific SAW task.

MVC measurements were taken at four points during the experimental protocol (Fig. 4.2). MVCs decreased post-fatigue for all strength measures ($p < 0.038$; Fig 4.7. There was also a significant differences between conditions for shoulder flexion MVC ($p = 0.035$). Subjects exhibited a greater decrease in shoulder flexion strength and increased imbalance of flexion/extension and internal/external rotation strength after the LIFT task (Fig. 4.6). Thus, the LIFT task was successful at specifically fatiguing the shoulder flexors.
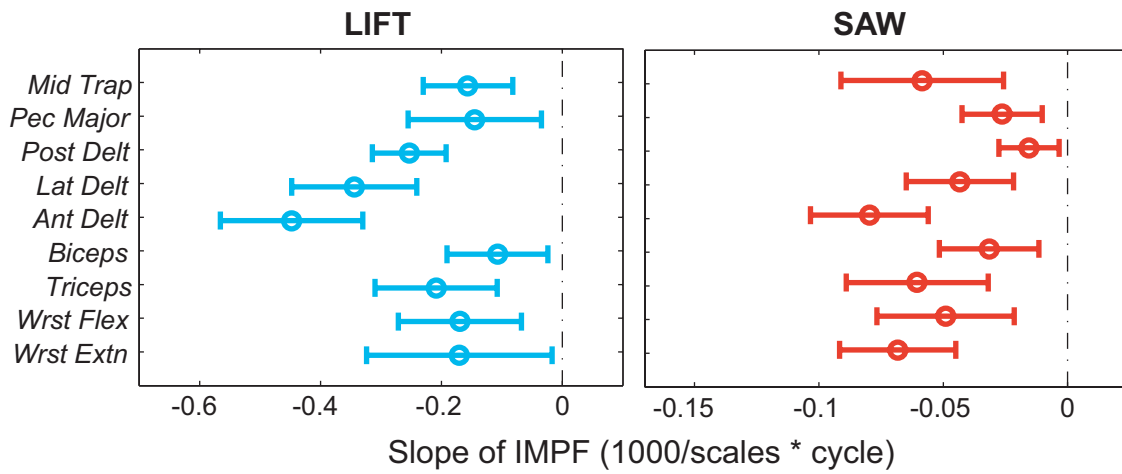
Figure 4.6 The slope of the IMNF vs. cycle curves are shown for each condition
Errorbars represent 95% confidence intervals about the mean of the 20 subjects. Subjects showed fatigue in all muscles as a result of both fatigue protocols.
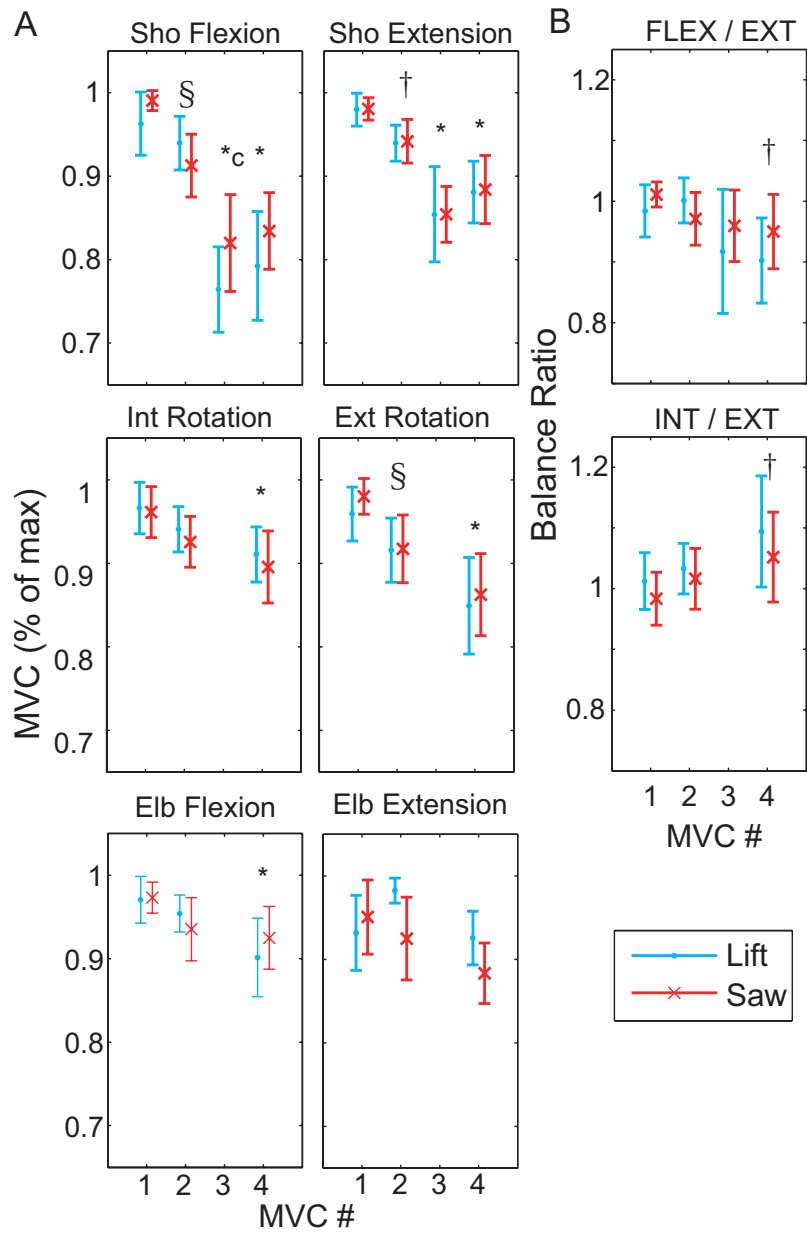
Figure 4.7: Results of MVC testing

MVC measures were taken at four time points in the experiment (Fig. 4.2A). **A)** MVCs are shown as a percent of maximum for Top: shoulder flexion and extension, Middle: shoulder internal and external rotation, Bottom: elbow flexion and extension. **B)** Balance ratios of shoulder flexion to extension and shoulder internal to external rotation MVCs are shown for each time point. Significant differences from MVC1 are shown for both fatigue protocols '*', the lifting protocol only '†', and the sawing protocol only '§'. Significant differences between conditions at that time point are represented by 'c'.

λ_s^* decreased post-fatigue at the shoulder (p=0.029; Fig. 4.8). The estimated marginal means showed that the pre/post difference was significant for lifting (p = 0.035) but not sawing (p = 0.241). There were no significant effects of fatigue on the local stability of elbow or wrist movements. There were also no significant differences between the two fatigue protocols. Finally, no differences in λ_L^* were found for any comparison (not shown).
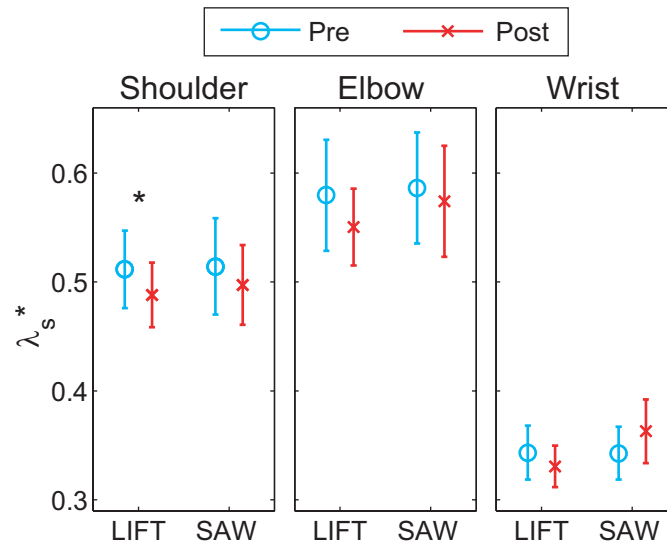
Figure 4.8: Mean values of λ_s^* for the shoulder, elbow and wrist.
Data are shown for are shown prior to fatigue and after either the sawing or lifting fatigue protocol. Errorbars are the 95% confidence intervals across subjects about the mean. '*' represent significant pre/post effects. 'o' represents the pre-fatigue sawing trials while 'x' denotes the post-fatigue sawing trials.
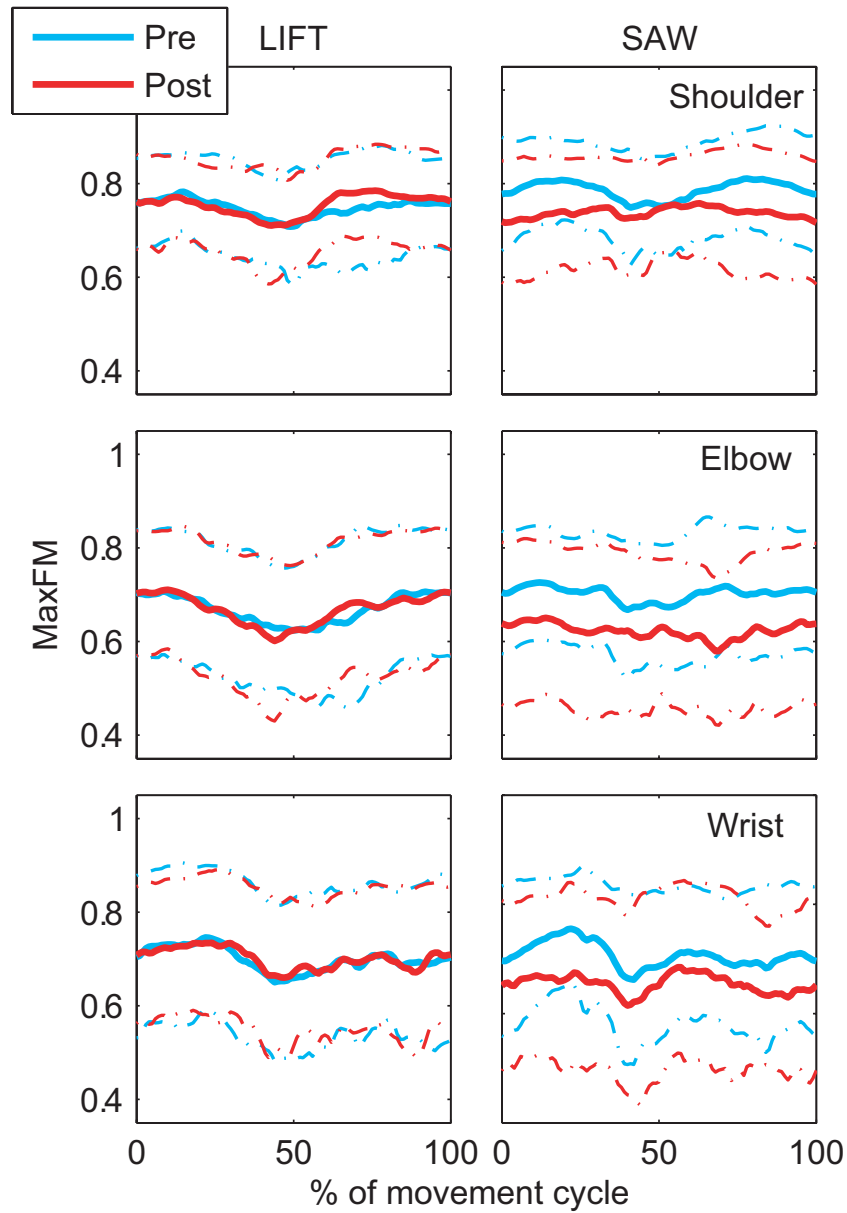
Figure 4.9: MaxFM across the movement cycle.
0% is at the start of the pushing phase, at 50%, the subject begins to pull the weight back toward them. 100% is the end of the pull phase.

Orbital stability of the elbow decreased significantly post-fatigue (p = 0.016), but did not change for the shoulder (p = 0.152) or wrist (p = 0.060). There were no significant differences between fatigue protocols and no significant protocol x fatigue

state interaction effects (elbow: $p = 0.054$, wrist: $p = 0.086$). The estimated marginal means revealed significant decreases in MaxFM for the shoulder and elbow post-fatigue for the SAW task ($p = 0.021$ and 0.013 respectively; Fig 4.9 & 4.10). There were no differences in orbital stability after the LIFT task.
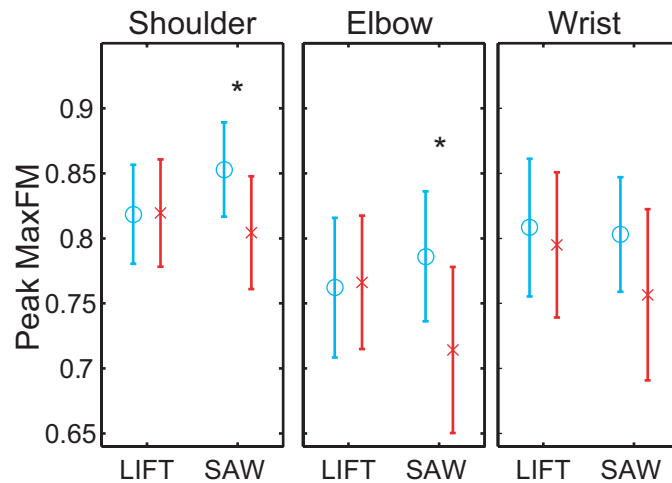
Figure 4.10: Peak MaxFM for each condition pre and post fatigue.
'○' represents the pre-fatigue sawing trials while 'x' denotes the post-fatigue sawing trials. Significant differences from pre to post-fatigue for that condition are denoted with '*'.

There was a significant decrease in cocontraction post-fatigue at the shoulder for the sawing condition ($p = 0.000$; Fig. 4.11). Cocontraction at the wrist decreased significantly post-fatigue ($p = 0.001$) for both conditions. There were no significant differences in cocontraction at the elbow. There were also no significant differences in cocontraction between fatigue tasks ($p > 0.05$).
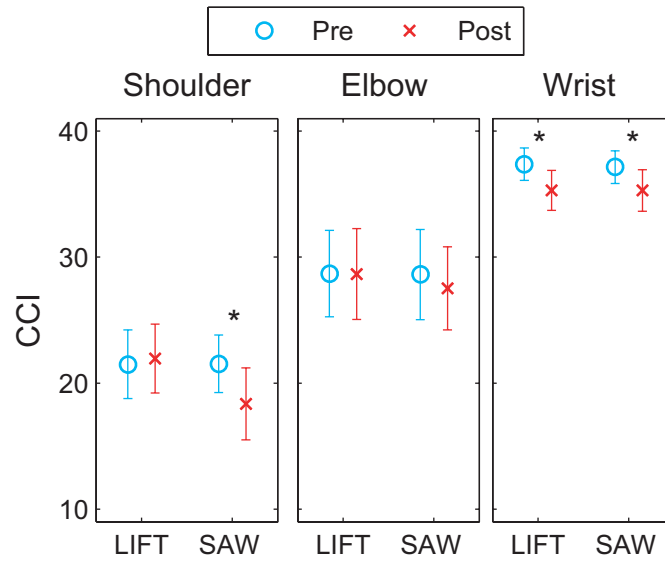
Figure 4.11: Cocontraction indicies (CCI) for the shoulder, elbow, and wrist pre- and post-fatigue.
'○' represents the pre-fatigue sawing trials while 'x' denotes the post-fatigue sawing trials. Significant differences from pre to post-fatigue for that condition are denoted with '*'.

4.5 DISCUSSION

In this study, we quantified the effect of muscle fatigue on movement stability during a repetitive sawing task. We tested the hypotheses that muscle strength imbalances would be generated by specific muscle fatigue of the shoulder flexors and that these imbalances would result in movement instability. Although minor muscle imbalances were seen post-fatigue, these did not lead to instability. In contrast, the subjects actually became more locally and orbitally stable post-fatigue. This was not accomplished through increased muscle cocontraction.

Previous research has shown that muscles respond slower post-fatigue (Wilder et al., 1996; Wojtys et al., 1996), which could lead to instability. However, there are many muscles around each joint which may not fatigue at the same rate (Kumar and Narayan, 1998). The lifting task here primarily fatigued the anterior deltoid muscle (Fig. 4.5). It is

possible that smaller accessory muscles that were not fatigued could compensate for decreased response time of the fatigued muscles thus maintaining constant stability of the movement. Although we attempted to fatigue only the shoulder flexor muscles, we also saw significant fatigue in the other muscles tested. The subjects had to grip the weight in their hands which may have caused fatigue of the wrist flexors and extensors. Subjects also likely eccentrically contracted the posterior deltoid to slow the lowering of the weight on the down phase. While this task may not have *specifically* fatigued of the shoulder flexors, it did fatigue the anterior deltoid to a greater degree than any other muscle (Fig. 4.5).

Subjects could have used muscle cocontraction to stiffen the muscles. This allows the intrinsic properties of the system to contribute more in responding to perturbations than muscle and reflex response with delays (Reeves et al., 2007). A few studies have found that subjects increase cocontraction in response to fatigue, presumably in an effort to maintain stability (Granata et al., 2001; Grondin and Potvin, In Press). Muscle fatigue also leads to increased force variability which can impair movement accuracy. To maintain accuracy during a task, people may cocontract their muscles (Gardner-Morse and Stokes, 1998; Gribble et al., 2003; van Dieën et al., 2003; Missenard et al., 2008a; Reeves et al., 2008). In other fatigue studies with accuracy requirements, subjects did not cocontract their muscles at the expense of decreased accuracy and precision of their movements post-fatigue (Huysmans et al., 2008; Missenard et al., 2008b). In this study, subjects presumably had to maintain stability of their joint movements while accurately matching the metronome timing. Our results show that subjects maintained constant accuracy post-fatigue (no changes in movement time or distance) without increasing cocontraction. They also did not exhibit impaired stability.

85

The cocontraction index used here is not unique. Many other indicies have been proposed (Falconer and Winter, 1985; Frost et al., 1997; Rudolph et al., 2001). The value numerical values differ depending on which index you use (Kellis et al., 2003). In this study, these indices were based only on the prime movers of the task. Thus, it is possible that the smaller accessory muscles either increased or decreased their activity, which would change the overall flexor to extensor activity ratio. However, these are the largest muscles, so we expect that they represent the bulk of the activity.

Despite making the task as dynamically equivalent as possible, differences between subjects remained, particularly in the MVC measures which decreased between 0 and 57%. One reason for this is that since this task was inherently redundant, there were numerous alternative modalities subjects could use to compensate for fatigue (Gates and Dingwell, 2008). The between-subject variability observed in this study was similar to that observed in previous studies of fatigue in complex multijoint tasks (Nussbaum, 2001; von Tscharner, 2002; Madigan and Pidcoe, 2003). Another possible explanation is that the different subjects fatigued to different degrees. Subjects could stop the fatigue task as soon as they felt they could no longer continue the task (RPE =10). This ''threshold'' could be different for different subjects, depending on their motivation level and previous experience pushing themselves past the early stages of fatigue. Those with prior exercise experience may also have recovered quicker from the fatigue task. Some subjects showed rapid recovery from the fatigue task and their MVC values were completely restored after the 'Post' trial while others showed continuous decreases.

In summary, subjects performed consistently accurate movements before and after fatigue. They were able to do this in spite of significant muscle fatigue and decreased muscle cocontraction. Subjects' shoulder movements became more locally stable after targeted fatigue of their shoulder flexors. Their shoulder and elbow movements became

more orbitally stable after general fatigue of the arm. These results suggest that subjects can compensate for muscle fatigue while performing multi-joint redundant tasks, in ways that maintain both movement stability and task precision.

Chapter 5: The Effect of Muscle Fatigue and Movement Height on Movement Stability and Variability

5.1 ABSTRACT

Performing repetitive manual tasks can lead to muscle fatigue, which may induce changes in motor coordination, movement stability, and kinematic variability. These changes may pre-dispose individuals to developing musculoskeletal injuries. Movements performed at or above shoulder height have been associated with increased shoulder injury risk. Ten healthy subjects performed a repetitive task similar to sawing continuously until volitional exhaustion. This task was synchronized with a metronome to control for movement timing. Subjects performed the sawing task at shoulder (High) and sternum (Low) height on two different days. Joint angles and muscle activity were monitored continuously. Local and orbital stability of the joint angles, kinematic variability, and peak angles were calculated for five bins of data spaced evenly throughout each trial. Subjects fatigued more quickly at the High height ($p = 0.007$). They also altered their kinematic patterns significantly in response to muscle fatigue. These changes were larger when the task was performed at the High height. Subjects also exhibited increased kinematic variability of their movements post-fatigue. Increases in variability and altered coordination did not lead to greater instability, however. Shoulder movements were more locally stable when the task was performed at the High height ($p = 0.003$). In contrast, shoulder and elbow movements were more orbitally unstable for the High condition ($p = 0.042$ and 0.040 respectively). Thus people adapt their movement strategies in multi-joint redundant tasks, possibly to maintain stability at the expense of increased variability.

5.2. INTRODUCTION

Performing manual tasks repeatedly can lead to muscle fatigue, which may induce changes in motor coordination (Viitasalo et al., 1993; Bonnard et al., 1994; Forestier and Nougier, 1998). Some changes in coordination may pre-dispose people to develope injuries by inducing poor biomechanics (Rodgers et al., 1994; Sparto et al., 1997; Mizrahi et al., 2000). Injury risk during fatiguing repetitive tasks may also be mediated by changes in variability and/or stability of the movement.

Greater variability might lead to injury by increasing the likelihood of extreme movements (Potvin and O'Brien, 1998). Conversely, increased variability might be protective, because it prevents the joints from constantly being loaded in the same manner (Hamill et al., 1999; Madeleine et al., 2003). Muscle fatigue can lead to increased muscle force unsteadiness proportional to the force level (Missenard et al., 2008a). This unsteadiness may in turn lead to increased kinematic and kinetic variability (Parnianpour et al., 1988; Selen et al., 2007). Muscle fatigue may also reduce co-activation (Missenard et al., 2008b), which can lead to increased variability (Gribble et al., 2003; Selen et al., 2005). In multi-joint dynamic tasks, people may alter their biomechanical coordination strategies (Sparto et al., 1997; Côté et al., 2002) or muscle activation patterns (Corcos et al., 2002; Goerlick et al., 2003). These adjustments may serve to minimize changes in overall kinematic variability.

Measures of variability, however, do not quantify the sensitivity of the neuromuscular control system to perturbations, i.e., 'stability' (Dingwell et al., 2000). Stability is defined as the ability of the body to correct for small perturbations quickly without tissue damage (Granata et al., 2004). This is actively controlled by muscle recruitment, muscle stiffness, and reflex responses (Granata et al., 2004). Since muscle

function is essential to stability, any factors affecting muscle responses could result in instability. Muscle fatigue causes decreased proprioception (Myers et al., 1999), increased muscle response times (Wilder et al., 1996; Wojtys et al., 1996), increased muscle compliance (Huang et al., 2006), altered reflexes (Freund, 1983; Wojtys et al., 1996), and changes in muscle coordination (Bonnard et al., 1994; Corcos et al., 2002). Any of these factors could lead to functional instabilities, possibly increasing the risk of in injury (McQuade et al., 1998). Repeated trunk flexion movements became more unstable after specific fatigue of the trunk extensors (Granata and Gottipati, 2008). In contrast, fatigue induced by prolonged walking caused subjects to slow down and their trunk movements during walking became more stable (Yoshino et al., 2004).

Although changes in movement patterns with fatigue are well documented for a variety of different tasks, these types of experiments traditionally used a pre versus post test approach so the time course over which these changes occur has not been observed. The conclusions of such studies may be limited since they not provide any information about what happens *during* the fatiguing process. Additionally, no studies have concurrently quantified kinematics, variability and dynamic stability so it's unclear whether the documented changes in coordination actually lead to instability and increased variability. It is also possible that changes in kinematics server to offset changes in variability and instability that may result from muscle fatigue.

The purpose of this study was to determine how kinematics, kinematic variability and dynamic stability of the arm were affected by muscle fatigue while subjects performed a repetitive task at a constant rate. Upper limb disorders are commonly associated with repetitive work performed with the arm elevated and abducted (Ohlsson et al., 1995), so this task was performed at both sternum and shoulder levels. We hypothesized that 1) Subjects would change their movement patterns more dramatically

90

when the task was performed at the High height since this was assumed to be more difficult to maintain, 2) Kinematic variability would increase with fatigue in response to increased neuromuscular noise, 3) Shoulder movements would become more locally unstable with fatigue, and 4) Movement variability and instability would be greater for movements performed at the High height.

5.3 METHODS

Subjects

Ten healthy right-handed subjects (four female, six male) participated. Their mean ± SD age, weight, and height were 27.9 ± 2.2 yr, 72.4 ± 18.2 kg and 1.73 ± 0.10 m, respectively. Prior to the experiment, all participants signed institutionally approved consent forms and were screened to ensure that no subject had a history of medications, surgeries, injuries, or illnesses that might have affected their upper extremity joint movements. To determine handedness, subjects completed a modified version of the Edinburgh Inventory (Oldfield, 1971). This inventory indicates the level of dominance of one hand over another. A score of 0/10 indicates a complete left-handed preference, while a score of 10/10 indicates a complete right-handed preference. All subjects scored at least 9/10 on the Edinburgh Inventory, indicating a strong right-handed dominance.

Experimental Protocol

Subjects performed a repetitive task at two different work heights on two separate visits to the laboratory spaced approximately one week apart. The order of testing was randomized. On each visit, subjects were seated in a device built to simulate a repetitive work task similar to sawing (Fig. 5.1). During each experiment, subjects made bi-

directional horizontal movements in the anterior-posterior direction with their right arm while holding a handle mounted to a metal platform sliding on a low friction track attached to a support frame. Inertial resistance was supplied by an adjustable set of weights mounted on the carriage. Therefore, the resisting load was always opposed to the direction of motion so that the arm extensors were the primary agonists during the pushing stroke, while the flexors were the primary agonists on the pulling stroke. Subjects performed this task synchronized with a metronome continuously until voluntary exhaustion.
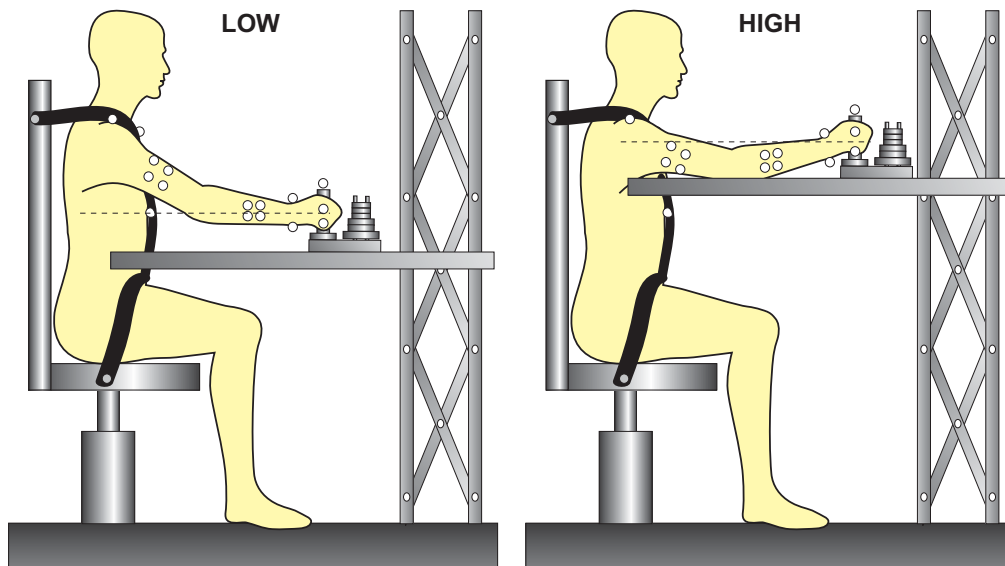
Figure 5.1 High/Low Experimental setup.
Subjects were seated in a high-back chair and restrained by belts across the waist and shoulders. A handle with an adjustable weight stack was able to slide with low friction across a horizontal track. This track was adjusted to either the level of the subject's sternum or their shoulder joint center.

The device was adjusted so that subjects sat with a knee angle of 90°. The height of the metal track was adjusted so the midpoint between the third and fourth finger was either at the level of the xiphoid process ('Low') or in line with the shoulder joint center ('High'). The horizontal position of the chair was adjusted to be comfortable for the

subject and to allow for a full range of motion. This was defined as a maximum point almost to full extension (no hyperextension) and a minimum point at the level of the sternum. Subjects also wore a five-point harness (Corbeau, Sandy, UT, USA) cross their waist and shoulders, to restrict trunk motion.

To ensure the task resistance was comparable across subjects, we first measured each subject's maximum pushing/pulling force using a second custom handle attached to a Baseline® dynamometer that was rigidly mounted on a table (Fig.2). Subjects alternately pushed and then pulled on this rigidly fixed handle with maximal effort three times for five seconds each time with 60 seconds of rest in between each attempt. The average of these six peak forces applied during each maximal effort defined that subject's maximum isometric pushing/pulling strength (MVC). This was used to set a target resistance of 15% MVC for each task. This percent was chosen from pilot testing to achieve complete fatigue in approximately 15 – 20 minutes.

Figure 5.2 Picture of set-up to determine maximum pushing/pulling force

Subjects were instructed to synchronize their movements with a metronome. To ensure that the task was dynamically equivalent across subjects, the frequency of the metronome was set to twice the average of the predicted resonant frequencies of the upper arm and forearm segments of each subject (2 beats per cycle) (Gates and Dingwell, 2008). The average frequency of movement was 1.07 Hz. To ensure that our results were

not influenced by learning effects, subjects were asked to perform a warm up trial, moving in time with the metronome, for a minimum of 30 seconds (~30 cycles) or until they felt completely comfortable with the task. Pilot testing confirmed that subjects were able to learn this simple task within just a few (< 10) movements (Gates and Dingwell, 2008). Subjects then rested for one minute to minimize any fatigue effects that may have occurred during this practice period.

Nineteen reflective markers were placed on the right arm and trunk to define the movements of four body segments. Markers were placed on the trunk at the right and left acromion processes, sternal notch, and seventh cervical vertebra. Clusters of four markers each were placed on the upper and lower arms to define the segments. The hand was defined by four markers at the radial and ulnar epicondyles of the wrist and third and fifth metacarpal-phalangeal joints. Additional markers were placed on the medial and lateral humeral epicondyles for a static calibration trial. A final marker was placed on the top of the handle to define the beginning and end of each cycle. The three-dimensional position of these markers was recorded continuously during all trials at 60 Hz using an eight camera Vicon-612 motion analysis system (Oxford Metrics, Oxford, UK).

Nine pre-amplified electromyography (EMG) surface electrodes (Delsys Inc., Boston, MA, USA) were attached to the dominant arm and torso muscles to record activity in the middle trapezius, pectoralis major, deltoid (anterior, lateral and posterior), triceps (lateral head), biceps, flexor carpi radialis, and extensor carpi radialis longus. Electrodes were positioned over each muscle according to accepted recommendations (Konrad, 2005). EMG signals were recorded at 1080 Hz using a Delsys Bagnoli-8 (Delsys Inc., Boston, MA, USA) system (differentially amplified with a gain of 1000, frequency bandwidth of 20–450 Hz, input impedance $>10^{15}/0.2$ Ω/pF, CMRR >80 dB) prior to A/D conversion. Additionally, subjects were asked to rate their perceived

94

exertion (RPE) every three minutes during each trial on a modified Borg scale (Borg, 1974; Borg, 1982).

Data Analysis

The *instantaneous* mean power frequency (IMPF) was calculated using wavelet transform methods, as this method is more accurate and robust than the Fourier transform for analyzing nonstationary signals (Hostens, 2004).   Briefly, a continuous wavelet transform (*CWT*) of the signal was taken (Matlab 7.0, Mathworks, Natick, MA, USA). The power density function, or 'Scalogram', of the *CWT* is

$$SCAL(\tau, s) = |CWT(s, \tau)|^2 \tag{5.2}$$

Where *s* represents the scale (frequency band) and τ is time.   The instantaneous mean frequency (IMNF) is calculated by

$$IMNF = \frac{\int_{ls}^{hs} s \times SCAL\ (s)ds}{\int_{ls}^{hs} SCAL\ (s)ds} \tag{5.3}$$

Where *ls* is the lowest scale of interest and *hs* is the highest.   The IMNF was then averaged over each cycle to give a single value per cycle. A 'debauchies' wavelet (db5) with a center frequency of 720 Hz at the lowest scale was used for all analyses.   This wavelet was scaled in 1-scale intervals from 1–38, which corresponds to center frequencies ranging from approximately 19–720 Hz.   IMNF values were averaged over each cycle to give a single IMNF per cycle.   These IMNF values quantified how the local fatigue state of each muscle changed across consecutive cycles during each trial. Localized muscle fatigue would cause the EMG mean frequencies to decrease (DeLuca, 1997).

Marker data were filtered using a fifth order Butterworth filter with a cutoff frequency of 15 Hz. Segment coordinate systems were calculated based on the marker positions with a least-squares algorithm (Veldpaus, 1988). The joint centers at each instant in time were then calculated based on the position of the joint markers during the static trial (Schmidt et al., 1999). Local coordinate systems were then defined using the International Society of Biomechanics' (ISB) recommendations for the shoulder and elbow (Wu et al., 2005) and a modified coordinate system for the trunk (Hingtgen et al., 2006) and wrist (Rao et al., 1996). The three dimensional movements of the right arm were determined using Euler angles. The rotation sequences used were in accordance with ISB recommendations (Wu et al., 2005). All joints were assumed to have three rotational degrees of freedom. The second rotational angle of the elbow, the carrying angle, was not analyzed since it changes only minimally due to the biomechanical constraints on the elbow joint.

The maximum angle ('PeakAng') within each cycle was identified and used to evaluate changes in overall kinematics. Variability was quantified as MeanSD: the average width of the standard deviation across the movement cycle (Dingwell and Marin, 2006). The mean values of IMNF, PeakAng, and MeanSD were calculated by splitting the data into five non-overlapping bins. Only the last 50 cycles in each bin were analyzed to maintain consistency across subjects and conditions.

Local dynamic stability was defined as the quantitative response of the system's state variables to small perturbations (Kang and Dingwell, 2006b). To calculate this we first defined a multi-dimensional state space for each joint consisting of its three rotational angles and angular velocities (except at the elbow, which had onlys two).

$$S(t) = \left[\theta_1(t), \theta_2(t), \theta_3(t), \dot{\theta}_1(t), \dot{\theta}_2(t), \dot{\theta}_3(t) \right] \qquad (5.4)$$

These state space descriptions were shown to adequately define the joint motion (Gates and Dingwell, In Press). The mean local divergence of nearest neighbor trajectories was calculated using a previously published algorithm (Rosenstein et al., 1993). For any trajectory in state space, that trajectory's nearest neighbor represents what might happen if a small local perturbation were applied to the system. Short-term local divergence exponents were estimated from the slopes of linear fits to curves using:

$$\lambda^*_s = \frac{1}{\Delta t} \left\langle \ln[d_j(t)] \right\rangle \tag{5.5}$$

where $\left\langle \ln[d_j(t)] \right\rangle$ represents the mean logarithm of the divergence, for all pairs of nearest neighbors, j, throughout a time span (Rosenstein et al., 1993). Positive exponents indicate local instability (i.e., small perturbations grow larger with time), and larger exponents indicate greater sensitivity to local perturbations.

Since the intrinsic time scales were different for each subject (i.e. different average cycle times), the time axes of these curves were re-scaled by multiplying by the average cycle frequency for each subject during each condition. Short-term exponents (λ^*_S) were calculated from the slopes of linear fits to the divergence curve between 0 and 1 cycle. Long-term exponents (λ^*_L) were calculated as the slope between 4 and 10 cycles (Dingwell et al., 2007). Since these divergence curves are sensitive to the number of cycles (Bruijn et al., 2009), only data from the last 50 cycles of each bin were used for consistency across subjects and conditions. This method is also sensitive to the number of points (Granata and England, 2006), so the data in each bin was resampled such that each series of 50 cycles had exactly 5000 points.
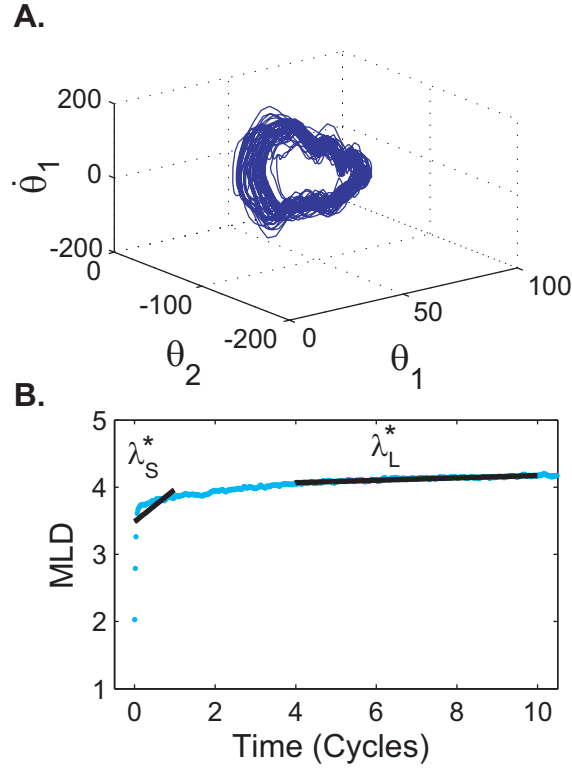
Figure 5.3: Methods to determine local divergence exponents.
A) A 3D projection of the full 6D state space of the shoulder is shown for one representative subject. $\dot{\theta}_1$ is humeral plane angular velocity, θ_1 is the humeral plane angle, and θ_2 is the shoulder elevation angle. **B)** The mean log divergence (MLD) curve (Eq. 5.5) for the data shown in A. The short-term local divergence exponent, λ_S^*, was calculated as the slope of this curve divergence (MLD) between 0 and 1 cycle. The long-term local divergence exponent, λ_L^*, was calculated as the slope of the curve between 4 and 10 cycles.

Second, orbital stability was quantified by calculating maximum Floquet Multipliers (FM) (Nayfeh and Balachandran, 1995) based on established techniques (Hurmuzlu et al., 1996; Kuo, 1999; Donelan et al., 2004). The state space data for each individual cycle were time-normalized to 101 samples (0% to 100%). We defined a Poincaré section for each percent of the movement cycle, which defined 101 Poincaré sections for the system. 0% and 100% were minimum positions of the handle marker while 50% was the maximum position (Fig. 4.5). The state space, S_k, for each cycle at

98

that Poincaré section evolved to the state at the following cycle, S_{k+1} according to the Poincaré map:

$$\mathbf{S}_{k+1} = F(\mathbf{S}_k) \tag{4.6}$$

The average trajectory across all cycles within a trial was chosen to represent the 'limit cycle' for the movement. Limit cycles correspond to single fixed points in each Poincaré plane (i.e., at each % of the cycle). Orbital stability at each Poincaré section was estimated by computing how quickly small perturbations away from these fixed points grow or decay, using a linearized approximation of equation 5.6:

$$[\mathbf{S}_{k+1} - \mathbf{S}^*] \approx J(\mathbf{S}^*)[\mathbf{S}_k - \mathbf{S}^*] \tag{4.7}$$

where k enumerates individual cycles, $\mathbf{S}_k$ is the system state for cycle k at that Poincaré section, and $\mathbf{S}^*$ is the system state at the fixed point. $J(\mathbf{S}^*)$ is the system Jacobian matrix for each Poincaré section. The FM are the eigenvalues of $J(\mathbf{S}^*)$ (Hurmuzlu and Basdogan, 1994; Nayfeh and Balachandran, 1995). In this case, $J(\mathbf{S}^*)$ is a 6 x 6 matrix so there were six eigenvalues. Since each Poincaré section occupied a 5 x 5 sub-space of S, only the first five eigenvalues were non-zero. If these FM had a magnitude < 1, perturbations shrank, on average, by the next cycle, and the system remained stable. In this case, larger FM indicates that movements are approaching instability (i.e. it takes longer for perturbations to be 'absorbed'). The magnitudes of the maximum FM for each percentage of the movement cycle were calculated for all cycles and pre- and post-fatigue. The maximum MaxFM across the movement cycle were recorded as 'MaxFM'. The magnitudes of the maximum FM ("Max FM") for each percent of the movement cycle were calculated for the data in each bin. Data were averaged across subjects to quantify differences between conditions and across bins.

Comparisons for peak angles (PeakAng), kinematic variability (MeanSD), dynamic stability (λ_s^*, λ_L^*, and MaxFM) and IMNF were made using 2-factor (Bin (1-5)

x Condition (High/Low)) repeated measures ANOVAs (SPSS Inc., Chicago, IL USA). The significance level was set at $p < 0.05$ for all comparisons. Least significant difference tests were performed to assess significance between bins for each condition and between conditions for each bin.

5.3 RESULTS

Subjects performed the task for significantly longer in the Low condition (24.1 ± 10.3 min) than the High condition (12 ± 3.9 min; $p = 0.007$). All subjects exhibited localized muscle fatigue as measured by decreased IMNF of the EMG signals (Fig. 5.4). These decreases were statistically significant for all nine muscles tested ($p < 0.032$). In addition, all subjects reported an RPE of 10 at the completion of the experiment.
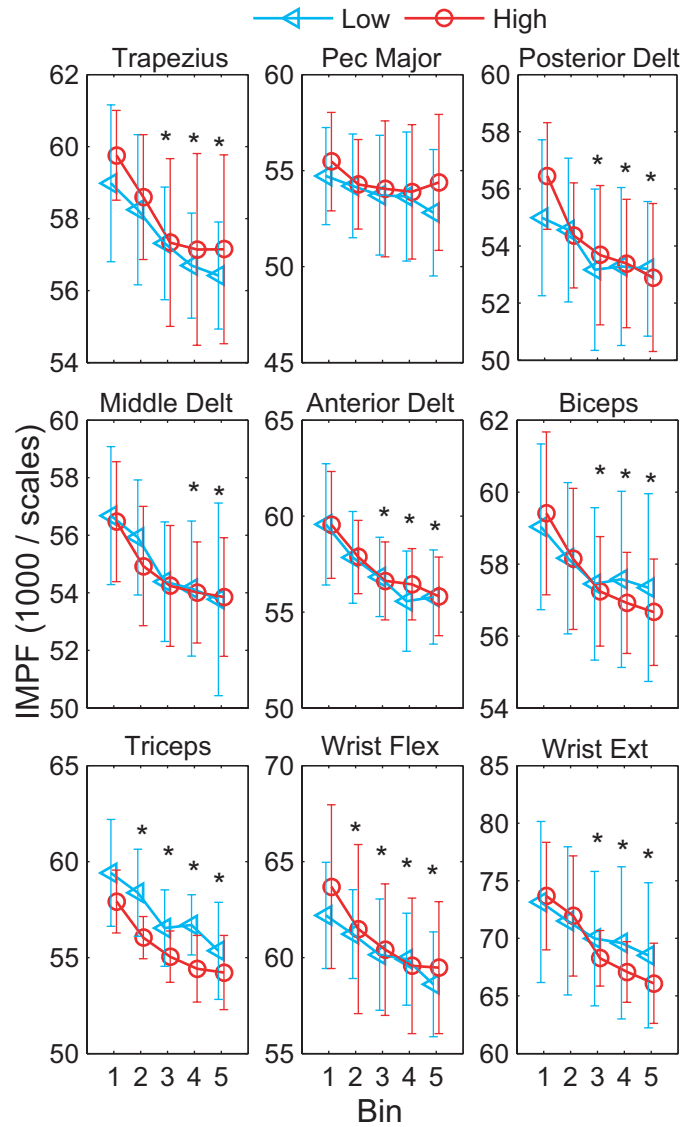
Figure 5.4: Instantaneous mean frequency (IMNF) across bins.

The average IMNF was calculated for each of 5 bins. The means across subjects are shown. Error bars are ±95% confidence intervals. A significant main effect for bin was found for all muscles (p < 0.032). There was no significant effect of condition for any muscle tested. Bins are offset for clarity. '*' represent bins which were significantly different from bin 1 for both conditions.
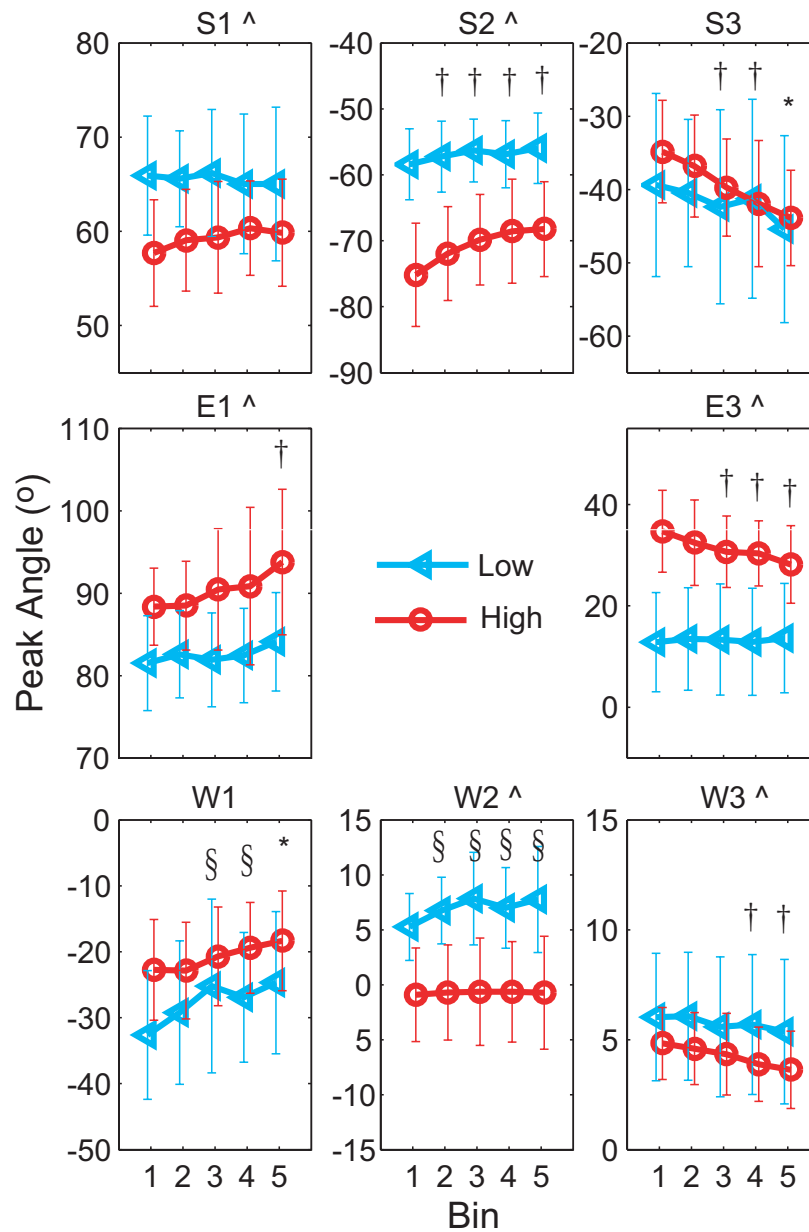
Figure 5.5: Peak angles across bins for both the High and Low condition.

The average maximum angle ('PeakAng') for each bin is shown for the High and Low conditions. The top row shows data for the shoulder joint angles (from left to right, humeral plane (S1), elevation angle (S2), rotation (S3) angles). The middle row is elbow flexion (E1) and pronation / supination (E3). The bottom row is the wrist flexion (W1), ab/adduction (W2) and pronation/supination (W3). '^' represents a significant condition effect, '†' represents bins which are significantly different from bin 1 for the high condition, '§' is for the low condition and '*' is for both conditions.
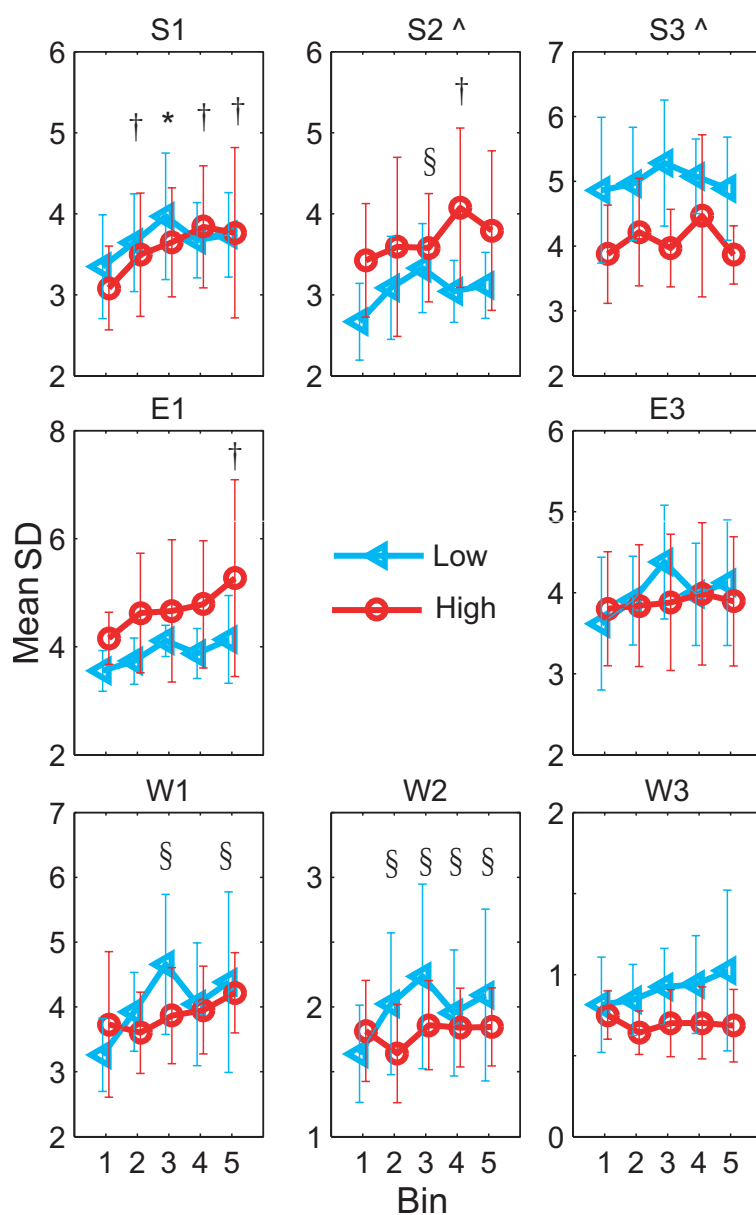
Figure 5.6: MeanSD angles across bins for both the High and Low conditions.

MeanSD for each joint angle is shown across the 5 bins. The top row shows data for the shoulder joint angles (from left to right, humeral plane (S1), elevation angle (S2), internal external rotation (S3)). The middle row is elbow flexion/extension (E1) and pronation/supination (E3). The bottom row is the wrist flexion/extension (W1), ab/adduction (W2) and pronation/supination (W3). '^' represents a significant condition effect, '†' represents bins which are significantly different from bin 1 for the high condition, '§' is for the low condition and '*' is for both conditions.

103

The average maximum angle ('PeakAng') the subjects achieved during each movement varied across the trial (Fig. 5.5). Subjects tended to lower (increased humeral 'negative' elevation (S2: p = 0.001), and externally rotate (S3: p = 0.000) their humeruses. They also increased their elbow extension (E1: p = 0.011) and decreased their wrist extension (W1: p = 0.002) and wrist abduction (W2: p = 0.008). There were significant High/Low condition effects for S1 (p = 0.044), S2 (p = 0.000), E1 (p = 0.003), E3 (p = 0.000), and W2 (p = 0.005). There were also a significant bin x condition interactions for S2 (p = 0.045) and E3 (p = 0.013).

The variability ('MeanSD') of the movements changed with condition and bin (Fig. 5.6). The humeral elevation angle (S2) was more variable for the High condition (p = 0.041), while humeral rotation angles (S3) were less variable (p = 0.012). There was a significant bin effect for the humeral plane angle (S1: p = 0.014), elbow flexion angle (E1: p = 0.023), wrist flexion (W1: 0.003) and wrist ab/adduction (W2: p = 0.038). These differences were relatively small, however ($< 2^{\circ}$).

Short-term (λ_s^*) and long-term (λ_L^*) local divergence exponents (Fig. 5.7), were calculated to quantify movement stability. Subjects exhibited more locally unstable shoulder movements over the short-term in the Low condition (p = 0.003). There were no significant main effects for either condition or bin for the long-term local divergence exponents. There were no differences in across bins for any variable.

Maximum Floquet multipliers were calculated as a secondary measure of movement stability. Movements were more orbitally unstable at the High height for the shoulder (p=0.042) and elbow (p = 0.040). There were no significant differences across bins, however.
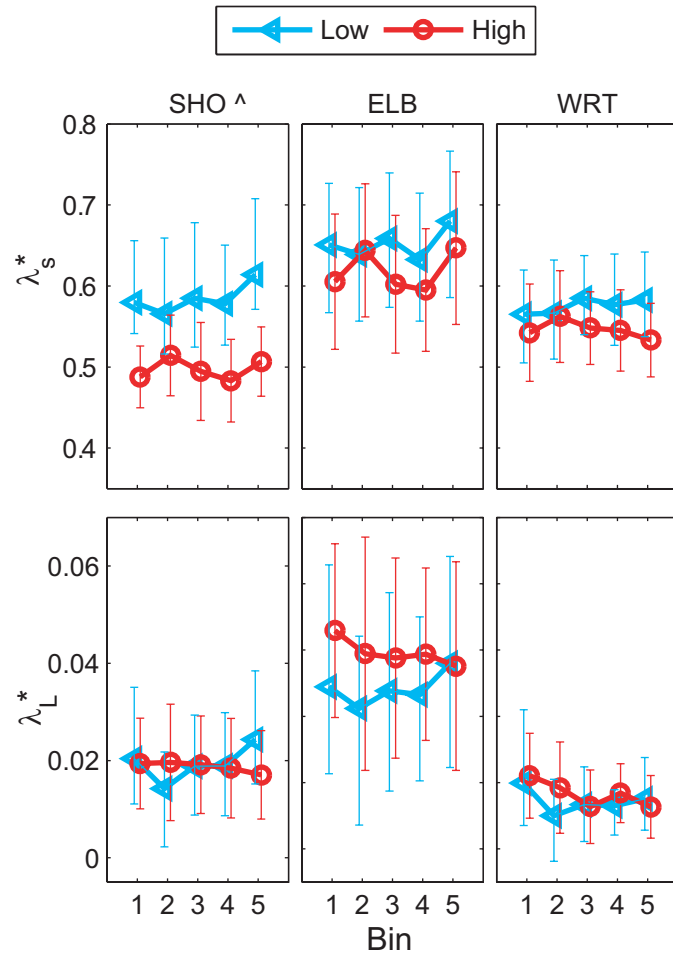
Figure 5.7: Local dynamic stability results for the shoulder, elbow, and wrist

The top row shows data for short-term exponents, λ_s^*. The bottom row is data for the long-term exponent, λ_L^*. Data is shown for the shoulder, elbow and wrist. There was significant main effect for condition (i.e. Low vs. High) at the shoulder for λ_s^* (p = 0.003). There were no significant differences across bins for any variable and no Low/High condition effects for any of the other five comparisons.
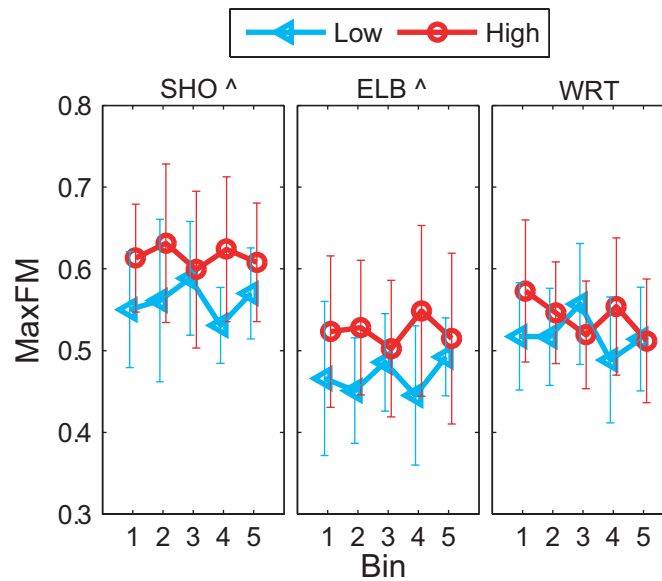
Figure 5.8: Orbital stability results for the shoulder, elbow and wrist

Data is shown for the shoulder (SHO), elbow (ELB) and wrist (WRT). MaxFM exhibited shows some differences between conditions (shoulder: $p = 0.042$, elbow: $p = 0.040$) where movemens were slightly less stable (larger MaxFM) for the High condition. There were no differences across bins. ^ represents a significant main effect for condition ($p < 0.05$).

5.4 DISCUSSION

Muscle fatigue can lead to increased variability (Parnianpour et al., 1988; Selen et al., 2007; Missenard et al., 2008a), and decreased stability (Granata and Gottipati, 2008) of repetitive movements. In multi-joint dynamic tasks, people can change their biomechanical coordination strategies (Sparto et al., 1997; Côté et al., 2002) or muscle activation patterns (Corcos et al., 2002; Goerlick et al., 2003). These adjustments could minimize changes in overall kinematic variability and movement stability. The purpose of this study was to determine how muscle fatigue affected kinematic variability, dynamic stability, and coordination during a repetitive task. This task was performed at two work heights. The High height required the arm to be elevated further against gravity and put the humerus in more impinged position relative to the scapula. This

106

presumable increased the difficulty of the task. The fatiguing protocol appeared to be effectively fatigue the muscles of the right arm. Each subject reported that their rate of perceived exertion was a 10 (on a scale of 10) when they completed the study. We also found significant decreases in instantaneous mean frequency of the EMG signals for both work heights (Fig 5.4).

Generally, the results supported about half of these hypotheses. Subjects altered their movement patterns in response to fatigue, predominantly in the High condition (Fig. 5.5). This supported our first hypothesis and is consistent with other studies on fatiguing repetitive movements (Sparto et al., 1997; Côté et al., 2002). Subjects also exhibited small but significant increases in kinematic variability with muscle fatigue (Fig. 5.6), thus supporting our second hypothesis. However, movement stability did not across the trial, contrary to our third hypothesis. Only variability of the humeral elevation angle was greater at the High height (Fig. 5.6). Additionally, movements at the higher height were more locally stable (Fig. 5.7) but less orbitally stable (Fig. 5.8) than those performed at the Low height. Thus our fourth hypothesis was largely unsupported. In and of themselves, the observed differences between the Low and High height conditions do not tell you why you see these changes. They could be related to biomechanical changes or they could be related to changes in neural control.

One reason for the lack of changes in stability may have been adjustments in movement speed. Decreasing speed has been shown to increase local stability (Dingwell and Marin, 2006; Granata and England, 2006). In the present study, we attempted to control for movement speed by having subjects synchronize their movements with a metronome. Subjects were largely able to maintain a constant cycle time across the trial ($p = 0.083$) for both conditions (Fig. 5.9). There were no specific targets for the movement distance, however, so some subjects adjusted their reaching distance across

bins (p = 0.021). This adjustment was different for the two heights (bin*cond: p = 0.002). The average speed therefore also varied across bins (bin: p = 0.008; bin*cond, p = 0.000). Using post-hoc analysis to explore these significant interaction effects, we found that temporal parameters were only affected when movements were performed at the high height. Subjects were not able to maintain a constant cycle time as dictated by the metronome. They tended to slow down and make shorter movements over the course of the experiment. Since subjects slowed down, it is possible that this may have offset any effect of fatigue on the stability of movements performed at the high height.
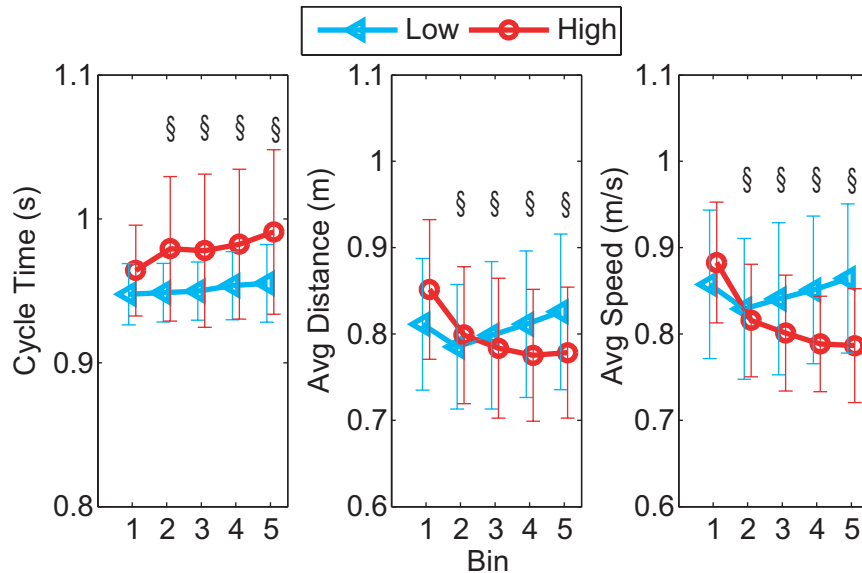
Figure 5.9 Average cycle times, distance and speed across bins.
Average data across subjects is shown for both the Low and High conditions. Error bars represent ±95% confidence intervals about the mean. § indicates bins that were statistically different from bin 1 for the High condition.

For most of the biomechanical and dynamic stability variables tested here, trends over time are difficult to indentify because of the large between subject variability, particularly for time to exhaustion. One reason for this is that, since this task was inherently redundant, there were numerous alternative modalities subjects could use to compensate for those that were altered by fatigue. For example, each subject showed a

unique pattern as to which muscles were most affected by fatigue during the task. This could be due to difference in muscle anatomy, muscle fiber type composition, training, etc. All of these factors could potentially affect which muscles fatigued first and to what extent. The differential effects of the task on fatigue led subjects to exhibiting different changes over time in their kinematics. The between-subject variability observed in this study was similar to that observed in previous studies of fatigue in complex multi-joint tasks (Nussbaum, 2001; von Tscharner, 2002; Madigan and Pidcoe, 2003; Voge and Dingwell, 2003).

While all subjects reported a RPE of 10 at the conclusion of the experiment, it is a subjective measure so the actual amount of fatigue might have been different. Also, in an effort to use the same number of trials for each subject we only analyzed the last 50 cycles of each bin. This was chosen to capture the later stages of fatigue. However, it is likely that some subjects were already beginning to experience the early stages of fatigue in bin #1 so comparisons made here do not directly illustrate 'no fatigue' versus fatigue, but rather changes throughout the fatiguing process.

In summary, subjects significantly altered their kinematic patterns in response to muscle fatigue. These changes were larger when the task was performed at a higher height. Subjects also exhibited increased variability of their movements post-fatigue. Increases in variability and altered coordination did not lead to decreased stability, however. Local stability of the shoulder decreased when movements were performed at a lower height. In contrast, orbital stability of the shoulder and elbow decreased for movements at the higher height. This research showed that people adopt their strategies in multi-joint redundant tasks, possibly to maintain stability at the expense of increased variability.

Chapter 6: Conclusion

SUMMARY

Repetitive stress injuries are common in the workplace where workers perform repetitive tasks continuously throughout the day. Muscle fatigue may lead to injury either directly through muscle damage or indirectly through changes in coordination, development of muscle imbalances, kinematic and muscle activation variability, and movement instability. It is difficult to separate these possible causes or to make generalizations about how fatigue affects movement since effects seem to be task dependent and highly variable amongst subjects. To better understand the role of muscle fatigue in injury, we studied how muscle fatigue and muscle imbalances affected the control of movement timing, variability, and stability during an upper extremity sawing task.

Previous research has suggested that muscles respond slower after significant muscle fatigue (Wilder et al., 1996; Wojtys et al., 1996). The muscles activations may also become more variable (Bruijn et al., 2009). Changes at the muscle level likely correlate to changes in the resulting kinematics. A few studies have shown decreased performance post fatigue (Jaric et al., 1999; Iwasa et al., 2005; Missenard et al., 2008b), while others have found that people retain the ability to reproduce movements or accurately hit a target (Côté et al., 2002; Heuer et al., 2002; Selen et al., 2007). This may be possible to the redundancy in human body which enables us to perform the same task with different combinations of muscle activity or different joint positions. In Aim #1 of this dissertation, we found that subjects were able to retain timing despite significant muscle fatigue. We further analyzed this data to determine how the subjects were controlling their movements and found that subjects made more frequent corrections to

their movements after fatigue. This supports work by Corbeil et al. (2003) which showed that subjects made more frequent corrections to their center of pressure during standing after significant muscle fatigue.

In this study we also decomposed variability into that which directly affected the 'goal' of maintaining time with the metronome and that which did not. Those solutions which met this goal lied on a 'goal equivalent manifold' (GEM) for the task. Mean deviations and variability perpendicular to the GEM were much smaller than those tangent to the GEM. Deviations perpendicular to the GEM were also corrected much more rapidly than those tangent to it. This indicates that subjects were trying to correct only those variations which adversely affected performance. This is an interesting finding since it illustrates that increases in overall variability are not necessarily bad. For example, when performing repetitive movements, it may be ideal to take advantage of this variability to maintain accuracy and yet prevent the joints from constantly being loaded in the same manner.

The delayed muscular responses mentioned above, may also lead to instability of the movement (Granata and Gottipati, 2008). One way to measure this is to look at the local dynamic stability of the movement using techniques from non-linear dynamics. While this concept is gaining increasing popularity in recent literature, it has yet to be determined how it can accurately be applied to studies of human movement. Recent research has focused on question such as: How many cycles should be included for a valid estimate of stability? (Bruijn et al., 2009) How long should the trials be? (Kang and Dingwell, 2006b) How many data points are necessary? (Rosenstein et al., 1994) Should the kinematic data be filtered or not? One question that had yet to be addressed was how to appropriately define the state space when the equations of motion governing the movement are unknown. In Aim 2 of this dissertation we explored the use of a variety of

state spaces that had been used in previous literature as well as exploring the possibility of using principal components analysis to define the state space. We found that for both defined nonlinear deterministic system and experimental data state spaces composed of the all state variables performed the best, while delay embedding of individual variables may also be a viable alternative. Overall the experimental trends persisted no matter which state space was used. This finding is important since it suggests that we should be able to make qualitative comparisons across studies which have used different state spaces. However, quantitative values of stability differed for the different state spaces. This suggests that in order to make quantitative comparisons across studies you must you the same state space definition.

Muscle fatigue may also lead to muscle imbalances (Alizadehkhaiyat et al., 2007) as the muscles surrounding the joint fatigue at different rates (Kumar and Narayan, 1998). These imbalances can lead to excessive movement in the direction that the unfatigued / less fatigued muscle operates. This would lead to decreased stability of the joint movement. In Aim #3 we found that primarily fatiguing the shoulder flexor muscles caused decreased force generating capacity of the muscles, increased force imbalances of the opposing muscle groups around the shoulder, and decreased cocontraction of the wrist muscles. In spite of these deleterious effects, subjects also exhibited increased local stability of their shoulder movements. In contrast, general fatigue of the arm resulted in decreased force generating capacity of the muscles, no changes in muscle balance, and decreased cocontraction at the shoulder and wrist. The general fatigue resulted in increased orbital stability of the shoulder and elbow movements but no changes in local stability. Together, these results suggest that neither specific fatigue of a muscle group nor general fatigue of the arm have a deleterious effect on movement stability. It is possible that neither protocol fatigued them to the point that

112

they could not quickly adapt their movements or that (as discussed in Aim #1) they simply applied more frequent corrections to their movements post-fatigue.

In multi-joint tasks, people may also alter their coordination patterns to delay the onset of fatigue or in response to painful muscles. These changes in coordination may also serve to limit kinematic variability which may arise out of the increased force variability associated with muscle fatigue (Bigland-Ritchie and Woods, 1984). They may also improve stability of the movement. In contrast, many changes in coordination that result from fatigue put the body in an improper posture that may increase the risk of injury (Sparto et al., 1997). Little is known about how these variables interact or the time course over which these changes are made. In Aim #4 we found that subjects adapted differently when task posture was modified. When movements were performed at a high height, subjects adapted to fatigue by slowing down and making shorter movements. They also dropped their arm from the extreme abducted posture. These changes made the subjects more variable in their kinematics while their stability remained constant. Subjects found the task to be less challenging at the lower height. At this height, they were able to maintain a constant movement distance and speed. They mainly exhibited altered coordination and increased variability at the wrist. Again, subjects showed no changes in local or orbital stability of their movements with fatigue. These results suggest that subjects can make adjustments to their coordination in ways that maintain stability. It seems that they are not trying to reduce kinematic variability.

INJURY MODEL REVISITED

In Chapter 1, we proposed the injury model shown in Figure 6.1. In the experiments presented in this dissertation, we showed that subjects did change their

coordination patterns in response to fatigue (Chapter 5). These changes did not appear to lead to an improper posture, since subjects showed decreased humeral (negative) elevation angles post-fatigue. Postures with the arm at or above shoulder level are associated with an increased risk of injury (Ohlsson, 1995). Subjects did not show a decreased ability to maintain movement timing after significant muscle fatigue (Chapter 2). Subjects may have been able to continue achieving the task goal by altering their control strategies. We found significant increases in variability of the kinematics post-fatigue (Chapter 5), but no changes in variability of the endpoint trajectories (Chapter 2). We believe this variability may be a good thing since it increases the number of ways subjects can perform the task so as to distribute the stresses to different tissues, while still allowing for accurate movements.
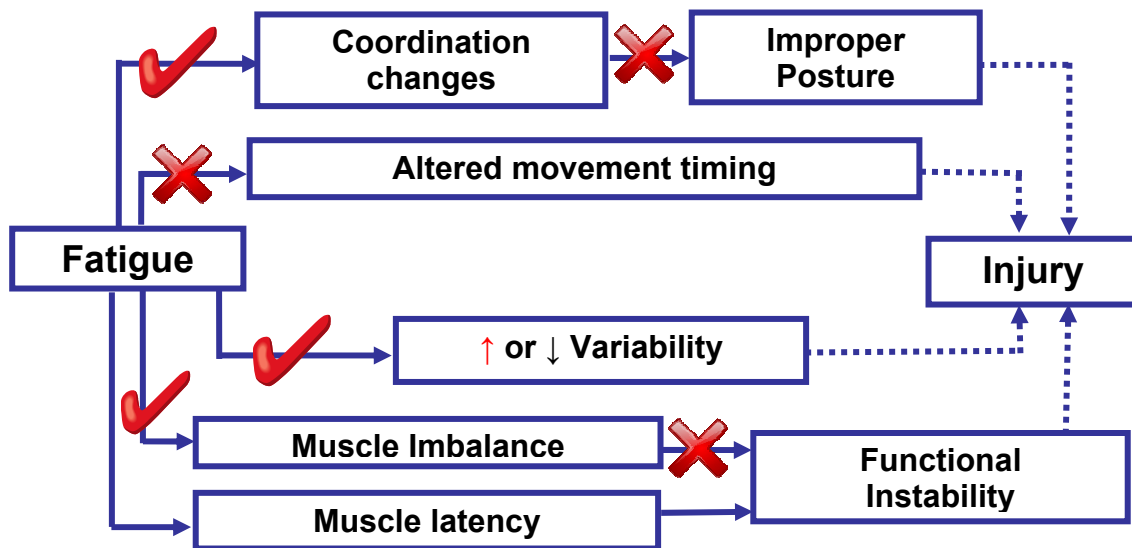
Figure 6.1: Updated injury model

Targeted muscle fatigue of the shoulder flexors did cause some, albeit small, increases in muscle imbalance at the shoulder (Chapter 4). This increased imbalance did not result in instability, however. These results suggest that subjects are able to adapt

their movements in response to fatigue in ways that maintain performance. Future work should focus on monitoring workers performing repetitive tasks continuously for extended periods of time. This could reveal the long-term adaptations people make to their movements and which may be associated with increased prevalence of injury.

Appendices

APPENDIX A. HEALTH HISTORY QUESTIONNAIRE

IRB #: 2007-06-0018   **Subject ID:** _____

Date of Birth (mm/dd/yy): _____   Age: _____
(Age less than 21 or greater than 35 excludes)

MALE: _____   FEMALE: _____

Height:_____ ft./in. = _____ in. × 0.0254 = _____ m

Weight: _____ lbs. × 0.4567 = _____ kg.

BMI (kg/m^2): _____ (BMI > 35 excludes)

1. Are you taking any medications on a regular basis?   Y / N
    (Exclusions include: Psychotropics, Antihistamines, Asthma Meds,
    Aldomet, Clonidine, Anti-Depressants, Anti-Anxiety Meds)

2. Any additional over- the -counter meds?   Y / N
    If yes, explain:

3. Do you have any disability or impairment that affects your arms or shoulders? Y / N
    (If yes, excludes.)

4. Have you had any broken bones, surgery, or injury to upper extremities?   Y / N
    If yes, explain:

5. Do you have arthritis? Does it cause pain or discomfort in your hands or arms? Y / N
    If yes to discomfort, excludes.

6. Have you had any significant medical problems within the last 10 years?   Y / N
    If yes, explain:

7. Do you have a history of neurological diseases likely to affect your ability to make
   reaching movements, including CVA (stroke), disc disease, peripheral neuropathy, or
   upper extremity weakness?
   If yes, exclude.   Y / N

116

8. Do you have any history of back problems, such as low back pain?　　　Y / N
　　　If yes, excludes.

9. Do you have any problems with standing balance?　　　Y / N
　　　If yes, excludes.

10. Do you have any drug and/or alcohol dependence?　　　Y / N
　　　If yes, excludes.

11. Do you have any significant visual impairments?　　　Y / N
　　　Examples: loss of binocular vision or the presence of double vision
　　　If yes, excludes.

12. Do you wear corrective lenses (glasses or contacts)?　　　Y / N
　　　If yes, are you (circle one):　　　Nearsighted / Farsighted
　　　If yes, do you wear bifocals:　　　Yes / No

13. Do you have any heart problems or coronary artery disease?　　　Y / N
　　　If yes, excludes.

14. Do you have hypertension?　　　Y / N
　　　If yes, excludes.

15. Do you have any lung or respiratory problems?　　　Y / N
　　　If yes, excludes.

16. Do you smoke? Pattern?　　　Y / N

17. Do you use alcohol? Pattern?　　　Y / N

18. Do you use caffeine (cola, coffee, etc.)? Pattern?　　　Y / N

19. Do you have any allergies that require medication?　　　Y / N
　　　If yes, explain.

Self-reported activity level:

How many times a week do you exercise?: _____

How long do you spend exercising on those days?: _____

What intensity level would you say you exercise at?: _____
　　　(e.g. "low", "moderate", or "hard")

APPENDIX B. HANDEDNESS SURVEY

IRB #:   **2005-02-0089**   **Subject ID:** _____

Which hand do you ***usually*** use to….

      Brush your teeth?   R _____   L _____

      Shave?   R _____   L _____

      Write?   R _____   L _____

      Move a computer mouse?   R _____   L _____

      Hold on top while using a broom?   R _____   L _____

      Hold your knife while cutting food?   R _____   L _____

      Throw a ball?   R _____   L _____

      Cut with scissors?   R _____   L _____

      Strike a match?   R _____   L _____

      Draw?   R _____   L _____

      Total: **R** _____   **L** _____

Criteria: Subjects must score at least 8 out of 10 for their right hand to be admitted to the study.

APPENDIX C: JOINT ANGLE CALCULATIONS

Locating Joint Centers (also see veldpaus.m)

The joint centers for the shoulder and elbow were found using the data from clusters of markers attached to the upper and lower arm using a least squares optimization method (Veldpaus, 1988). This is done by first, calculating the position of the center of the marker cluster, a, from a calibration trial.

$$a = \frac{1}{m}\sum_{i=1}^{m} a_i \qquad\qquad (C-1)$$

where m is the number of markers. Next, the distribution matrix, A, is calculated from equation 2. This matrix depends on the relative position vectors (a_i- a) of each of the markers with respect to the center.

$$A = \frac{1}{m}\sum_{i=1}^{m} (a_i - a)(a_i - a)^T \qquad\qquad (C-2)$$

These values do not change throughout the trial. For each frame of data, the new marker center, p, is calculated. From this we calculate the matrices G and P

$$\hat{G} = \frac{1}{m}\sum_{i=1}^{m} (\hat{p}_i - \hat{p})(a_i - a)^T \qquad\qquad (C-3)$$

$$\hat{P} = \frac{1}{m}\sum_{i=1}^{m} (\hat{p}_i - \hat{p})(\hat{p}_i - \hat{p})^T \qquad\qquad (C-4)$$

We then minimize the least squares function $f(\hat{r}, \hat{H})$ defined by:

$$f(\hat{r}, \hat{H}) = \frac{1}{m}\sum_{i=1}^{m} \left[\left(\hat{p}_i - a - \hat{r} - \hat{H}(a_i - a)\right)^T \times \left(\hat{p}_i - a - \hat{r} - \hat{H}(a_i - a)\right) \right] \qquad (C-5)$$

Where the vector $\hat{r}$ and the matrix $\hat{H}$ assumed to be the best approximations for the translation vector, r and the rotation matrix, R.

After much matrix manipulation, we find

$$\beta_1^2 - 2\beta_2 = g_1^2 \qquad\qquad (C-6)$$

$$\beta_2^2 = 2\beta_1 g_3 + g_2^2 \qquad\qquad (C-7)$$

119

Where

$$g_1{}^2 = tr(G^T G) = j_1 \qquad \text{(C-8)}$$

$$g_2{}^2 = tr(G^T G)^a = j_2 \qquad \text{(C-9)}$$

$$g_3 = \det(G) = j_3 \qquad \text{(C-10)}$$

Substituting these expressions, we get

$$\beta_1{}^2 - 2\beta_2 - j_1 = 0 \qquad \text{(C-11)}$$

$$\beta_2{}^2 - 2\beta_1 j_3 - j_2 = 0 \qquad \text{(C-12)}$$

which can then be solved in Matlab using optimization (veldpaus.m).

From these, we can find the rotation matrix R using

$$R = (G^a + \beta_1 G) \cdot C^{-1} \qquad \text{(C-13)}$$

where,

$$C = G^T G + \beta_2 I \qquad \text{(C-14)}$$

The translation vector, d can then be found using

$$d = p - a \qquad \text{(C-15)}$$

Finally, the location of the joint center (JC) is found as

$$JC = (\hat{R} \cdot (JC_{ref} - a)) + a + d \qquad \text{(C-16)}$$

The 3rd metacarpal joint center was found using the method described by (Rao et al., 1996). First, we define a unit vector from the ulnar styloid (UF) to the radial styloid (RF)

$$\vec{j}_h = \frac{\overrightarrow{RF} - \overrightarrow{UF}}{\left|\overrightarrow{RF} - \overrightarrow{UF}\right|} \qquad \text{(C-17)}$$

i_h is perpendicular to the plane containing RF, UF, and the fifth metatarsal head (5H)

$$k_{temp} = \frac{\overrightarrow{RF} - \overrightarrow{5H}}{\left|\overrightarrow{RF} - \overrightarrow{5H}\right|} \qquad \text{(C-18)}$$

$$\vec{i}_h = \vec{j}_h \times \overrightarrow{k_{temp}} \qquad \text{(C-19)}$$

120

And

$$\vec{k_h} = \vec{i_h} \times \vec{j_h}$$

(C-20)

Now we define a new plane with the third metacarpal

$$k_{temp} = \frac{\overrightarrow{RF} - \overrightarrow{3H}}{\left| \overrightarrow{RF} - \overrightarrow{3H} \right|}$$

(C-21)

$$\vec{i_{h2}} = \vec{j_h} \times \vec{k_{temp}}$$

(C-22)

$$\vec{k_{h2}} = \vec{i_{h2}} \times \vec{j_h}$$

(C-23)

Then we rotate the second plane about jh until it lies in the first plane

$$\theta = \vec{i_h} \bullet \vec{i_{h2}}$$

(C-24)

$$3JC = \begin{bmatrix} \cos\theta & 0 & -\sin\theta \\ 0 & 1 & 0 \\ \sin\theta & 0 & \cos\theta \end{bmatrix} \cdot 3H$$

(C-25)
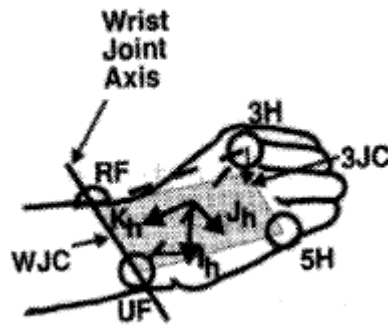
Illustration of the local coordinate system of the hand (from (Rao et al., 1996))

Defining Local Coordinate Systems

The coordinate system of the hand was defined according to Rao et al. (Rao et al., 1996).

Y_h: The line from the wrist joint center (WJC) to 3H

X_h: The line perpendicular to the plane formed by Y_h, RF and UF

Z_h: The common line perpendicular to the X_h and Y_h axis
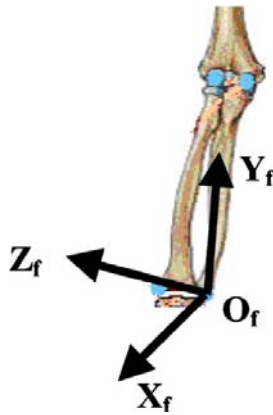
Illustration of the forearm coordinate system from (Wu et al.).

The coordinate system of the forearm was defined according to ISB recommendations (Wu et al., 2005)

O_h: The origin is at the ulnar styloid (UF)

Y_f: The line connecting the ulnar styloid to the joint center of the elbow pointing proximally

X_f: The line perpendicular to the plane through the ulnar styloid, radial styloid and midpoint between EL and EM, pointing forward

Z_h: The common line perpendicular to the X_f and Y_f axis, pointing to the right

The coordinate system of the humerus was defined using the 2nd option of ISB recommendations (Wu et al., 2005)

Y_h: The line connecting the shoulder joint center (SJC) and the elbow joint (EJC) center pointing toward SJC

122

Z_h: The common line perpendicular to the plane formed by Y_h and $Y_{f,}$ pointing to the

right.

X_h: The common line perpendicular to the Z_h and Y_h-axis, pointing forward

The coordinate system of the trunk was defined using (Hingtgen et al., 2006)

O_t: The origin is the midpoint between the left and right acromion processes

Z_t: The line from the left to right acromion processes

Y_t: A line perpendicular to the plane formed by Z_t and a line from the origin to the

clavicle

X_t: The common line perpendicular to the Y_t and Z_t axes

Calculating Joint Angles (also see jointangles.m)

The rotational transformation matrices were calculated from the unit vector matrices of

each coordinate system (Robertson et al., 2004).

$$T_d = \begin{bmatrix} i_{dx} & i_{dy} & i_{dz} \\ j_{dx} & j_{dy} & j_{dz} \\ k_{dx} & k_{dy} & k_{dz} \end{bmatrix} \tag{C-26}$$

$$T_p = \begin{bmatrix} i_{px} & i_{py} & i_{pz} \\ j_{px} & j_{py} & j_{pz} \\ k_{px} & k_{py} & k_{pz} \end{bmatrix} \tag{C-27}$$

Where T_d is the unit vector matrix for the distal segment and T_p is the unit vector matrix

for the proximal segment. The rotational transformation matrix is then

$$T_R = [T_D][T_P]^T = \begin{bmatrix} i_d \cdot i_p & i_d \cdot j_p & i_d \cdot k_p \\ j_d \cdot i_p & j_d \cdot j_p & j_d \cdot k_p \\ k_d \cdot i_p & k_d \cdot j_p & k_d \cdot k_p \end{bmatrix} \tag{C-28}$$

123

The rotation sequence for the humerus relative to the thorax (often referred to as the shoulder joint) (Wu, 2005) is Y-X-Y order
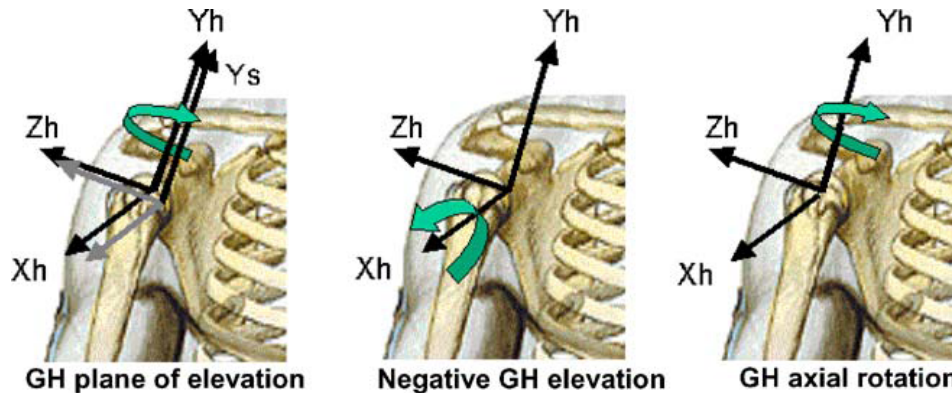
Illustration of glenohumeral (shoulder) joint angles (from (Wu et al., 2005)).

1) First, rotate γ_h about the Y_t axis

$$[R_y] = \begin{bmatrix} \cos\gamma & 0 & -\sin\gamma \\ 0 & 1 & 0 \\ \sin\gamma & 0 & \cos\gamma \end{bmatrix} \qquad (C\text{-}29)$$

2) Rotate β about the X_h axis

$$[R_x] = \begin{bmatrix} 1 & 0 & 0 \\ 0 & \cos\beta & \sin\beta \\ 0 & -\sin\beta & \cos\beta \end{bmatrix} \qquad (C\text{-}30)$$

3) Rotate γ_2 about the Y_h axis

$$[R_y] = \begin{bmatrix} \cos\gamma_2 & 0 & -\sin\gamma_2 \\ 0 & 1 & 0 \\ \sin\gamma_2 & 0 & \cos\gamma_2 \end{bmatrix} \qquad (C\text{-}31)$$

The angles are determined from the transformation matrix

$$\Re(t) = [R_{y2}] \cdot [R_x] \cdot [R_y] \qquad (C\text{-}32)$$

124

$$\mathfrak{R}(t) = \begin{bmatrix} \cos(\gamma_h)_2 & 0 & -\sin(\gamma_h)_2 \\ 0 & 1 & 0 \\ \sin(\gamma_h)_2 & 0 & \cos(\gamma_h)_2 \end{bmatrix} \begin{bmatrix} 1 & 0 & 0 \\ 0 & \cos\beta & \sin\beta_h \\ 0 & -\sin\beta_h & \cos\beta_h \end{bmatrix} \begin{bmatrix} \cos\lambda_h & 0 & -\sin\lambda_h \\ 0 & 1 & 0 \\ \sin\lambda_h & 0 & \cos\lambda_h \end{bmatrix} \quad \text{(C-33)}$$

$$\mathfrak{R}(t) = \begin{bmatrix} \cos\gamma_2\cos\gamma_1 - \sin\gamma_2\sin\gamma_1 & \sin\gamma_2\sin\beta & -\sin\gamma_1\cos\gamma_2 - \sin\gamma_2\cos\beta\cos\gamma_1 \\ \sin\beta\sin\gamma_1 & \cos\beta & \sin\beta\cos\gamma_1 \\ \cos\gamma_1\sin\gamma_2 + \sin\gamma_1\cos\gamma_2\cos\beta & -\sin\beta\cos\gamma_2 & -\sin\gamma_1\sin\gamma_2 + \cos\gamma_1\cos\gamma_2\cos\beta \end{bmatrix}$$

$$\text{(C-34)}$$

From here, the angles were calculated:

Plane Angle (about Y_h-axis):

$$\gamma_1(t) = \tan^{-1}\left(\frac{\mathfrak{R}_{2,1}/\sin\beta}{\mathfrak{R}_{2,3}/\sin\beta}\right) \quad \text{(C-35)}$$

Negative Elevation Angle (about X_h-axis):

$$\beta(t) = -\cos^{-1}(\mathfrak{R}_{2,2}) \quad \text{(C-36)}$$

Internal/External Rotation (about z''-axis):

$$\gamma_2(t) = \tan^{-1}\left(\frac{\mathfrak{R}_{1,2}/\sin\beta}{\mathfrak{R}_{3,2}/\sin\beta}\right) \quad \text{(C-37)}$$

Here we assume that sin(β) is negative.

The rotation sequence for the elbow and wrist was (Z-X-Y). This is solved similarly to the shoulder

$$\mathfrak{R}(t) = [R_y]\cdot[R_x]\cdot[R_z] \quad \text{(C-38)}$$

$$\mathfrak{R}(t) = \begin{bmatrix} \cos\alpha\cos\gamma - \cos\alpha\sin\beta\sin\gamma & \cos\alpha\sin\beta\sin\gamma - \cos\gamma\sin\alpha & \cos\beta\sin\gamma \\ \cos\beta\sin\alpha & \cos\alpha\cos\beta & -\sin\beta \\ \cos\gamma\sin\alpha\sin\beta - \cos\alpha\sin\gamma & \cos\alpha\cos\gamma\sin\beta - \sin\alpha\sin\gamma & \cos\beta\cos\gamma \end{bmatrix} \quad \text{(C-39)}$$

From here, the angles were calculated:

Flexion / Extension (about Z_h-axis):

$$\alpha(t) = \sin^{-1}\left(\Re_{2,3}\right)$$

(C-40)

Carrying Angle (Elbow) (about X_h'-axis):

$$\beta(t) = -\sin^{-1}\left(\frac{\Re_{1,3}}{\cos\alpha}\right)$$

(C-41)

Ulnar / Radial Deviation (Wrist)
Pronation / Supination (about Y_h-axis):

$$\gamma(t) = \sin^{-1}\left(\frac{\Re_{2,1}}{\cos\alpha}\right)$$

(C-42)

APPENDIX D: STATISTICS - SPSS CODE

Syntax code

```
GLM
s2 BY bin cond subject
/RANDOM = subject
/METHOD = SSTYPE(3)
/EMMEANS = TABLE(bin)
/EMMEANS = TABLE(cond)
/EMMEANS = TABLE(bin*cond) COMPARE(bin) ADJ(LSD)
/EMMEANS = TABLE(bin*cond) COMPARE(cond) ADJ(LSD)
/CRITERIA = ALPHA(0.05)
/DESIGN = bin cond bin*cond subject(bin) subject(cond).
```

Example output

Between-Subjects Factors

		N
bin	1	20
	2	20
	3	20
	4	20
	5	20
cond	1	50
	2	50
subject	1	10
	2	10
	3	10
	4	10
	5	10
	6	10
	7	10
	8	10
	9	10
	10	10

Tests of Between-Subjects Effects

Dependent Variable:s2

Source		Type III Sum of Squares	df	Mean Square	F	Sig.
Intercept	Hypothesis	901883.175	1	901883.175	288.660	.000
	Error	28203.304	9.027	3124.381[a]		
bin	Hypothesis	81.443	4	20.361	1.060	.391
	Error	691.768	36	19.216[b]		
cond	Hypothesis	3159.126	1	3159.126	1.013	.341
	Error	28077.378	9	3119.709[c]		
bin * cond	Hypothesis	61.166	4	15.291	1.051	.395
	Error	523.559	36	14.543[d]		
subject(bin)	Hypothesis	691.768	36	19.216	1.321	.204
	Error	523.559	36	14.543[d]		
subject(cond)	Hypothesis	28077.378	9	3119.709	214.512	.000
	Error	523.559	36	14.543[d]		

a. MS(subject(bin)) + MS(subject(cond)) - MS(Error)

b. MS(subject(bin))

c. MS(subject(cond))

d. MS(Error)

Expected Mean Squares[a,b]

Source	Variance Component			
	Var(subject(bin))	Var(subject(cond))	Var(Error)	Quadratic Term
Intercept	2.000	5.000	1.000	Intercept, bin, cond, bin * cond
bin	2.000	.000	1.000	bin, bin * cond
cond	.000	5.000	1.000	cond, bin * cond
bin * cond	.000	.000	1.000	bin * cond
subject(bin)	2.000	.000	1.000	
subject(cond)	.000	5.000	1.000	
Error	.000	.000	1.000	

a. For each source, the expected mean square equals the sum of the coefficients in the cells times the variance components, plus a quadratic term involving effects in the Quadratic Term cell.

b. Expected Mean Squares are based on the Type III Sums of Squares.

Estimated Marginal Means

1. bin

Dependent Variable:s2

bin	Mean	Std. Error	95% Confidence Interval	
			Lower Bound	Upper Bound
1	95.935	.853	94.206	97.665
2	95.928	.853	94.198	97.657
3	95.103	.853	93.373	96.832
4	94.119	.853	92.390	95.849
5	93.753	.853	92.023	95.482

2. cond

Dependent Variable:s2

cond	Mean	Std. Error	95% Confidence Interval	
			Lower Bound	Upper Bound
1	89.347	.539	88.253	90.441
2	100.588	.539	99.494	101.682

3. bin * cond

Estimates

Dependent Variable:s2

bin	cond	Mean	Std. Error	95% Confidence Interval	
				Lower Bound	Upper Bound
1	1	88.938	1.206	86.492	91.384
	2	102.933	1.206	100.487	105.379
2	1	89.943	1.206	87.497	92.389
	2	101.912	1.206	99.467	104.358
3	1	90.168	1.206	87.723	92.614
	2	100.037	1.206	97.591	102.483
4	1	89.058	1.206	86.612	91.504
	2	99.180	1.206	96.735	101.626
5	1	88.628	1.206	86.182	91.073
	2	98.878	1.206	96.432	101.324

Pairwise Comparisons

Dependent Variable:s2

cond	(I) bin	(J) bin	Mean Difference (I-J)	Std. Error	Sig.[a]	95% Confidence Interval for Difference[a]	
						Lower Bound	Upper Bound
1	1	2	-1.005	1.705	.559	-4.464	2.454
		3	-1.231	1.705	.475	-4.689	2.228
		4	-.120	1.705	.944	-3.579	3.339
		5	.310	1.705	.857	-3.149	3.769
	2	1	1.005	1.705	.559	-2.454	4.464
		3	-.225	1.705	.896	-3.684	3.233
		4	.885	1.705	.607	-2.574	4.344
		5	1.315	1.705	.446	-2.144	4.774
	3	1	1.231	1.705	.475	-2.228	4.689
		2	.225	1.705	.896	-3.233	3.684
		4	1.110	1.705	.519	-2.348	4.569
		5	1.541	1.705	.372	-1.918	4.999
	4	1	.120	1.705	.944	-3.339	3.579
		2	-.885	1.705	.607	-4.344	2.574
		3	-1.110	1.705	.519	-4.569	2.348
		5	.430	1.705	.802	-3.029	3.889
	5	1	-.310	1.705	.857	-3.769	3.149
		2	-1.315	1.705	.446	-4.774	2.144
		3	-1.541	1.705	.372	-4.999	1.918
		4	-.430	1.705	.802	-3.889	3.029
2	1	2	1.021	1.705	.553	-2.438	4.480
		3	2.896	1.705	.098	-.563	6.355
		4	3.753*	1.705	.034	.294	7.212
		5	4.055*	1.705	.023	.596	7.514
	2	1	-1.021	1.705	.553	-4.480	2.438
		3	1.876	1.705	.279	-1.583	5.334
		4	2.732	1.705	.118	-.727	6.191
		5	3.034	1.705	.084	-.424	6.493
	3	1	-2.896	1.705	.098	-6.355	.563
		2	-1.876	1.705	.279	-5.334	1.583
		4	.856	1.705	.619	-2.602	4.315
		5	1.159	1.705	.501	-2.300	4.618
	4	1	-3.753*	1.705	.034	-7.212	-.294
		2	-2.732	1.705	.118	-6.191	.727

	3	-.856	1.705	.619	-4.315	2.602
	5	.302	1.705	.860	-3.156	3.761
5	1	-4.055	1.705	.023	-7.514	-.596
	2	-3.034	1.705	.084	-6.493	.424
	3	-1.159	1.705	.501	-4.618	2.300
	4	-.302	1.705	.860	-3.761	3.156

Based on estimated marginal means

a. Adjustment for multiple comparisons: Least Significant Difference (equivalent to no adjustments).

*. The mean difference is significant at the 0.05 level.

Univariate Tests

Dependent Variable:s2

cond		Sum of Squares	df	Mean Square	F	Sig.
1	Contrast	17.980	4	4.495	.309	.870
	Error	523.559	36	14.543		
2	Contrast	124.628	4	31.157	2.142	.096
	Error	523.559	36	14.543		

Each F tests the simple effects of bin within each level combination of the other effects shown. These tests are based on the linearly independent pairwise comparisons among the estimated marginal means.

4. bin * cond

Estimates

Dependent Variable:s2

bin	cond	Mean	Std. Error	95% Confidence Interval	
				Lower Bound	Upper Bound
1	1	88.938	1.206	86.492	91.384
	2	102.933	1.206	100.487	105.379
2	1	89.943	1.206	87.497	92.389
	2	101.912	1.206	99.467	104.358
3	1	90.168	1.206	87.723	92.614
	2	100.037	1.206	97.591	102.483
4	1	89.058	1.206	86.612	91.504
	2	99.180	1.206	96.735	101.626
5	1	88.628	1.206	86.182	91.073
	2	98.878	1.206	96.432	101.324

Pairwise Comparisons

Dependent Variable:s2

bin	(I) cond	(J) cond	Mean Difference (I-J)	Std. Error	Sig.[a]	95% Confidence Interval for Difference[a]	
						Lower Bound	Upper Bound
1	1	2	-13.995[*]	1.705	.000	-17.454	-10.536
	2	1	13.995[*]	1.705	.000	10.536	17.454
2	1	2	-11.970[*]	1.705	.000	-15.428	-8.511
	2	1	11.970[*]	1.705	.000	8.511	15.428
3	1	2	-9.868[*]	1.705	.000	-13.327	-6.410
	2	1	9.868[*]	1.705	.000	6.410	13.327
4	1	2	-10.123[*]	1.705	.000	-13.581	-6.664
	2	1	10.123[*]	1.705	.000	6.664	13.581
5	1	2	-10.250[*]	1.705	.000	-13.709	-6.791
	2	1	10.250[*]	1.705	.000	6.791	13.709

Based on estimated marginal means

*. The mean difference is significant at the 0.05 level.

a. Adjustment for multiple comparisons: Least Significant Difference (equivalent to no adjustments).

Univariate Tests

Dependent Variable:s2

bin		Sum of Squares	df	Mean Square	F	Sig.
1	Contrast	979.342	1	979.342	67.340	.000
	Error	523.559	36	14.543		
2	Contrast	716.345	1	716.345	49.256	.000
	Error	523.559	36	14.543		
3	Contrast	486.936	1	486.936	33.482	.000
	Error	523.559	36	14.543		
4	Contrast	512.325	1	512.325	35.228	.000
	Error	523.559	36	14.543		
5	Contrast	525.343	1	525.343	36.123	.000
	Error	523.559	36	14.543		

Each F tests the simple effects of cond within each level combination of the other effects shown. These tests are based on the linearly independent pairwise comparisons among the estimated marginal means.

132

APPENDIX E: MATLAB CODE

Least Squares Optimization Program: veldpaus.m

```matlab
%==========================================================================
% Deanna Gates
% Last modified: 1/3/07
% Description: Uses the least squares method given in, Veldpaus, F. 'A least-sqares algorithm for the
equiform transformation from spatial marker coordinates' J. Biomechanics 21, 45-54. 1988.
% to find the transformation matrix from global to local coordinates

%Input: A matrix of marker data (MK), size Nx12 [RUP1 RUP2 RUP3 RUP4] and
%the position of the cluster markers and joint center during calibration.
%Ouput: The position of the joint center at each instance in time
%==========================================================================
function jc = veldpaus(MK, MK_ref, jc_ref)

global h1 h2

m = 4;  %Number of markers in the cluster
N=length(MK); %Find the length of the data

%Fix matrix size
j=1;
for i=1:m
    ai(:,i) = MK_ref(1,j:j+2)';
    j=j+3;
end

%Find the postition of the center Po of the marker distribution at calibration time (eq. 2.1)
a = mean(ai,2);

for i=1:N
    sump = MK(i,1:3)' + MK(i,4:6)' + MK(i,7:9)' + MK(i,10:12)';
    p = (1/m)*sump; % p is position measured at time=i (equation 3.3)

    j=1;
    for k=1:m
%Find the distribution matrix A of the relative position of markers with respect to the middle at t=0 (eq.
2.2)
        Atemp(:,:,k) = (ai(:,k)-a)*(ai(:,k)-a)';

        %G is the difference between relative measured position at t=0 and t=i (equation 3.4)
        Gtemp(:,:,k) = (MK(i,j:j+2)'-p)*(ai(:,k)-a)';

%Find the distribution matrix P of the relative position of markers with respect to the middle for time=i (eq.
3.5)
        Ptemp(:,:,k) = (MK(i,j:j+2)'-p)*(MK(i,j:j+2)'-p)';
        j=j+3;
    end
```

133

```matlab
    A = mean(Atemp,3);
    G = mean(Gtemp,3);
    P = mean(Ptemp,3);

    %Check the rank of G to ensure that it is greater than 2
     if rank(G)>2
        g1 = sqrt(trace(G'*G)); %4.12
        g2 = sqrt(trace(adjoin(G'*G)));
        g3 = det(G);
        h1 = g2/(g1^2);
        h2 = (g1*g3)/g2^2;
        %Next, call an optimization routine.
        x0 = [1; 1];          % Make a starting guess at the solution
        options = optimset('TolFun', 10^-10, 'Display','off');
        x = fsolve(@veld,x0,options);
        beta1 = x(1)*g1;
        beta2 = x(2)*g2;
        D = G'*G + beta2*eye(3);  %equation 4.9
        R1 = (adjoin(G) + beta1*G)*inv(D); %equation 4.10

        d1 = p - a; %Translation vector of the center of the cluster
        s= beta1/trace(A); %should be close to one.  Then it behaves like a rigid body

        jc(i,:) = ((R1*(jc_ref(1,1:3)'- a)) + a + d1)';
     end
end
```

veld.m
```matlab
function F = veld(x)
global h1 h2
F= [(x(1)^2 - 2*h1*x(2) - 1); (x(2)^2 -2*h2*x(1) - 1)];
```

134

Joint Angle Program: jointangles.m

```
%==============================================================
% Deanna Gates
% Written: 5/24/06
% Last Modified: 10/6/06

% Calculate the three dimensional joint angles
% This requires the function file findnorm.m to calculate unit vectors
% Lab coordinate system  + X-Axis is direction of push, + Y-Axis - right arm across body,
%                  + Z-Axis - up
% Input: Mat file with smooth trajectories from calmarkerdata.m
%==============================================================
clear, close all
warning off

%File information

for trial =[1:40]
    %File Information
    datadir = 'C:\ViconData\NoBiLab\P0020\CSV Files\';
    subjectids = ['P06l'; 'P06g'; 'P07l'; 'P07g'; 'S01l'; 'S01g'; 'S02l'; 'S02g'; 'S03l'; 'S03g';.
                'S04l'; 'S04g'; 'S05l'; 'S05g'; 'S06l'; 'S06g'; 'S08l'; 'S08g'; 'S11l'; 'S11g'; ...
                'S12l'; 'S12g'; 'S13l'; 'S13g'; 'S14g'; 'S14l'; 'S15l'; 'S15g'; 'S16g'; 'S16l';...
                'S17g'; 'S17l'; 'S18l'; 'S18g'; 'S19l'; 'S19g'; 'S20l'; 'S20g'; 'S09g'; 'S09l'];
    Circums = [32.0 32.0 38.0 38.0 37.5 37.5 25.5 25.5 32.0 32.0 ...
            40.0 40.0 44.5 44.5 31.0 31.0 39.0 39.0 28.5 28.5 ...
            35.5 35.5 32.0 32.0 39.0 39.0 39.5 39.5 37.5 37.5 ...
            35.5 35.5 43.0 43.0 41.0 41.0 39.0 39.0 38.5 38.5];

    subjectid = subjectids(trial,:);
    Circum = Circums(trial);
    TrialType = 'Pre';

    %Read in the matfile of marker trajectories
    load([datadir 'Marker Data\' subjectid '_' TrialType '_m15.mat']);
    %Read in the matfile of joint centers
    load([datadir 'Joint Angles\' subjectid '_' TrialType '_jc15.mat']);

    %Filter Joint Centers
    sampfreq = 120; cutoff =15; %choose lowpas cuttoff (Hz)
    [b,a] = butter(5, (2 * cutoff) / sampfreq);
    R3JC = filtfilt(b,a,R3JC);    ELJC = filtfilt(b,a,ELJC);    SHJC = filtfilt(b,a,SHJC);

    %++++++++++++++++++ Joint Coordinate Systems +++++++++++++++++++++++++++++++++++
    % Follows 2.3.6 of G. Wu et al., 2005 'ISB recommendations...'

    %****** Coordinate System of Hand (Metatarsals) *******
    %Definition of coordinate system taken from Rao et al. 1996
    WRJC = (RWRA + RWRB)/2;
    USRS = RWRA - RWRB;
    Ym = findnorm(R3JC, WRJC);
    Xm = -cross(USRS,Ym);
```

135

```matlab
Xm = Xm./repmat(sqrt(sum(Xm.^2,2)),1,3);
Zm = cross(Xm,Ym);
 %****** Coordinate System of Forearm *******
% Origen at ulnar styloid (RWRB)

%The Y axis of the forearm, Yf, is the line connecting the ulnar styloid to the joint center of the elbow
pointing proximally
Yf = findnorm(RWRB,ELJC);

%The X-axis of the forearm, Xf, is the line perpendicular to the plane through the ulnar styloid, radial
styloid and midpoint between EL and EM pointing forward
Xf = cross(Yf,USRS);    Xf = Xf./repmat(sqrt(sum(Xf.^2,2)),1,3);
%Z-axis is common line perpendicular to the Xf and Yf-axis, pointing to the right.
Zf = cross(Xf,Yf);

%****** Coordinate System of Humerus *******
%ISB guidelines 2nd option (section 2.3.5)

%The Y axis of the humerus, Yh, is the line connecting shoulder joint center and the elbow joint center
pointing toward the SHJC
Yh = findnorm(ELJC,SHJC);
%Z-axis is common line perpendicular to the plane formed by Yh and Yf pointing to the right.
Zh = cross(Yh,Yf); Zh = Zh./repmat(sqrt(sum(Zh.^2,2)),1,3);
    %The X-axis of the humerus, Xh, is the common line perpendicular to the Zh and Yh-axis, pointing
forward
Xh = cross(Yh,Zh);

%****** Coordinate System of Trunk *******
%Taken form Hingtgen et al. 2006
%Origen in midpoint between acromium markers
tc=1/2*(RSHO+LSHO);
Zt=findnorm(LSHO,RSHO);
temp=findnorm(tc,CLAV);
Yt = cross(Zt,temp); Yt = Yt./repmat(sqrt(sum(Yt.^2,2)),1,3);
clear temp
Xt = cross(Yt,Zt);

%+++++++++++++++++++++++++++ Rotation Matrices +++++++++++++++++++++++++++++++
%Origin of local coordinate systems (for figures)
dm = WRJC;
dt = CLAV;
df = RWRB + repmat(0.57*distance(RWRB,ELJC),1,3).*Yf;
dh = SHJC - repmat(0.436*distance(ELJC,SHJC),1,3).*Yh;

% preallocate space to save memory
elbowangles = zeros(length(Xm),3); wristangles = zeros(length(Xm),3);
shoangles = zeros(length(Xm),3);

for i=1:length(Xf)

    Rm = 52; %For the wrist
    Rf = [Xf(i,:); Yf(i,:); Zf(i,:)]; %For the forearm
    Rh = [Xh(i,:); Yh(i,:); Zh(i,:)]; %For the humerus
    Rt = [Xt(i,:); Yt(i,:); Zt(i,:)]; %For the thorax
```

```matlab
         %Rotation matrix where hand is distal segment and forearm is proximal
        RotWrist = Rm*Rf';
        %Rotation matrix where forearm is distal segment and humerus is proximal
        RotElbow = Rf*Rh';
        %Rotation matrix where humerous is distal segment and thorax is proximal
        RotSho = Rh*Rt';

        %Motion for the wrist joint (hand relative to forearm Z-X-Y order
        wristangles(i,:) = rot_zxy(RotWrist);
        %Motion for the elbow joint (forearm relative to humerus, Z,X,Y order)
        elbowangles(i,:) = rot_zxy(RotElbow);
        %Motion for the shoulder joint (humerus relative to thorax Y-X-Y order)
        shoangles(i,:) = rot_yxy(RotSho);
    end

    elbowangles(:,3) = elbowangles(:,3) + repmat(90,length(elbowangles),1);

    save([datadir 'Joint Angles\' subjectid '_' TrialType '_jointangles15.mat'], 'shoangles','elbowangles',
'wristangles')
    clear
end
```

Timing Errors Code: DFA_Timing Errors.m

```matlab
%=======================================================================%
%Written by Deanna Gates on 11/21/06

% DFA timing errors
% Input:  1) HAND marker mins /maxs from file Subject#_TrialType_minmax1080.mat
%         2) Metronome data from csv file (example 'S18_low_force.csv ')
% Output: 1) Error between measurements and 2) Alpha values from DFA analysis
% This code requires the function files:  1. gemanalysis.m, 2. findnorm.m, 3. DFA.m
%=======================================================================%
clear, close all

for subject = 1:14
    %File information
    datadir = 'C:\Documents and Settings\Deanna\My Documents\P0008\GEM Paper\Data Files\';
    subjectids = ['S02'; 'S03'; 'S07'; 'S08'; 'S09'; 'S11';'S13';'S14'; 'S16'; 'S17'; 'S18'; 'S22';'S01';'P08'];
    TrialType = 'low';
    subjectid = subjectids(subject,:);
    Height = [1.6 1.73 1.88 1.88 1.61 1.66 1.565 1.665 1.73 1.8 1.66 1.79 1.685 1.82];
    ArmLength = Height(subject);

    %Import MET data
    load([datadir 'Metronome Data\' subjectid '_' TrialType '_MET.mat']); pack

    %Find location of beeps from Metronome
    try Met=Metdata;
        catch
    end
    k=1;
    for i=1:length(Met)-1
        if Met(i)>1
            if k ==1
                ind(k)=i;
                k=k+1;
                %Make sure that the next max is at least 50 points away
            elseif k>1 & i - ind(k-1) > 50
                ind(k) = i;
                k=k+1;
            end
        end
    end

%Import min/max from HAND marker trajectories
    load([datadir 'Marker Data\' subjectid '_' TrialType '_m20.mat']);
    %Up sample the hand data to 1080 Hz
    xi = (1:length(HAND))./60;
    xf = (1:length(HAND)*18)./1080;
    HAND_up = interp1(xi,HAND,xf,'cubic');

    %load min/max
    load([datadir 'MinMax\' subjectid '_' TrialType '_minmax1080.mat']);
    %----------------Calculate Basic Parameters (Distance/Velocity/Cycle Time)-------------------------
```

```matlab
for i=2:length(Mins)-1
    if Maxs(i)<Mins(i)
        CycleTime(i-1) = (Maxs(i+1)-Mins(i)).*(1/1080);
        Dist(i-1) = (HAND_up(Maxs(i+1),1) - HAND_up(Mins(i),1))/1000;
        Vel(i-1) = Dist(i-1)/CycleTime(i-1);
    else
        CycleTime(i-1) = (Maxs(i)-Mins(i)).*(1/1080);
        Dist(i-1) = (HAND_up(Maxs(i),1) - HAND_up(Mins(i),1))/1000;
        Vel(i-1) = Dist(i-1)/CycleTime(i-1);
    end
end
Dist = Dist/ArmLength;
freq = 1 / (mean(diff(ind))/1080);
Vel = Vel / (ArmLength * freq);

% Determine the GEM
[perpindist meandist] = gemanalysis(Dist',Vel',1);
X = Dist';
Y=Vel';
slope = freq/freq;
x = 0:0.01:0.6;
gem = slope*x;
neggem = -(1/slope)*x ;
num = 224;

% Perform DFA Analysis on Pre-Fatigue Data
figure(subject)
[npre Fpre spre Rpre ppre] = DFA(perpindist(2:num+1,1));
[npre2 Fpre2 spre2 Rpre2 ppre2] = DFA(meandist(2:num+1,1));
[ndpre Fdpre sdpre Rdpre pdpre] = DFA(Dist(2:num+1));
[nvpre Fvpre svpre Rvpre pvpre] = DFA(Vel(2:num+1));

% Perform DFA Analysis on Post-Fatigue Data
[npost Fpost spost Rpost ppost ] = DFA(perpindist(end-num:end-1,1));
[npost2 Fpost2 spost2 Rpost2 ppost2] = DFA(meandist(end-num:end-1,1));
[ndpost Fdpost sdpost Rdpost pdpost] = DFA(Dist(end-num:end-1));
[nvpost Fvpost svpost Rvpost pvpost] = DFA(Vel(end-num:end-1));

SD_perp = [std(perpindist(2:num+1,1)) std(perpindist(end-num:end-1,1))];
SD_mean = [std(meandist(2:num+1,1)) std(meandist(end-num:end-1,1))];

Mean_perp = [mean(perpindist(2:num+1,1)) mean(perpindist(end-num:end-1,1))];
Mean_mean = [mean(meandist(2:num+1,1)) mean(meandist(end-num:end-1,1))];

%----------------------- Calculate the timing error-------------------------------------------------------
t = 1:length(HAND_up);
Marker_ind = sort([Mins Maxs]);

%Find places where they missed the beep
for i=1:length(Marker_ind)
    %look around it and see which point is closest
    temperror = ind  - Marker_ind(i);
    [k m] = min(abs(temperror));
    error(i) = (ind(m)-Marker_ind(i))./1080;
```

139

```
    end

    %Pre / Post
  [npre3 Fpre3 spre3 Rpre3 ppre3] = DFA(error(2:num*2+1));
  [npost3 Fpost3 spost3 Rpost3 ppost3] = DFA(error(end-num*2:end-1));

  SD_error = [std(error(2:num*2+1)) std(error(end-num*2:end-1))];
  SD_dist = [std(Dist(1,2:num+1)) std(Dist(1,end-num:end-1))];;
  SD_vel = [std(Vel(2:num+1)) std(Vel(end-num:end-1))];

  Mean_error = [mean(error(2:num*2+1)) mean(error(end-num*2:end-1))];
  Mean_dist = [mean(Dist(1,2:num+1)) mean(Dist(1,end-num:end-1))];;
  Mean_vel = [mean(Vel(2:num+1)) mean(Vel(end-num:end-1))];
  table = [npre' Fpre' npost' Fpost' npre2' Fpre2' npost2' Fpost2' ndpre' Fdpre' ndpost' Fdpost' nvpre' Fvpre'
nvpost' Fvpost'];
  table2 = [npre3' Fpre3' npost3' Fpost3'];


  Rtable = [Rpre ppre Rpost ppost Rpre2 ppre2 Rpost2 ppost2 Rdpre pdpre Rdpost ...
       pdpost Rvpre pvpre Rvpost pvpost Rpre3 ppre3 Rpost3 ppost3];
   save([datadir subjectid '_' TrialType '_DFAresults_all3.mat'], 'npre', 'Fpre','spre', 'npre2', 'Fpre2', 'spre2',
'npost', 'Fpost', 'spost', 'npost2', 'Fpost2', 'spost2','ndpre','Fdpre','sdpre','nvpre','Fvpre','svpre', 'ndpost',
'Fdpost', 'sdpost','nvpost','Fvpost','svpost', 'npre3', 'Fpre3', 'spre3', 'npost3', 'Fpost3', 'spost3')
   save([datadir subjectid '_' TrialType '_VAR2.mat'], 'SD_mean', 'SD_perp', SD_error','SD_dist','SD_vel')
   save([datadir subjectid '_' TrialType '_MEAN2.mat'], 'Mean_mean', 'Mean_perp', 'Mean_error',
'Mean_dist', 'Mean_vel')
   save([datadir subjectid '_' TrialType '_timing.mat'], 'error', 'Dist', 'Vel','perpindist','meandist')
   save([datadir subjectid '_' TrialType '_Rtable.mat'], 'Rtable')
   clear
end
```

Goal Equivalent Manifold Analysis Code: gemanalysis.m

```matlab
%=========================================================================%
%Written by Deanna Gates 3/28/06

% This code decomposes errors in X and Y into deviations (delta) tangent and
% perpindicular to the goal equivalent manifold (GEM)
% Input:  1) column vectors of X and Y data,  2) slope (GEM)
% Output: 1) Delta decomposed into two directions
%=========================================================================
function [delta_p delta_t] = gemanalysis(X, Y, slope)

N = length(X);

%Plot Error and GEM
x = min(X):0.01:max(X);
gem = slope*x;
yi = mean(Y) + slope*mean(X);
neggem = -slope*x + yi;

%Define unit vectors perpindicular and tangent to the GEM
et = findnorm([0 0 0], [1 slope 0]);
ep = findnorm([0 0 0], [-slope 1 0]);

%Make a vector for all points
p = [X Y zeros(N,1)];

%Calculate distance using a dot product
delta_p = dot(repmat(ep,N,1),p,2);
delta_t = dot(repmat(et,N,1),p,2);
```

141

Detrended Fluctation Analysis Code: DFA.m

```
%=======================================================================
% Written by Deanna Gates, 12/1/05
% Modified 6/30/06 to calculate the error by starting the bins at the beginning of the trial and then % by
starting at the end and taking the average of the two (to reduce error of small bins at end).
% Modified 7/5/06 to split into 50 bins evenly distributed from 4 to 400 on log-log scale.
% Modified 12/4/07 to give the adjusted R2 values for the n v F plot for a linear, quadratic, and  cubic
regression

% Input: A column vector of time series of data (stride times) and the order of the fit within the bins.  Set to
1 for a linear fit as a default
% Output:
% 1) n1 which contains the bin lengths used.
% 2) F1 which contains the RMS fluctuation of the detrended time series corresponding to each  bin
length,n
3) p1, the fit for log(n) vs. log(F).  p1(1,1) is the scaling exponent
% 4) Rvals are the R2 values for the constant term R2 = 0, linear fit,
% quadratic fit and cubic fit
% 5) pvals, the p value for the constant term, linear term, squared term
% and cubed term of the regression
 =======================================================================
function [n1 F1 p1 Rvals pvals]=DFA(x,o)

% order of the polynomial to fit the data in each window
try order = o;
   catch order = 1;
end

warning off

N=length(x); %number of points in time series

%integrate the entire time series
M=mean(x);
for k=1:N
   y_int(k,1) = sum(x(1:k) - M); %make column vector of integrated series
end

%binlength=round(logspace(log10(4),log10(56),35));%After removing duplicate points, this finds
% 25 equally spaced points on log-log scale between 4 and 50
binlength = round(logspace(log10(4),log10(N/4),20)); %After removing duplicate points, this finds
% 50 equally spaced points on log-log scale between 4 and 400

% initialize matrices
error=zeros(N,length(binlength));
yn=zeros(N,length(binlength));
yn2=zeros(N,length(binlength));

%Calculate the root-mean square fluctuation of the detrended series for all possible bin sizes
for i=1:length(binlength)
```

```matlab
    n(i)=binlength(i);
    %Do a least squares fit to the data for each bin
    k=(1:N)'; % A column vector representing the x-axis, or index of the time series
    j=1;
    while j<N
        temparray=j:j+(n(i)-1);
        b=temparray(find(temparray<=N)); %If number of bin size is not even, cut off extra points and fit the
partial bin at the end
        p=polyfit(k(b,1),y_int(b,1),order); %fit the time series for the bin
        yn(b,i)=polyval(p,k(b,1)); %find the value of the straight line at each k
        j=j+n(i);
        clear p b
    end
    error(:,i) = y_int(:,1)-yn(:,i); %find the difference between the integrated time series and the best fit line
end
 %Repeat, starting from the end of the data
for i=1:length(binlength)
    n(i)=binlength(i);
    %Do a least squares fit to the data for each bin
    k=(1:N)'; % A column vector representing the x-axis, or index of the time series
    j=N;
    while j>0
        temparray=j-(n(i)-1):j;
        b=temparray(find(temparray>0)); %If number of bin size is not even, cut off extra points and fit the
partial bin at the end
        p=polyfit(k(b,1),y_int(b,1),order); %fit the time series for the bin
        yn2(b,i)=polyval(p,k(b,1)); %find the value of the straight line at each k
        j=j-n(i);
        clear p b
    end
    error2(:,i) = y_int(:,1)-yn2(:,i); %find the difference between the integrated time series and the best fit
line
end

%Sum the detrended time series for each k (column)
S1=(1/N)*sum(error.^2);
S2=(1/N)*sum(error2.^2);
S=(S1+S2)/2;

%Calculate the RMS fluctuation of the detrended series
F=S.^0.5;

z=1;
for i=2:length(binlength)     %Remove all duplicate bin lengths (may exist due to rounding).
    if n(i)>n(i-1)
        n1(z)=n(i);
        F1(z)=F(i);
        z=z+1;
    end
end

%Find the scaling exponent, p1(1,1) (the slope of a linear line relating log(F) to log(n))
[p1] = polyfit(log10(n1),log10(F1),1);
```

```
[R2_linear R2adj_quad R2adj_cubic] = adjRsquare(log10(n1)',log10(F1)');

%Are the fits significant?
xs = log10(n1)' - repmat(mean(log10(n1)),length(n1),1);
x = [xs xs.^2 xs.^3];
[Coefficients, S_err, XTXI, R_sq, F_val, Coef_stats, Y_hat, residuals, covariance] = mregress(log10(F1)',x,
1);

Rvals = [ 0; R2_linear; R2adj_quad; R2adj_cubic];
pvals = Coef_stats(:,4);
```

References

Alizadehkhaiyat, O., Fisher, A.C., Kemp, G.J., Frostick, S.P., 2007. Strength and fatigability of selected muscles in the upper limb: Assessing muscle imbalance relative to tennis elbow. Journal of Electromyography and Kinesiology 4, 428-36.

Arihara, M., Sakamoto, K., 1999. Contribution of motor unit activity enhanced by acute fatigue to physiological tremor of finger. Electromyography and Clinical Neurophysiology 39, 235-247.

Aschersleben, G., 2002. Temporal control of movements in sensorimotor synchronization. Brain and Cognition 48 (1), 66-79.

Barr, A.E., and Barbe, A.F., 2002. Pathophysiological tissue changes associated with repetitive movement: A review of the evidence. Physical Therapy 82 (2), 173-187.

Basmajian, J., DeLuca, C.J., 1985. Muscles alive: Their functions revealed by electromyography. Lippincott Williams & Wilkins, Philadelphia, PA.

Beukeboom, C., Birmingham, T.B., Forwell, L., Ohrling, D., 2000. Asymmetrical strength changes and injuries in athletes training on a small radius curve indoor track. Clin J Sport Med 10 (4), 245-50.

Bigland-Ritchie, B., Woods, J.J., 1984. Changes in muscle contractile properties and neural control during human muscular fatigue. Muscle Nerve 7 (9), 691-699.

Billaut, F., Basset, F.A., Falgairette, G., 2005. Muscle coordination changes during intermittent cycling sprints. Neuroscience Letters 380 (3), 265-269.

Bock, O., 1993. Early stages of load compensation in human aimed arm movements. Behavioral Brain Research 55 (1), 61-68.

Boden, L.I., Galizzi, M., 1999. Economic consequences of workplace injuries and illnesses: Lost earnings and benefit adequacy. American Journal of Industrial Medicine 36 (5), 487-503.

Bonnard, M., Sirin, A.V., Oddsson, L., Thorstensson, A., 1994. Different strategies to compensate for the effects of fatigue revealed by neuromuscular adaptation processes in humans. Neuroscience Letters 166 (1), 101-105.

Borg, G.A., 1974. Perceived exertion. Exercise and Sports Science Review 2, 131-153.

Borg, G.A., 1982. Psychophysical bases of perceived exertion. Medicine and Science in Sports and Exercise 14 (5), 377-381.

Bove, M., Tacchino, A., Novellino, A., Trompetto, C., Abbruzzese, G., Ghilardi, M.F., 2007. The effects of rate and sequence complexity on repetitive finger movements. Brain Research 1153, 84-91.

Bowman, T.G., Hart, J.M., McGuire, B.A., Palmier, R.M., Ingersoll, C.D., 2006. A functional fatiguing protocol and deceleration time of the shoulder from an internal rotation perturbation. Journal of Athletic Training 41 (3), 275-279.

Bruijn, S.M., van Dieën, J.H., Meijer, O.G., Beek, P.J., 2009. Statistical precision and sensitivity of measures of dynamic gait stability. Journal of Neuroscience Methods 178 (2), 327 - 333.

Burgess-Limerick, R., 2003. Squat, stoop, or something in between? International Journal of Industrial Ergonomics 31 (3), 143-148.

Burnham, R.S., May, L., Nelson, E., Steadward, R., Reid, D.C., 1993. Shoulder pain in wheelchair athletes. The role of muscle imbalance. American Journal of Sports Medicine 21 (2), 238-42.

Butterfield, T.A., Herzog, W., 2005. Quantification of muscle fiber strain during in vivo repetitive stretch-shortening cycles. J Appl Physiol 99 (2), 593-602.

Buzzi, U.H., Stergiou, N., Kurz, M.J., Hageman, P.A., Heidel, J., 2003. Nonlinear dynamics indicates aging affects variability during gait. Clinical Biomechanics 18 (5), 435-443.

Chen, Y., Ding, M., Kelso, J.A.S., 1997. Long memory processes ($1/f^{\alpha}$ type) in human coordination. Physical Review Letters 79 (22), 4501-4504.

Clewley, R.H., Guckenheimer, J.M., Valero-Cuevas, F.J., 2008. Estimating effective degrees of freedom in motor systems. IEEE Transactions on Biomedical Engineering 55 (2), 430-442.

Corbeil, P., Blouin, J., Begin, F., Nougier, V., Teasdale, N., 2003. Perturbation of the postural control system induced by muscular fatigue. Gait Posture 18, 92-100.

Corcos, D.M., Jiang, H.Y., Wilding, J., Gottlieb, G.L., 2002. Fatigue induced changes in phasic muscle activation patterns for fast elbow flexion movements. Experimental Brain Research 142 (1), 1-12.

Côté, J.N., Mathieu, P.A., Levin, M.F., Feldman, A.G., 2002. Movement reorganization to compensate for fatigue during sawing. Experimental Brain Research 146 (3), 394-398.

Côté, J.N., Raymond, D., Mathieu, P.A., Feldman, A.G., Levin, M.F., 2005. Differences in multi-joint kinematic patterns of repetitive hammering in healthy, fatigued and shoulder-injured individuals. Clinical Biomechanics 20 (6), 581-590.

Cusumano, J.P., Cesari, P., 2006. Body-goal variability mapping in an aiming task. Biological Cybernetics 94 (5), 367-79.

Daffertshofer, A., Lamoth, C.J.C., Meijer, O.G., Beek, P.J., 2004. Pca in studying coordination and variability: A tutorial. Clinical Biomechanics 19 (4), 415-428.

DeLuca, C.J., 1984. Myoelectrical manifestations of localized muscular fatigue in humans. Critical Reviews in Biomedical Engineering 11 (4), 251-279.

DeLuca, C.J., 1997. The use of surface electromyography in biomechanics. Journal of Applied Biomechanics 13, 135-163.

Ding, M., Chen, Y., Kelso, J.A.S., 2002. Statistical analysis of timing errors. Brain Cognition 48 (1), 98-106.

Dingwell, J., Robb, R., Troy, K., Grabiner, M., 2008. Effects of an attention demanding task on dynamic stability during treadmill walking. Journal of NeuroEngineering and Rehabilitation 5 (1), 12.

Dingwell, J.B., Cusumano, J.P., 2000. Nonlinear time series analysis of normal and pathological human walking. Chaos 10 (4), 848-863.

Dingwell, J.B., Cusumano, J.P., Sternad, D., Cavanagh, P.R., 2000. Slower speeds in neuropathic patients lead to improved local dynamic stability of continuous overground walking. Journal of Biomechanics 33 (10), 1269-1277.

Dingwell, J.B., Kang, H.G., 2007. Differences between local and orbital dynamic stability during human walking. Journal of Biomechanical Engineering 129, 586-593.

Dingwell, J.B., Kang, H.G., Marin, L.C., 2007. The effects of sensory loss and walking speed on the orbital dynamic stability of human walking. Journal of Biomechanics 40 (8), 1723-1730.

Dingwell, J.B., Marin, L.C., 2006. Kinematic variability and local dynamic stability of upper body motions when walking at different speeds. Journal of Biomechanics 39 (3), 444 - 452.

Donelan, J.M., Shipman, D.W., Kram, R., Kuo, A.D., 2004. Mechanical and metabolic requirements for active lateral stabilization in human walking. Journal of Biomechanics 37 (6), 827 - 835.

England, S.A., Granata, K.P., 2007. The influence of gait speed on local dynamic stability of walking. Gait & Posture 25 (2), 172 - 178.

Falconer, K., Winter, D., 1985. Quantitative assessment of cocontraction at the ankle joint during walking. Electromyography and Clinical Neurophysiology 25, 135-149.

Farina, D., Fattorini, L., Felici, F., Filligoi, G., 2002. Nonlinear surface emg analysis to detect changes of motor unit conduction velocity and synchronization. Journal of Applied Physiology 93, 1753-1763.

Forestier, N., Nougier, V., 1998. The effects of muscular fatigue on the coordination of a multijoint movement in human. Neuroscience Letters 252 (3), 187-190.

Franklin, D.W., So, U., Kawato, M., Milner, T.E., 2004. Impedance control balances stability with metabolically costly muscle activation. Journal of Neurophysiology 92 (5), 3097-105.

Fraser, A.M., Swinney, H.L., 1986. Independent coordinates for strange attractors from mutual information. Physical Review A 33 (2), 1134-1140.

Freund, H.J., 1983. Motor unit and muscle activity in voluntary motor control. Physiol Rev 63, 387-436.

Friden, J., Seger, J., Ekblom, B., 1988. Sublethal muscle fibre injuries after high-tension anaerobic exercise. European Journal of Applied Physiology 57, 360-368.

Frost, G., Dowling, J., Dyson, K., Bar-Or, O., 1997. Cocontraction in three age groups of children during treadmill locomotion. Journal of Electromyography and Kinesiology 7 (3), 179-186.

Full, R.J., Kubow, T., Schmitt, J., Holmes, P., Koditschek, D.E., 2002. Quantifying dynamic stability and maneuverability in legged locomotion. Integrative and Comparative Biology 42 (1), 149-157.

Gandevia, S.C., 2001. Spinal and supraspinal factors in human muscle fatigue. Physiological Review 81 (4), 1725-1789.

Gardner-Morse, M.G., Stokes, I.A.F., 1998. The effects of abdominal muscle coactivation on lumbar spine stability. Spine 23 (1), 86-91.

Gates, D.H., and Dingwell, J.B., 2007. Peripheral neuropathy does not alter the fractal dynamics of stride intervals of gait. J Appl Physiol 102 (3), 965-71.

Gates, D.H., Dingwell, J.B., 2008. The effects of neuromuscular fatigue on task performance during repetitive goal-directed movements. Experimental Brain Research 187 (4), 573-585.

Gates, D.H., Dingwell, J.B., In Press. A comparison of different state spaces for local dynamic stability analyses. Journal of Biomechanics.

Gates, D.H., Su, J.L., Dingwell, J.B., 2007. Possible biomechanical origins of the long-range correlations in stride intervals of walking. Physica A 380, 259-270.

Goerlick, M., Brown, J.M.M., Groeller, H., 2003. Short-duration fatigue alters neuromuscular coordination of trunk musculature: Implications for injury. Applied Ergonomics 34 (4), 317-325.

Gordon, A.M., Westling, G., Cole, J.K., Johansson, R.S., 1993. Memory representations underlying motor commands used during manipulation of common and novel objects. Journal of Neurophysiology 69 (6), 1789-1796.

Granata, K.P., England, S.A., 2006. Stability of dynamic trunk movement. Spine 31 (10), E271-6.

Granata, K.P., Gottipati, P., 2008. Fatigue influences the dynamic stability of the torso. Ergonomics 51 (8), 1258-1271.

Granata, K.P., Orishimo, K.F., Sanford, A.H., 2001. Trunk muscle coactivation in preparation for sudden load. Journal of Electromyography and Kinesiology 11 (4), 247-254.

Granata, K.P., Slota, G.P., Wilson, S.E., 2004. Influence of fatigue in neuromuscular control of spinal stability. Hum Factors 46 (1), 81-91.

Gribble, P.L., Mullin, L.I., Cothros, N., Mattar, A., 2003. Role of cocontraction in arm movement accuracy. Journal of Neurophysiology 89 (5), 2396-405.

Grondin, D.E., Potvin, J.R., In Press. Effects of trunk muscle fatigue and load timing on spinal responses during sudden hand loading. Journal of Electromyography and Kinesiology.

Hagg, G.M., Milerad, E., 1997. Forearm extensor and flexor muscle exertion during simulated gripping work - an electromyographic study. Clinical Biomechanics 12, 39-43.

Hamill, J., van Emmerick, R.E.A., Heiderscheit, L.L., 1999. A dynamical systems approach to lower extremity running injuries. Clin Biomech 14, 297-308.

Hausdorff, J.M., Peng, C.K., Ladin, Z., Wei, J.Y., Goldberger, A.L., 1995. Is walking a random walk? Evidence for long-range correlations in stride interval of human gait. Journal of Applied Physiology 78 (1), 349-358.

Heuer, H., Schulna, R., Luttmann, A., 2002. The effects of muscle fatigue on rapid finger oscillations. Experimental Brain Research 147, 124-134.

Hingtgen, B., McGuire, J.R., Wang, M., Harris, G.F., 2006. An upper extremity kinematic model for evaluation of hemiparetic stroke. Journal of Biomechanics 39 (4), 681-8.

Hof, A.L., 1996. Scaling gait data to body size. Gait & Posture 4, 222-223.

Hostens, I., Seghers, J., Spaepen, A. and Ramon, H., 2004. Validation of the wavelet spectral estimation technique in biceps brachii and brachioradialis fatigue assessment during prolonged low-level static and dynamic contractions. Journal of Electromyography and Kinesiology 14, 205-215.

Huang, C.-T., Hwang, I.-S., Huang, C.-C., Young, M.-S., 2006. Exertion dependent alternations in force fluctuations and limb acceleration during sustained fatiguing contraction. Eur J Appl Physiol 97, 362-371.

Hunter, S.K., Duchateau, J., Enoka, R.M., 2004. Muscle fatigue and the mechanisms of task failure. Exercise and Sport Science Reviews 32 (2), 44-49.

Hurmuzlu, Y., Basdogan, C., 1994. On the measurement of dynamic stability of human locomotion. Journal of Biomechanical Engineering 116 (1), 30-36.

Hurmuzlu, Y., Basdogan, C., Stoianovici, D., 1996. Kinematics and dynamic stability of the locomotion of post-polio patients. Journal of Biomechanical Engineering 118 (3), 405 - 411.

Huysmans, M.A., Hoozemans, M.J.M., van der Beek, A.J., de Looze, M.P., van Dieën, J.H., 2008. Fatigue effects on tracking performance and muscle activity. Journal of Electromyography and Kinesiology 18 (3), 410-419.

Iwasa, K., Miyamoto, K., Shimizu, K., 2005. Effects of erector spinae muscle fatigue on trunk repositioning accuracy in forward and lateral flexion. J Back & Musculoskeletal Rehab 18 (3), 61-66.

Janda, V., 1993. Muscle strength in relation to muscle length, pain and muscle imbalance. In: Ringdahl, K.H. (Eds.). Muscle strength. Churchill Livingstone, Edinburgh.

Jaric, S., Blesic, S., Milanovic, S., Radovanovic, S., Ljubisavljevic, M., Anastasijevic, R., 1999. Changes in movement final position associated with agonist and antagonist muscle fatigue. European Journal of Applied Physiology 80 (5), 467-471.

Jordan, K., Challis, J.H., Cusumano, J.P., Newell, K.M., 2009. Stability and the time-dependent structure of gait variability in walking and running. Human Movement Science 28 (1), 113-128.

Kamien, M., 1990. A rational management of tennis elbow Sports Medicine 9, 173-191.

Kang, H.G., Dingwell, J.B., 2006a. A direct comparison of local dynamic stability during standing and walking. Experimental Brain Research 172 (1), 35 - 48.

Kang, H.G., Dingwell, J.B., 2006b. Intra-session reliability of local dynamic stability of walking. Gait & Posture 24 (3), 386-390.

Kang, H.G., Dingwell, J.B., 2008. Effects of walking speed, strength and range of motion on gait stability in healthy older adults. Journal of Biomechanics 41 (14), 2899-2905.

Kantz, H., Schreiber, S., 2004. Nonlinear time series analysis, 2nd ed.

Kellis, E., Arabatzi, F., Papadopoulos, C., 2003. Muscle co-activation around the knee in drop jumping using the co-contraction index. Journal of Electromyography and Kinesiology 13 (3), 229-38.

Kennel, M.B., Brown, R., Abarbanel, H.D.I., 1992. Determining embedding dimension for phase-space reconstruction using a geometrical construction. Physical Review A 45 (6), 3403-3411.

Keogh, J.P., Nuwayhid, I., Gordon, J.L., Gucer, P.W., 2000. The impact of occupational injury on injured worker and family: Outcomes of upper extremity cumulative trauma disorders in maryland workers. American Journal of Industrial Medicine 38 (5), 498-506.

Kilbom, A., Makarainen, M., Sperling, L., Kadefors, R., Liedberg, L., 1993. Tool design, user characteristics and performance: A case study on plate-shears. Applied Ergonomics 24 (3), 221-30.

Kim, H.J., Chung, S., Kim, S., Shin, H., Lee, J., Kim, S., Song, M.Y., 2006. Influences of trunk muscles on lumbar lordosis and sacral angle. European Spine Journal 15, 409-414.

Konrad, P. 2005. The abc of emg: A practical introduction to kinesiological electromyography, Noraxon, Inc.

Kumar, S., 2001. Theories of musculoskeletal injury causation. Ergonomics 44 (1), 17-47.

Kumar, S., Narayan, Y., 1998. Spectral parameters of trunk muscles during fatiguing isometric axial rotation in neutral posture. J Electromyogr Kinesiol 8 (4), 257-67.

Kuo, A.D., 1999. Stabilization of lateral motion in passive dynamic walking. The International Journal of Robotics Research 18 (9), 917-930.

Latash, M.L., Scholz, J.P., Schöner, G., 2002. Motor control strategies revealed in the structure of motor variability. Exercise & Sport Sciences Reviews 30 (1), 26-31.

Latko, W.A., Armstron, T.J., Franzblau, A.L., Ulin, S.S., Werner, R.A., Albers, J.W., 1999. Cross-sectional study of the relationship between repetitive work and the prevalence of upper limb musculoskeletal disorders. American Journal of Industrial Medicine 36, 248-259.

Lee, H., Granata, K.P., 2008. Process stationarity and reliability of trunk postural stability. Clinical Biomechanics 23 (6), 735-742.

Levenstein, C., 1999. Economic losses from repetitive strain injuries. Occupational Medicine 14 (1), 149-161.

Lieber, R.L., Woodburn, T.M., Friden, J., 1991. Muscle damage induced by eccentric contractions of 25% strain. Journal of Applied Physiology 70 (6), 2498-507.

Lorist, M.M., Kernell, D., Meijman, T.F., Zijdewind, I., 2002. Motor fatigue and cognitive task performance in humans. Journal of Physiology 545 (1), 313-319.

Lucidi, C.A., Lehman, S.L., 1992. Adaptation to fatigue of long duration in human wrist movements. Journal of Applied Physiology 73 (6), 2596-2603.

MacIsaac, D., Parker, P.A., Scott, R.N., 2001. The short-time fourier transform and muscle fatigue assessment in dynamic contractions. Journal of Electromyography and Kinesiology 11 (6), 439-449.

Madeleine, P., Lundager, B., Voigt, M., Arendt-Nielsen, L., 1999. Shoulder muscle co-ordination during a chronic and acute experimental neck-shoulder pain. An occupational study. European Journal of Applied Physiology 79, 127-140.

Madeleine, P., Lundager, B., Voigt, N., Arendt-Nielson, L., 2003. Standardized low-load repetitive work: Evidence of different motor control strategies between experienced workers and a reference group. Applied Ergonomics 34, 533-542.

Madigan, M.L., Pidcoe, P.E., 2003. Changes in landing biomechanics during a fatiguing landing activity. Journal of Electromyography and Kinesiology 13 (5), 491-198.

Mair, S.D., Seaber, A.V., Glisson, R.R., Garret, W.E., 1996. The role of fatigue in susceptibility to acute muscle strain injury. American Journal of Sports Medicine 24 (2), 137-143.

Manor, B., Wolenski, P., Li, L., 2008. Faster walking speeds increase local instability among people with peripheral neuropathy. Journal of Biomechanics 41 (13), 2787-2792.

151

Maraun, D., Rust, H.W., Timmer, J., 2004. Tempting long-memory - on the interpretation of dfa results. Nonlinear Processes in Geophysics 11, 495-503.

Marras, W.S., and Granata, K.P., 1997. Changes in trunk dynamics and spine loading during repeated trunk exertions. Spine 22 (21), 2564-70.

McQuade, K.J., Dawson, J., Smidt, G.L., 1998. Scapulothoracic muscle fatigue associated with alteration in scapulohumeral rhythm kinematics during maximum resistive shoulder elevation. Journal of Orthopedic and Sports Physical Therapy 28 (2), 74-80.

Missenard, O., Mottet, D., Perrey, S., 2008a. Muscular fatigue increases signal-dependent noise during isometric force production. Neuroscience Letters 437 (2), 154-7.

Missenard, O., Mottet, D., Perrey, S., 2008b. The role of cocontraction in the impairment of movement accuracy with fatigue. Experimental Brain Research 185 (1), 151-6.

Mizrahi, J., Verbitsky, O., OIsankov, E., 2000. Fatigue-related loading imbalances on the shank in running: A possible factor in stress fractures. Annals of Biomedical Engineering 28, 463-469.

Myers, J.B., Guskiewicz, K.M., Schneider, R.A., Prentice, W.E., 1999. Proprioception and neuromuscular control of the shoulder after muscle fatigue. Journal of Athletic Training 34 (4), 362-367.

Nayfeh, A.H., Balachandran, B., 1995. Applied nonlinear dynamics: Analytical, computational, and experimental methods. Wiley Series in Nonlinear Science.

Niemuth, P.E., Johnson, R.J., Myers, M.J., Thieman, T.J., 2005. Hip muscle weakness and overuse injuries in recreational runners. Clinical Journal of Sports Medicine 15 (1), 14-21.

Nussbaum, M.A., 2001. Static and dynamic myoelectric measures of shoulder muscle fatigue during intermittent dynamic exertions of low to moderate intensity. European Journal of Applied Physiology 85 (3-4), 299-309.

O'Boyle, D.J., Freeman, J.S., Cody, F.W.J., 1996. The accuracy and precision of timing of self-paced, repetitive movements in subjects with parkinson's disease. Brain 119 (1), 51-70.

Ohlsson, K., Attewell, R.G., Pålsson, B., Karlsson, B., Balogh, I., Johnsson, B., Ahlm, A., Skerfving, S., 1995. Repetitive industrial work and neck and upper limb disorders in females. Am J Ind Med 27 (5), 731-747.

Oldfield, R.C., 1971. The assessment and analysis of handedness: The edinburgh inventory. Neuropsychologia 9 (97-113), 97-113.

Parnianpour, M., Nordin, M., Kahanovitz, N., Frankel, V., 1988. The triaxial coupling of torque generation of trunk muscles during isometric exertions and the effect of fatiguing isoinertial movements on the motor output and movement patterns. Spine 13 (9), 982-92.

Pedersen, J., Lonn, J., Hellstrom, F., Djupsjobacka, M., Johansson, H., 1999. Localized muscle fatigue decreases the acuity of the movement sense in the human shoulder. Medicine and Science in Sports and Exercise 31, 1047-1052.

Peng, C.K., Buldyrev, S.V., 1993. Finite-size effects on long-range correlations: Implications for analyzing DNA sequences. Physical Review E 47 (5), 3730-3733.

Peng, C.K., Buldyrev, S.V., Havlin, S., Simons, M., Stanley, H.E., Goldberger, A.L., 1994. Mosaic organization of DNA nucleotides. Physical Review E 49 (2), 1685-1689.

Peng, C.K., Havlin, S., Stanley, H.E., Goldberger, A.L., 1995. Quantification of scaling exponents and crossover phenomena in nonstationary heartbeat time series. Chaos 5 (1), 82-87.

Potvin, J.R., O'Brien, P.R., 1998. Trunk muscle co-contraction increases during fatiguing, isometric, lateral bend exertions. Spine 23, 774-781.

Pransky, G., Snyder, T., Dembe, A., Himmelstein, J., 1999. Under-reporting of work-related disorders in the workplace: A case study and review of the literature. Ergonomics 42 (1), 171-182.

Psek, J.A., Cafarelli, E., 1993. Behavior of coactive muscles during fatigue. Journal of Applied Physiology 74 (1), 170-175.

Rao, S.S., Bontrager, E.L., Gronley, J.K., Newsam, C.J., Perry, J., 1996. Three-dimensional kinematics of wheelchair propulsion. IEEE Transactions on Rehabilitation Engineering 4 (3), 152-60.

Reeves, N., Everding, V., Cholewicki, J., Morrisette, D., 2006. The effects of trunk stiffness on postural control during unstable seated balance. Experimental Brain Research 174 (4), 694-700.

Reeves, N.P., Cholewicki, J., Milner, T., Lee, A.S., 2008. Trunk antagonist co-activation is associated with impaired neuromuscular performance. Experimental Brain Research 188 (3), 457-63.

Reeves, N.P., Narendra, K.S., Cholewicki, J., 2007. Spine stability: The six blind men and the elephant. Clinical Biomechanics 22 (3), 266-274.

Robertson, D.G., Caldwell, G.E., Hamill, J., Kamen, G., Whittlessey, S.N., 2004. Research methods in biomechanics. Human Kinetics, Champaign.

Rodgers, M.M., Gayle, G.W., Figoni, S.F., Kobayashi, M., Lieh, J., Glaser, R.M., 1994. Biomechanics of wheelchair propulsion during fatigue. Archives of Physical Medicine and Rehabilitation 75 (1), 85-93.

Rodgers, M.M., McQuade, K.J., Rasch, E.K., Keyser, R.E., Finley, M.A., 2003. Upper-limb fatigue-related joint power shifts in experienced wheelchair users and nonwheelchair users. Journal of Rehabilitation Research and Development 40 (1), 27-37.

Rosenstein, M.T., Collins, J.J., DeLuca, C.J., 1993. A practical method for calculating largest lyapunov exponents from small data sets. Physica D 65, 117 - 134.

Rosenstein, M.T., Collins, J.J., Deluca, C.J., 1994. Reconstruction expansion as a geometry-based framework for choosing proper delay times. Physica D 73, 82–98.

Rudolph, K.S., Axe, M.J., Buchanan, T.S., Scholz, J.P., Snyder-Mackler, L., 2001. Dynamic stability in the anterior cruciate ligament deficient knee. Knee Surgery, Sports Traumatology, Arthroscopy 9 (2), 62-71.

Sainburg, R.L., Ghez, C., Kalakanis, D., 1999. Intersegmental dynamics are controlled by sequential anticipatory, error correction, and postural mechanisms. Journal of Neurophysiology 81 (3), 1045-1056.

Schmidt, R., Disselhorst-Klug, C., Silny, J., Rau, G., 1999. A marker-based measurement procedure for unconstrained wrist and elbow motions. Journal of Biomechanics 32, 615-621.

Scholz, J.P., Schöner, G., 1999. The uncontrolled manifold concept: Identifying control variables for a functional task. Experimental Brain Research 126 (3), 289-306.

Schöner, G., Scholz, J.P., 2007. Analyzing variance in multi-degree-of-freedom movements: Uncovering structure versus extracting correlations. Motor Control 11, 259-275.

Segal, A.D., Orendurff, M.S., Czerniecki, J.M., Shofer, J.B., Klute, G.K., 2008. Local dynamic stability in turning and straight-line gait. Journal of Biomechanics 41 (7), 1486-93.

Selen, L.P., Beek, P.J., van Dieen, J.H., 2005. Can co-activation reduce kinematic variability? A simulation study. Biological Cybernetics 93 (5), 373-81.

Selen, L.P.J., Beek, P.J., van Dienn, J.H., 2007. Fatigue-induced changes of impedance and performance in target tracking. Experimental Brain Research 181, 99-108.

Slota, G.P., Granata, K.P., Madigan, M.L., 2008. Effects of seated whole-body vibration on postural control of the trunk during unstable seated balance. Clinical Biomechanics 23 (4), 381-6.

Sparto, P.J., Parnianpour, M., Reinsel, T.E., Simon, S., 1997. The effect of fatigue on multijoint kinematics and load sharing during a repetitive lifting test. Spine 22 (22), 2647-2654.

Stergiou, N., Moraiti, C., Giakas, G., Ristanis, S., Georgoulis, A.D., 2004. The effect of the walking speed on the stability of the anterior cruciate ligament deficient knee. Clinical Biomechanics 19 (9), 957-963.

Stokes, I.A.F., Gardner-Morse, M., Henry, S.M., Badger, G.J., 2000. Decrease in trunk muscular response to perturbation with preactivation of lumbar spinal musculature. Spine 25 (15), 1957-1964.

Strange, A.J., Berg, W.P., 2007. Fatigue-induced adaptive changes of anticipatory postural adjustments. Exp Brain Res 178 (1), 49-61.

Strogatz, S.H., 1994. Nonlinear dynamics and chaos: With applications to physics, biology, chemistry, and engineering. Addison-Wesley, New York, New York.

Takens, F., 1981. Detecting strange attractors in turbulence. In: Rand, D., Young, L.S. (Eds.). Dynamical systems and turbulence, warwick 1980. Springer-Verlag, Berlin, 898, pp. 366-381.

U.S. Bureau of Labor Statistics 2005. Http://stats.Bls.Gov/iif/oshcdnew.Htm. 2007.

Valachi, B., Valachi, K., 2003. Mechanisms leading to musculoskeletal disorders in dentistry. Journal of the American Dental Association 134 (10), 1344-50.

van Dieën, J.H., Kingma, I., van der Bug, J.C.E., 2003. Evidence for a role of antagonistic cocontraction in controlling trunk stiffness during lifting. Journal of Biomechanics 36 (12), 1829-1836.

van Duinen, H., Renken, R., Maurits, N., Zijdewind, I., 2007. Effects of motor fatigue on human brain activity, an fmri study. NeuroImage 35 (4), 1438-1449.

Veldpaus, F.E., Woltring, H.J., and Dortmans, L.J., 1988. A least-squares algorithm for the equiform transformation from spatial marker co-ordinates. Journal of Biomechanics 21 (1), 45-54.

Viitasalo, J.T., Hamalainen, K., Mononen, H.V., Salo, A., Lahtinen, J., 1993. Biomechanical effects of fatigue during continuous hurdle jumping. Journal of Sports Sciences 11 (6), 503-509.

Voge, K.R., Dingwell, J.B., 2003. Relative timing of changes in muscle fatigue and movement coordination during a repetitive one-hand lifting task. In. Proc 25th int conf of ieee embs, Cancun, Mexico.

von Tscharner, V., 2002. Time-frequency and principal-component methods for the analysis of emgs recorded during a mildly fatiguing exercise on a cycle ergometer. J Electromyogr Kinesiol 12 (6), 479-492.

Wang, H.K., Cochrane, T., 2001. Mobility impairment, muscle imbalance, muscle weakness, scapular asymmetry and shoulder injury in elite volleyball athletes. Journal of Sports Medicine and Physical Fitness 41 (3), 403-410.

Wilder, D.G., Aleksiev, A.R., Magnusson, M.L., Malcolm, P.H., Spratt, K.F., Goel, V.K., 1996. Muscular response to sudden load: A tool to evaluate fatigue and rehabilitation. Spine 21 (22), 2628-2639.

Wing, A., Daffertshofer, A., Pressing, J., 2004. Multiple time scales in serial production of force: A tutorial on power spectral analysis of motor variability. Human Movement Science 23, 569-590.

Winter, D.A., 2005. Biomechanics and motor control of human movement, 3rd ed.

Wojtys, E.M., Wylie, B.B., Huston, L.J., 1996. The effects of muscle fatigue on neuromuscular function and anterior tibial translation in healthy knees. American Journal of Sports Medicine 24 (5), 615-621.

Wu, G., van der Helm, F.C., Veeger, H.E., Makhsous, M., Van Roy, P., Anglin, C., Nagels, J., Karduna, A.R., McQuade, K., Wang, X., Werner, F.W., Buchholz, B., 2005. Isb recommendation on definitions of joint coordinate systems of various joints for the reporting of human joint motion--part ii: Shoulder, elbow, wrist and hand. Journal of Biomechanics 38 (5), 981-992.

Yoshino, K., Motoshige, T., Araki, T., Matsuoka, K., 2004. Effect of prolonged free-walking fatigue on gait and physiological rhythm. Journal of Biomechanics 37 (8), 1271-1280.

Vita

Deanna Helene Gates was born on December 25, 1979 in Washington, D.C to her parents, Jean and Gerald Gates. Deanna grew up in Alexandria, VA where she graduated from Mount Vernon High School in 1998. She received a B.S. with Distinction in Mechanical Engineering from the University of Virginia in 2002. She then attended Boston University where she received an M.S. in Biomedical Engineering in 2004 under the guidance of Paolo Bonato in the Motion Analysis Laboratory at Spaulding Rehabilitation Hospital. Deanna worked as a Research Engineer at Spaulding Rehabilitation Hospital in Boston, MA for the next year (2004-2005). In the fall of 2005, Deanna began graduate school at the University of Texas at Austin. Deanna has published 4 journal articles, presented her research at 6 conferences and won an award for best student presentation at the 12th Annual Gait and Clinical Movement Analysis Society Meeting in 2007. She also was awarded a Continuing Fellowship from the University of Texas at Austin, to support her last year of study.

Permanent address: 8524 Wagon Wheel Rd.
                    Alexandria, VA 22309

This dissertation was typed by the author.